U.S. Department
of Transportation
**Federal Railroad
Administration**

Effect of Hollow-Worn Wheels on Wheel and Rail Interaction with North American Freight Cars

Office of Research and
Development
Washington, D.C. 20590

DOT/FRA/ORD-

November 2002
Draft Report

REPORT DOCUMENTATION PAGE

Form approved

OMB No. 0704-0188

1. AGENCY USE ONLY *(Leave blank)*	2. REPORT DATE	3. REPORT TYPE AND DATES COVERED
	November 2002	

4. TITLE AND SUBTITLE

Effect of Hollow-Worn Wheels on Wheel and Rail Interaction with North American Freight Cars

5. FUNDING NUMBERS

DTFR53-93-C-00001
Task Order 126

6. AUTHOR(S)

Kevin Sawley and Russell Walker

7. PERFORMING ORGANIZATION NAME(S) AND ADDRESS(ES)

Transportation Technology Center, Inc.
P.O. Box 11130
Pueblo, CO 81001

8. PERFORMING ORGANIZATION REPORT NUMBERS

9. SPONSORING/MONITORING AGENGY NAME(S) AND ADDRESS(ES)

U.S. Department of Transportation
Federal Railroad Administration
Office of Research and Development
1120 Vermont Avenue, NW
Washington, DC 20590

10. SPONSORING/MONITORING AGENCY REPORT NUMBER

11. SUPPLEMENTARY NOTES

12a. DISTRIBUTION/ABAILABILITY STATEMENT

This document is available through National Technical Information Service, Springfield, VA 22161

12b. DISTRIBUTION CODE

13. ABSTRACT

This report examines the effect that hollow-worn wheels have on wheel and rail interaction for typical North American freight cars on tangent and curved track. Hollow wear tends to reduce the speed of which hunting starts and can increase the rail roll moment. However, hollow wear is not the sole controller of wheel and rail interaction. Other important factors include rail shape, wheel flange wear, track gages, and wheel back-to-back spacing.

14. SUBJECT TERMS

Wheel wear
Vehicle stability
Lateral forces
Derailment risk

15. NUMBER OF PAGES

39 plus appendices

16. PRICE CODE

17. SECURITY CLASSIFICATION	18. SECURITY CLASSIFICATION OF THIS PAGE	19. SECURITY CLASSIFICATION OF ABSTRACT	20. LIMITATION OF ABSTRACT
UNCLASSIFIED	UNCLASSIFIED	UNCLASSIFIED	SAR

NSN 7540-01-280-5500

Standard Form 298 (Rec. 2-89)
Prescribed by ANSI/NISO Std. 239.18
298-102

EXECUTIVE SUMMARY

The Federal Railroad Administration contracted with Transportation Technology Center, Inc. to perform analysis and testing of the effect of hollow-worn wheels on wheel and rail interaction.

Both the modeling and the tests indicate that hollow wear decreases the speed at which vehicle hunting* is likely to start, and increases the standard deviation of lateral car body acceleration at speeds below the onset of hunting. However, the loaded tangent track simulations do not indicate that hollow-worn wheels necessarily lead to high L/V forces

A more detailed analysis of the NUCARS output indicates that the vehicle instabilities produced by hollow-worn wheels may be different from those produced by non-hollow-worn wheels.

Results further imply that vehicle stability depends critically on the interaction between wheel and rail geometries. The geometry parameters that influence interaction include:

- Detailed transverse wheel profiles, not just the degree of hollow wear.
- Detailed transverse rail profiles, though these likely have a lesser effect than the wheel profiles.
- Diameter difference at the tread between the two wheels on the axle. This has a major effect on the way the axle runs along the rail.
- The amount of flange wear on the wheelsets and the wheel back-to-back spacing, which influence the flangeway clearance.
- The amount of gage face wear on the rails, and the track gage, both of which influence flangeway clearance.

This study, and the associated Association of American Railroads Strategic Research Initiative project, has led to a much better understanding of the effect of hollow wear on vehicle stability and safety. The studies have also identified areas where knowledge of wheel profiles is deficient, and areas where further work is needed to better understand the way that combined wheel and rail geometry (especially the geometry of hollow wheels) influences wheel and rail interaction and hence railroad safety.

---

* A sudden increase in standard deviation of lateral car body acceleration.

Table of Contents

List of Figures

List of Tables

1.0 INTRODUCTION

The Federal Railroad Administration (FRA) contracted with Transportation Technology Center, Inc. (TTCI) to perform analysis and testing of the effect of hollow-worn wheels on vehicle safety.

Hollow-worn wheels represent the end-life condition of the typical North American freight car wheel. As such, these wheels are present on a significant number of freight cars. Figure 1 shows the distribution of hollow-worn wheels found from a survey of wheel profiles undertaken in the late 1990s.[1] Under loaded vehicle conditions, the presence of hollow-worn wheels can produce excessively high lateral loads, by causing trucks to warp (take up a parallelogram shape). When combined with the action of the hollow wheel "false flange" on the field side of the rail, it is possible that these increased lateral forces can increase the risk of derailment from rail rollover. It also has been reported that hollow-worn wheels cause increased incidence of hunting of empty vehicles and may represent a derailment hazard.

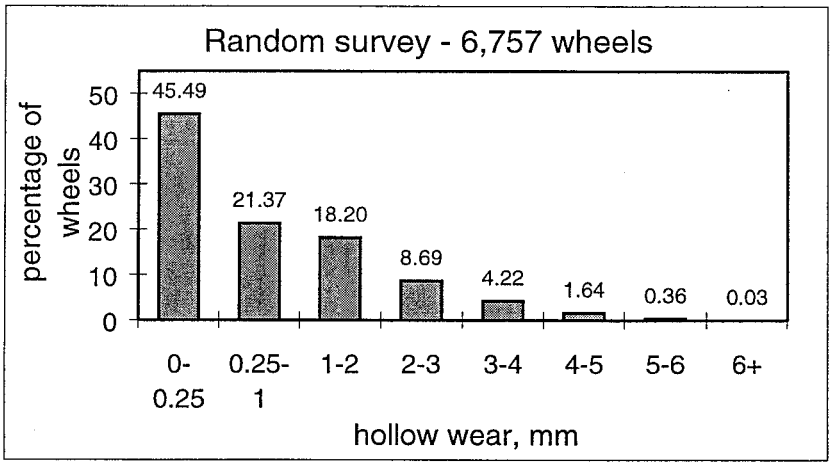

Figure 1: Distribution of Hollow-Worn Wheels in North America

The purpose of this investigation was to identify the consequence of running hollow-worn wheels on loaded and empty revenue freight service cars under conditions that may represent hazardous situations. The car types investigated are a bulkhead flat car and a rail compatible vehicle (RCV) consisting of a highway trailer especially configured for rail operation. The RCV modeled for this program consists of a single highway trailer mounted between two railroad bogies. The railroad bogies are high-speed freight trucks designed for use at speeds up to 90

mph. The truck center spacing is 47-feet 1-inch. A full-scale test was performed to compare the vehicle response when new wheels with AAR1B profiles are installed compared to revenue service hollow-worn wheels. A NUCARS[TM*] model of the test was completed and used as a calibration for subsequent NUCARS modeling efforts.

1.1 Objective

The objective of this project was to investigate the safety implications of hollow-worn wheels interacting with typical worn rails.

1.2 Description of a Hollow Wheel

Initially, we intended to characterize the performance of hollow-worn wheels in terms of their hollowness, H, which is defined here as the difference between the largest radius on the field edge of the tread and the smallest radius on the inside of the tread (see Figure 2). We thought that the wheel profile's performance could be directly and solely related to its hollowness. However, early work showed this not to be the case. Instead, the performance of a wheelset is related to the:

- profile of the two wheels of the wheelset,
- difference in radius between the two wheels of the wheelset, and
- gage clearance (defined by back to back spacing, flange wear, and track gage).

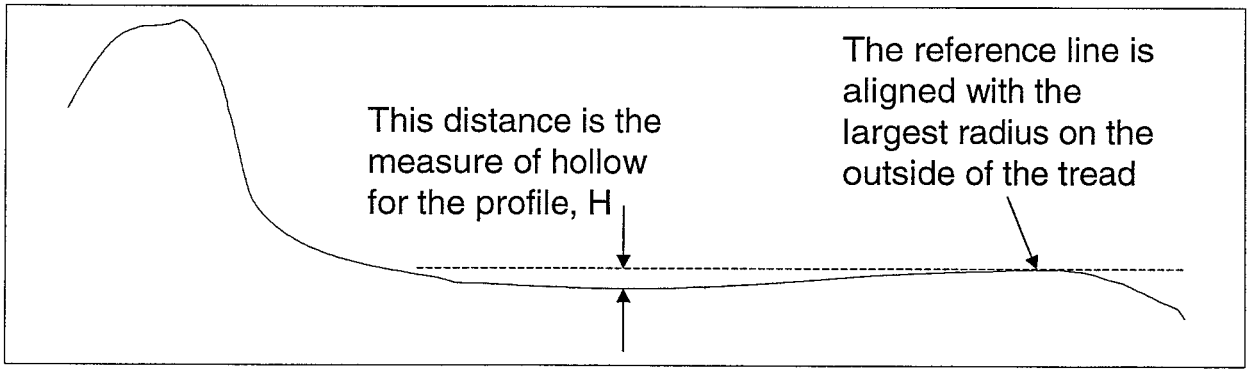

Figure 2. A Hollow-Worn Wheel Showing How Hollowness is Defined

* Trademark of Transportation Technology Center, Inc.

The best indicator of the high-speed stability performance of a wheelset is its rolling radius difference (RRD) graph. (An example is shown in Figure 3.) The RRD graph shows the difference in rolling radius between the left and right wheel of a wheelset for a range of wheelset lateral shifts. This graph is specific to a wheelset and rail pair.

1.3 ASSUMPTIONS

This study uses the following wheel and rail profile assumptions:

- The radii of the wheels on a wheelset are equal at the flange tip.
- Measured wheel profiles found from the work of reference 1 and used in this study may need rotation to correct for measurement errors. In all cases the rotations used are those calculated in reference 1.
- There is no rotation of the wheel or rail transverse profiles under vertical or lateral loads.

When work on this program began, a normal assumption was that the two wheels of a wheelset had identical radii at the tapeline. We soon realized that this assumption led to large errors when the two wheels of a wheelset have different amounts of tread wear. The reference position for the wheel radius was moved to the top of the flange because little or no wear should occur at that point. The validity of the assumption then is only dependent on the accuracy of the machining or casting process, rather than the wear of the profile.

In the study of reference 1, wheel profiles were measured with the Miniprof™* wheel profilometer manufactured by Greenwood Engineering, Denmark. The Miniprof attaches to the back of a wheel with magnets. Unfortunately, due to variations in the back of the wheel, and variations in the profilometers themselves, there is often some rotation introduced in the measurement. The wheel profiles used for this study were adjusted to account for this rotation.

No adjustments were made to the wheel and rail profile measurements to account for the changes in wheel rail interaction due to axle bending or rail roll under load.

* Trademark of Greenwood Engineering A/S

2.0 PROFILE AND MODELING PROCEDURES

2.1 SELECTION OF WHEEL PROFILES

Initial work in this area was done under the Association of American Railroads' (AAR) Strategic Research Initiative Program and focused on the use of idealized hollow wheel profiles. TTCI engineers created a standard set of profiles with various degrees of hollowing. Several assumptions were made to create these original profiles:

- The radii at tapeline of the two wheels of a wheelset were identical
- The profile of the two wheels of a wheelset were identical
- As hollowing increased, flange wear increased, so that a hollow wheel that was nearly condemnable for flange height was also nearly condemnable for flange thickness.

It was eventually realized that these assumptions were not general in practice and that deviating from these assumptions had a significant effect on the performance of a wheelset, especially considering vehicle stability.

A wide range of real wheel profiles was measured as part of this AAR program. These profiles were used to produce a database of wheelsets that included wheelsets typical of the majority in North American service plus a number of wheelsets with advanced hollow wear. This database was termed the FRA Hollow Wheel Profile Database and was used extensively for this study. It contains 66 measured wheelsets.

Work in the AAR program has led to much better understanding of the relationship of wheel/rail geometry to vehicle stability and has identified improvements to the ways in which wheel and rail profile data is handled for use in dynamic modeling. These include:

- Improved knowledge of the role of the RRD graph. This graph plots the difference in the radii (at the wheel/rail contact positions) of the two wheels of a wheelset as the wheelset is shifted laterally between the rails. The central slope of this graph and the wheelset lateral shift positions at zero rolling radius difference are critical to vehicle stability.
- Defining where the two wheels on a wheelset have the same radius. In the past, dynamic analyses, by default, have tended to assume that the wheels have the same radii at the tapeline near the tread center. This assumption is unlikely to be valid for wheels showing dissimilar tread wear. Hence, in this study, following work in the AAR program, it is assumed that wheels have the same radii at the flange tip.
- The importance of considering other factors than depth of hollow. Work in the AAR program has shown that, as well as the detailed rail profiles, vehicle stability depends on

the detailed shapes of the two wheel profiles, the RRD graph, and the gage clearance (defined by back to back spacing, flange wear, and track gage).

Figure 2 is a graph of rolling radius difference of a wheelset with some of the key features labeled.

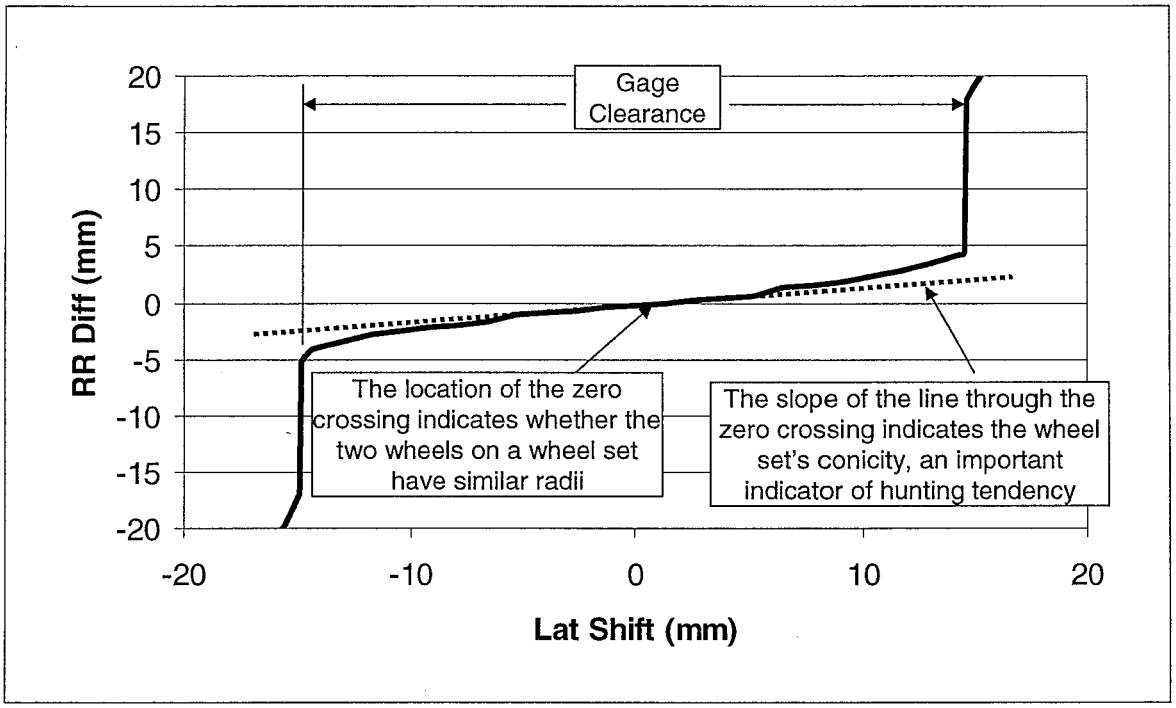

Figure 3. A Sample RRD Graph with the Key Features Labeled

The wheelsets in the FRA Hollow Wheel Profile Database were matched geometrically against a number of rail pairs at a track gage of 56.5 inches and moved laterally to generate RRD graphs. The rail pairs included the design AREMA 136-RE rails, two pairs of typical tangent-worn rails, and one pair of typical curve-worn rails. This generated numerous RRD graphs. These were used to identify five wheelsets, with various combinations of hollowing, flange wear, and wheel radius mismatch, which gave a wide range of RRD characteristics. The five wheelsets were then re-matched against the rail pairs at track gages of 56 and 57 inches. Finally, five wheelset/rail pair profile combinations were chosen for further modeling. High-speed stability simulations used new and tangent-worn rail profiles, whereas curving simulations used new and curve-worn rail profiles. These profile combinations gave RRD graphs that encompassed the range of behaviors seen throughout this initial exercise.

These five wheelset/rail pair combinations were:

- New AAR 1B narrow flange wheels on new AREMA 136-RE rail at 56.5-inch gage. Figure 4 shows the wheel and rail profiles (with the points of profile correspondence), and the resulting RRD graph. This RRD graph shows the normal new wheel/new rail situation. It has a central slope of approximately 0.1.
- Moderately worn AAR 1B wide flange wheels on new AREMA 136-RE rail with 57-inch gage (see Figure 5). This RRD graph shows a higher slope compared to Figure 4.
- Hollow-worn wheels with mismatched wheel diameters on tangent worn rail with 57-inch gage (see Figure 6). This RRD graph shows a central slope of approximately zero, which implies that the wheelset will have little ability to steer. The RRD graph also shows a vertical offset that implies the wheelset will run offset from the track centerline in tangent track.
- Hollow-worn wheels with flange wear on tangent worn rail at 56.5-inch gage (see Figure 7). The central part of the RRD graph has a negative slope. This implies that the wheelset will have negative steering. That is, if the wheelset moves to the right (or left), the geometry will tend to move it further right (or left). Hence in tangent track the wheelset would be expected to run against one of the rails, possibly moving to the other rail, if given sufficient lateral impact force from the track geometry.
- Hollow-worn wheels with very little flange wear on Transportation Technology Center's (TTC's) Transit Test Track (tangent) rail (see Figure 8). Although the wheels are hollow, the RRD graph now has a very high central slope that is likely to encourage hunting.

Table 1 lists hollow wear and flange wear details for the 10 wheels used in these wheelsets. Profile combinations using curve worn rails were substituted for the last three combinations for curving simulations (see Figures 9 to 11).

Table 1: Details of Wheel Hollow Wear and Flange Wear of Modeled Wheelsets

Wheelset	Wheel filename		Hollow wear, mm	Flange wear*, mm
1	AAR1B Narrow Flange	Left	0	0
		Right	0	0
2	Moderately worn AAR1B Wide Flange (2NED)	Left	0	0.03
		Right	0	0.14
3	Hollow-worn wheelset with wheel radius mismatch (11NED)	Left	0.61	2.59
		Right	0.37	2.83
4	Hollow-worn wheelset with flange wear (21NED)	Left	2.93	8.49
		Right	3.01	8.99
5	Hollow-worn wheelset with minimal flange wear (3-6#22)	Left	4.06	1.55
		Right	3.93	1.12

* Wear loss at the flange gage point

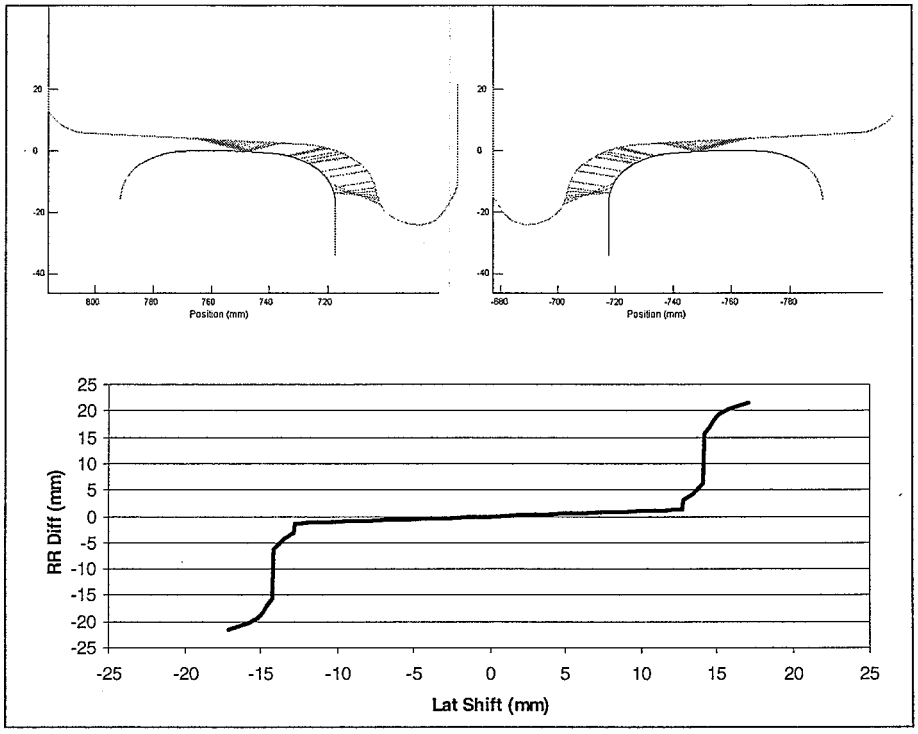

Figure 4. Contact of New AAR1B Narrow Flange Wheel on AREMA 136-RE Rail, 10-inch Crown Radius, 1:40 Cant, at a Gage of 56.5 inches. (AAR1BNF_13610140_565.WNT)

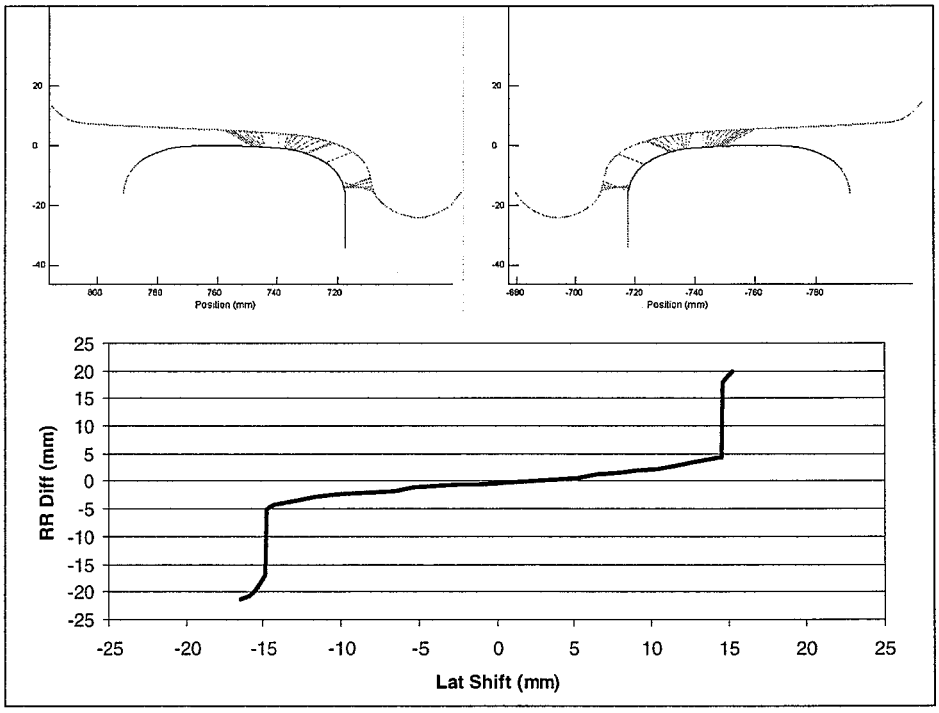

Figure 5. Contact of Moderately Worn AAR1B Wide Flange Wheel on AREMA 136-RE Rail, 10-inch Crown Radius, 1:40 cant, at a Gage of 57.0 inches. (2NED_13610140_570.WNT)

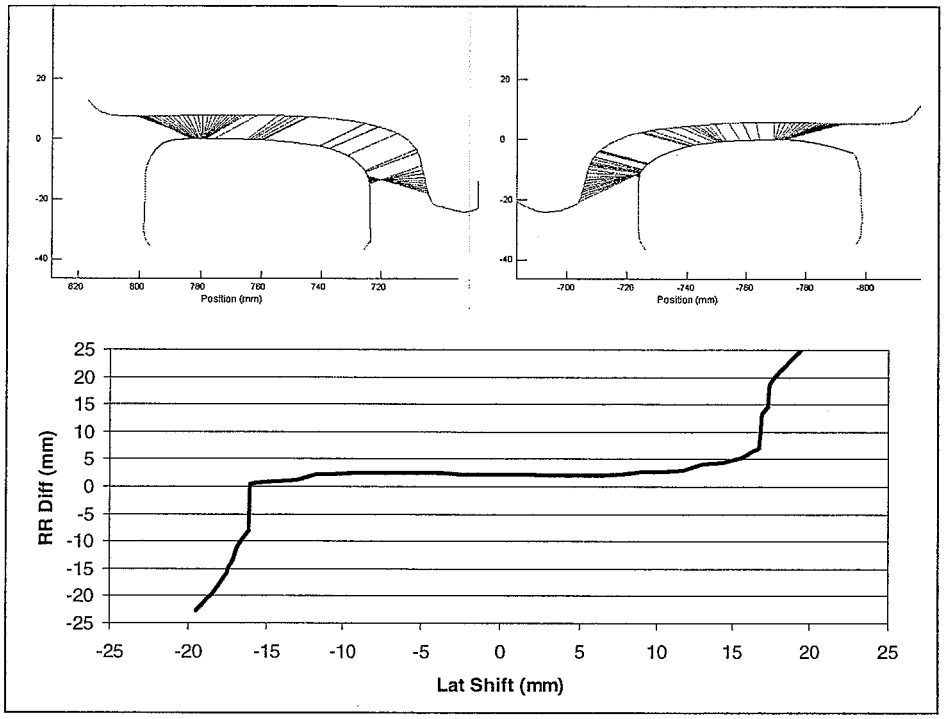

Figure 6. Contact of Hollow-Worn Wheel with Wheel Radius Mismatch on Tangent Worn Rail at a Gage of 57.0 inches. (11NED_Eggleston-95_570.WNT)

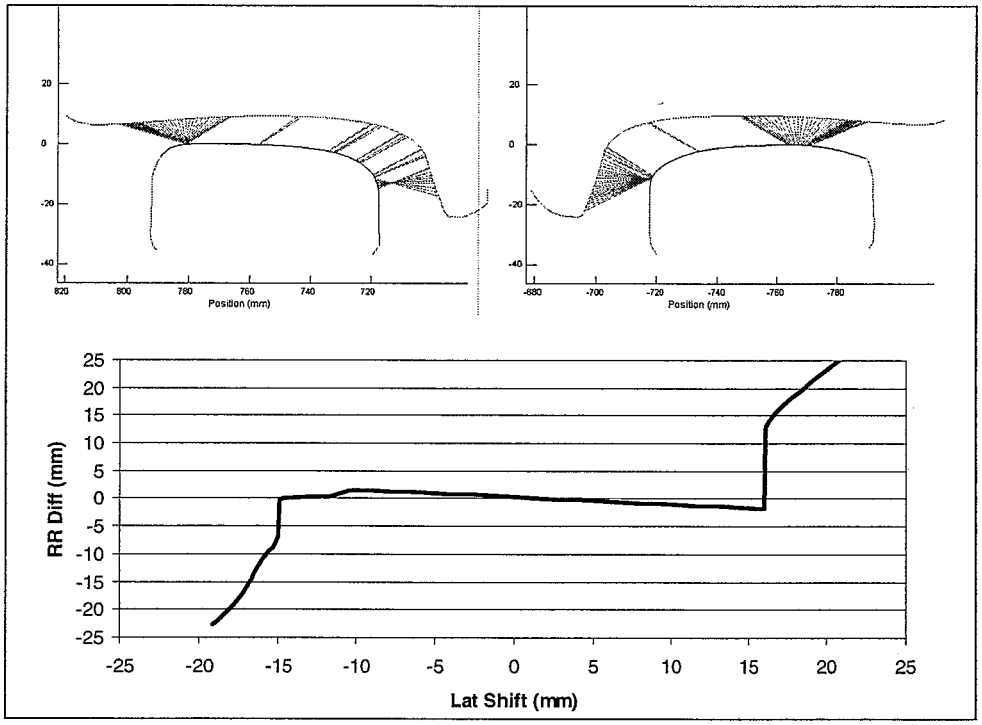

Figure 7. Contact of Hollow Worn Wheel on Tangent Worn Track at a Gage of 56.5 inches. (21NED_Eggleston-95_565.WNT)

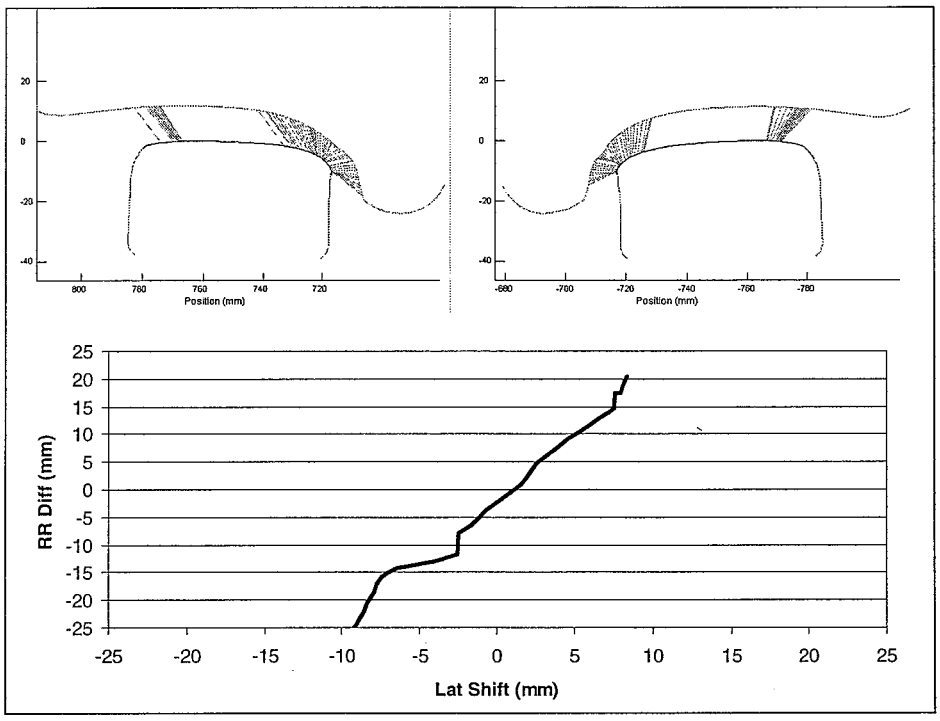

Figure 8. Contact of a Hollow Worn Wheel with Minimal Flange Wear on TTC'S TTT at a Gage of 56.5 inches. (3-6#22_TTT-14CCW_565.WNT)

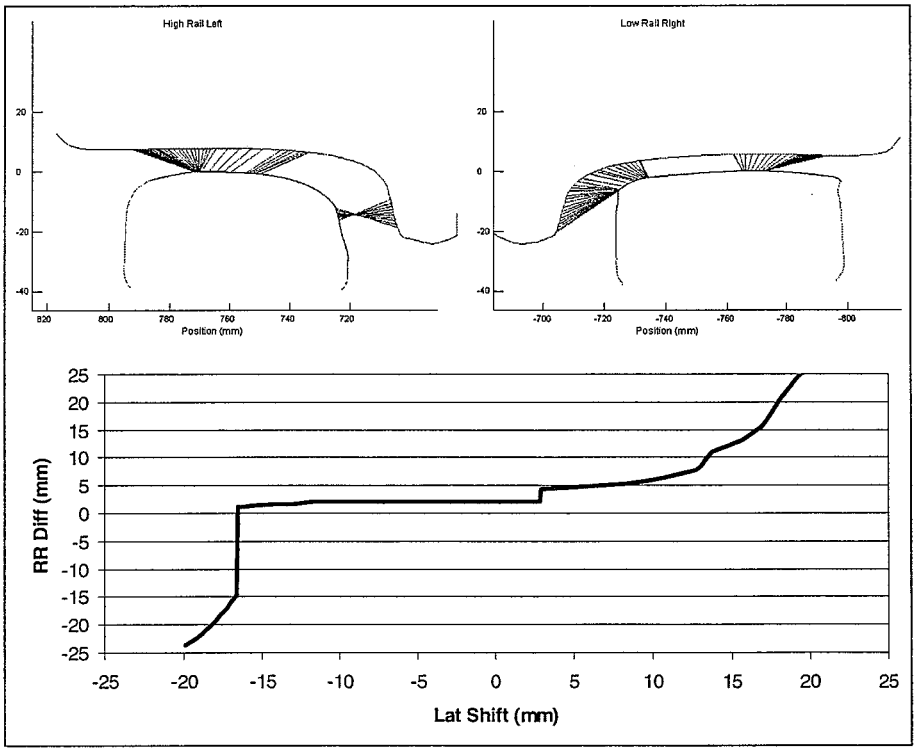

Figure 9. Contact of a Hollow-Worn Wheel with Mismatched Wheel Radii on Curve Worn Rail at a Gage of 57.0 inches. (11NED_44-154_570.WNT)

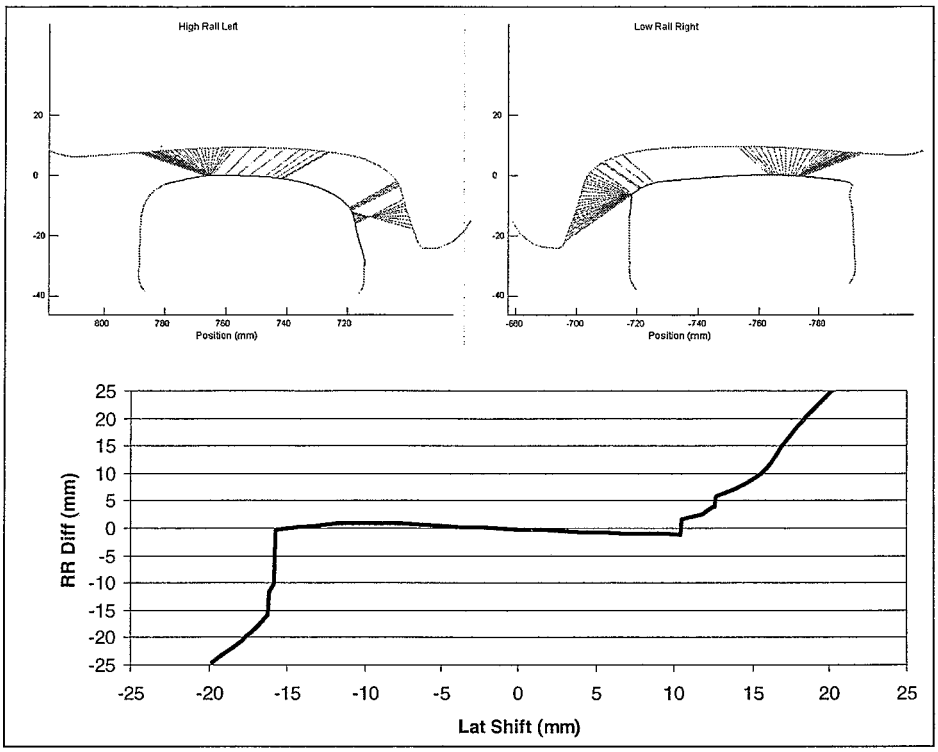

Figure 10. Contact of a Hollow-Worn Wheel on a Curve Worn Rail at a Gage of 56.5 inches. (21NED_44-154_565.WNT)

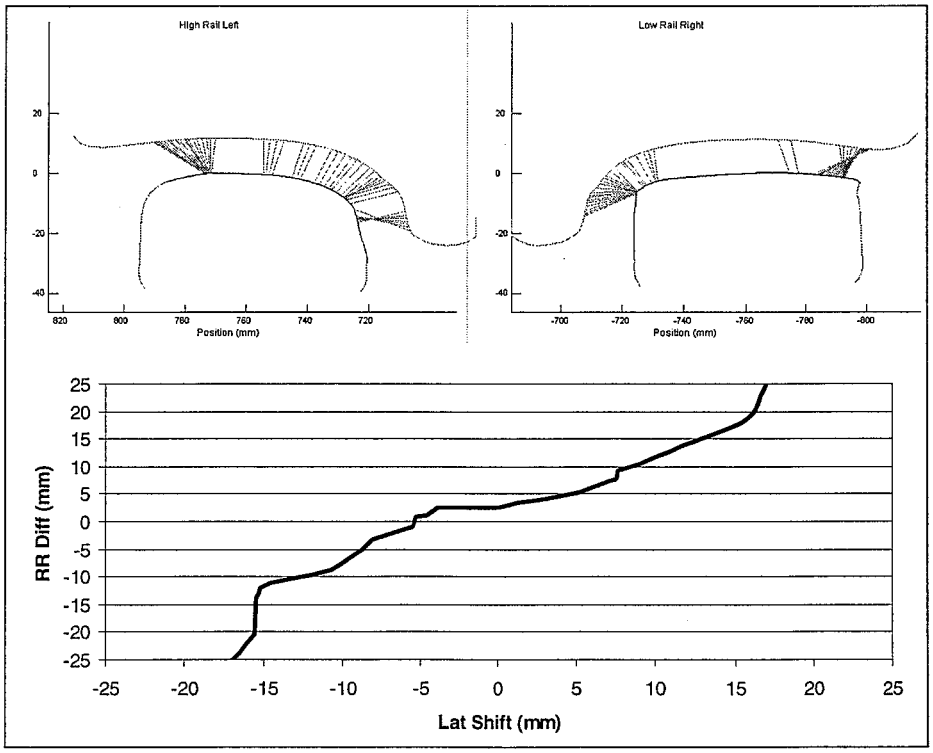

Figure 11. Contact of a Hollow-Worn Wheel with Minimal Flange Wear on a Curve Worn Rail at a Gage of 57.0 inches. (3-6#22_44-154_570.WNT)

2.2 Empty High-Speed Stability Modeling

The objective of these simulations was to determine the onset speed of hunting. An empty bulkhead flatcar and an empty RCV were modeled using the NUCARS vehicle dynamic modeling software. The track geometry input data was taken from TTC's Transit Test Track. Simulations were performed at speeds ranging from 20 mph to 70 mph for the bulkhead flatcar and 20 mph to 90 mph for the RCV. As described in Section 2.1, the wheel-rail geometries simulated represented five distinct shapes of the RRD graph.

The onset speed of hunting was defined in three separate ways:

- When the standard deviation of car body acceleration over 2000 feet exceeds 0.13 g. Termed car body hunting in the data tables.
- When the standard deviation of axle acceleration (over the whole run) exceeds 0.13 g. Termed axle hunting in the data tables.
- When the axle displacement is seen to cyclically shift from flange contact on one rail to flange contact on the other rail for more than 50 percent of the run. Termed flange-to-flange oscillations in the data tables.

In most cases, the onset speed was consistent between the three definitions (any deviations are discussed later in the appropriate sections).

2.3 Loaded High-Speed Stability Modeling

The objective of these simulations was to determine if hollow-worn wheels could induce hunting in loaded cars. (Hunting is normally an empty car phenomenon.) The loaded high-speed stability modeling was performed in the same manner as the empty modeling, except that axle sum lateral/vertical force (L/V) ratios, truck side L/V ratios, and rail rollover moments were calculated for each run. Axle sum and truck side L/V ratios were compared to the limits found in M-1001, Chapter XI of the AAR *Manual of Standards and Recommended Practices.*

Rail rollover moments are not normally found in vehicle performance criteria so a simple method to evaluate the moments was adopted. Figure 12 shows a typical rail with a set of forces input from a wheel. A case with two-point contact is shown. The tangential and normal forces are resolved into the vertical and lateral forces. The moments produced by these forces are summed about the field corner of the rail, point O in the figure. Positive moments tend to roll the rail

inward of point O while negative moments tend to roll the rail outward of point O. The two moments produced by wheels on the same side of a truck are summed. Any truck side moment less than zero is assumed to be likely to cause rail rollover. This is a very conservative limit for rail roll moments as it neglects the effect of the rail restraint system.

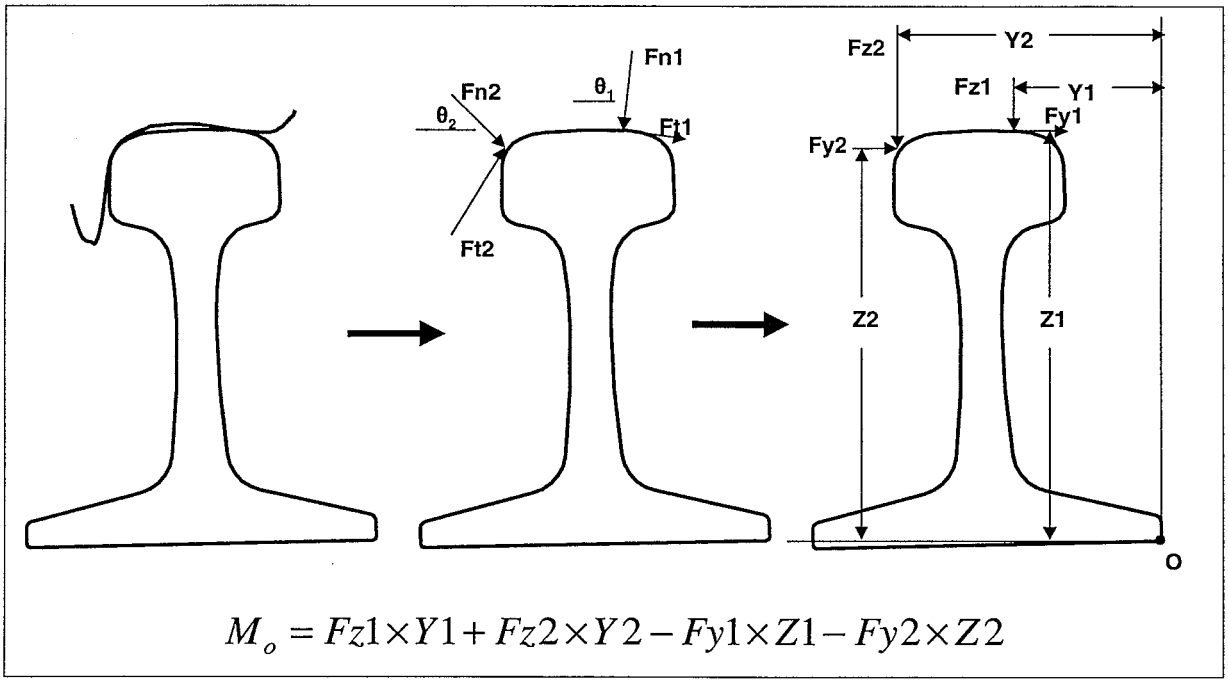

$$M_o = Fz1 \times Y1 + Fz2 \times Y2 - Fy1 \times Z1 - Fy2 \times Z2$$

Figure 12. Diagram Showing Method of Calculating Rail Roll Moments

2.4 Loaded Curving Modeling

The objective of these simulations was to determine the likely effect of hollow-worn wheels on the risk of derailment from rail rollover. Simulations of the loaded bulkhead flat car and the loaded RCV were performed for two 4-degree curves (right hand and left hand). The spirals and constant curve sections were 300 feet long. Three speeds were chosen corresponding to balance running, 3-inch underbalance and 3-inch overbalance. Data is presented in the form of wheel, axle sum, and truck side L/V and rail rollover moments.

3.0 MODELING VALIDATION TESTS

The objective of this phase of work was to demonstrate that the NUCARS software is capable of modeling hollow wheel/rail interaction with reasonable accuracy. A bulkhead flatcar was selected for this exercise. After vehicle characterization, the car was instrumented and tested at a range of speeds on the TTT. The vehicle was also modeled using the NUCARS software. Results from NUCARS were then compared with the test results.

We must stress that NUCARS modeling results cannot be compared directly to measured results from actual vehicles unless the test conditions are closely monitored and all characteristics carefully modeled in the NUCARS simulation. Although NUCARS and similar simulation models are made to be as close as possible a representation of the real vehicles, they should, in general, be used only as a comparison tool against other simulation modeling results. Factors such as rail and wheel profiles, track roughness, and ballast structure can result in significant differences between the simulation models and test conditions. However, similar changes should produce similar results, and as such, NUCARS can be used as a very effective tool to investigate potential directions of change or areas of improvements.

3.1 Vehicle Description

A bulkhead flatcar, TTPX 81550, was selected for the testing phase of the project. The car is owned by TTX Company and used by them as a standard test vehicle.*

The car has a 60-foot 8-inch deck, is 48-feet over truck centers, and is 68-feet over strikers. It is equipped with ASF ride control trucks with eight D5 inner coils and eight D5 outer coils. Roller side bearings were installed in the car for this test. The light weight of the car is 81,200 pounds. The load limit is 181,800 pounds.

* TTCI is grateful for permission from TTX for the use of this car in part of the research program.

3.2 Vehicle Characterization Test

A characterization test is required to determine the mass moments of inertia of the test vehicle, which are required inputs for NUCARS system files. The test procedure consists of:

- Removing the damping (friction wedges in this case) from the suspension
- Shimming out the side bearing clearance so the suspension can be approximated as a linear system
- Applying instrumentation to measure the motions of the vehicle
- Exciting resonance for the five rigid body modes of vibration:
  - Bounce
  - Pitch
  - Yaw
  - Lower Center Roll
  - Upper Center Roll
- Calculating the mass moments of inertia for the car body using the mass of the body and the frequencies of the five modes of vibration

This characterization test was done just before the track test so that the same instrumentation setup could be used. The vehicle was excited by lifting one side or end of the car with a forklift and then sliding the fork out from under the car body. This method was repeated at different points on the car until data was available for all five modes of vibration.

3.3 Warp Stiffness Test

One of the trucks from the test car was removed and placed under a flatcar modified for warp stiffness characterization tests. In this test, the center plate of the car sits on a thrust bearing that is placed in the center bowl to eliminate the turning resistance between the car body and truck bolster. Axles with independently rotating wheels are installed in the truck to eliminate the turning resistance between the truck and the track. Displacement transducers are mounted between the bolster and side frames to measure the warp angle. Two hydraulic cylinders are mounted longitudinally, each attached at one end to a truck side frame and at the other end to the car body. The hydraulic cylinders are then cycled out of phase with each other to warp the truck.

The longitudinal loads of each hydraulic cylinder and the warp angle between the side frame and truck bolster are measured. Figure 13 is a picture of the truck with the hydraulic cylinder

attached. Visible in this photo are the independently rotating wheels, the displacement transducers for measuring warp angle, the end of the hydraulic cylinder, and the load cell.

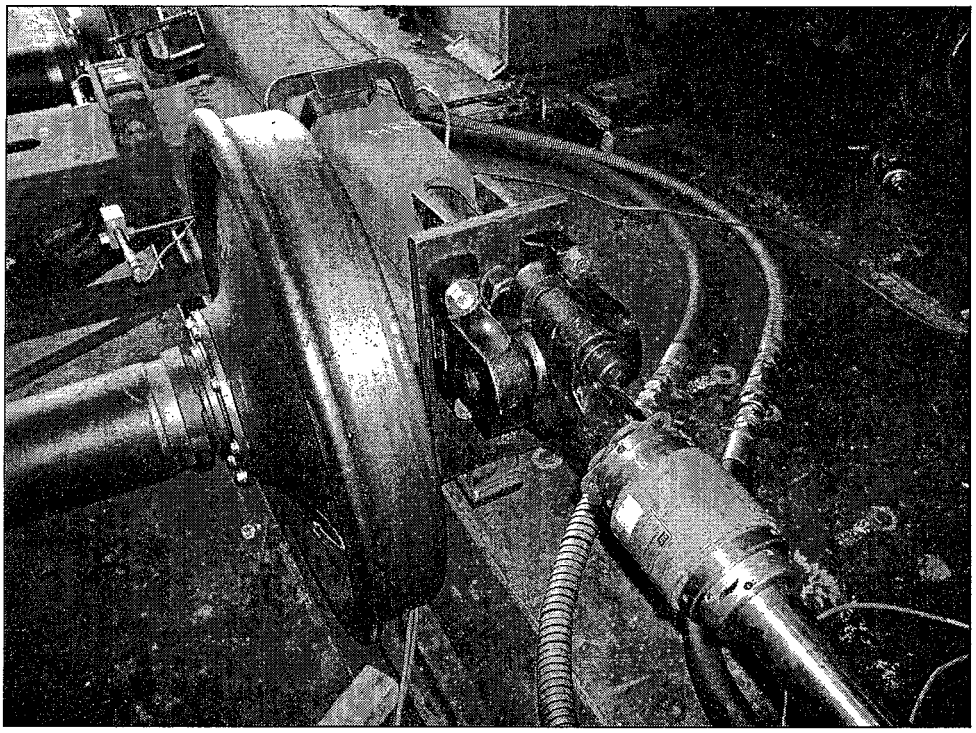

Figure 13. Photo Showing the Warp Test Setup with the Car Body Removed

3.4 Truck Rotation Test

The truck rotation test is performed to measure the friction moment between the car body and truck bolster. It is conducted by placing one truck of the vehicle on an air bearing table, and jacking the other end of the car so that the car body is level. The truck on the air table is then rotated by means of two hydraulic cylinders connected to the air table through load cells. The rotation of the bolster is measured by a longitudinal string potentiometer mounted to measure the fore-aft movement of the edge of the bolster as it yaws relative to the car body.

3.5 Track Test

The track test was performed with the bulkhead flatcar TTPX 81550. The car was the last car in a train consisting of a locomotive, an instrumentation coach, and the test car. Tests were performed according to M-1001, Chapter XI of the AAR *Manual of Standards and Recommended Practices.*

Data was low-pass filtered at 15 Hz and digitized at 200 samples per second. The following instrumentation was used for the track test (some of the channels were added specifically for the characterization test described in Section 3.2).

- Lateral and vertical accelerometers on the deck above each truck bolster
- Lateral accelerometers mounted on the top of each bulkhead
- Lateral accelerometers on the left bearing adapter of each axle
- String potentiometers between the truck bolster and side frames to measure the lateral suspension displacement and truck warp
- String potentiometers between the car body and bolster of each truck to measure truck rotation

The "new" wheelsets used for the test had recently turned wheels (less than 5,000 miles) with AAR1B narrow flange profiles. The worn wheelsets selected were from revenue service and included wheels with moderate hollow wear. Table 2 lists the details of the wear of these worn wheelsets as installed for the first series of worn-wheel tests. These tests are termed Configuration 1. Table 2 shows that the wheelsets in Configuration 1 are diagonally worn within a truck; e.g., the L1 and R2 wheels are hollow, whereas the R1 and L2 are not. To test whether the way the wheelsets are installed influences the stability, tests were done using a second wheelset configuration. In Configuration 2, the first and fourth axles were turned round to give the configuration shown in Table 3 where each truck has hollow-worn wheels only on one side.

Table 2: Details of Worn Wheelsets in Configuration 1

Axle No.	Wheel ID	Hollow Wear, mm	Flange Wear, mm*
1	L1	1.9	26.6
	R1	No hollow	34.0
2	L2	No hollow	34.3
	R2	2.6	26.8
3	L3	1.3	30.5
	R3	No hollow	32.6
4	L4	No hollow	30.6
	R4	1.0	29.6

* Measured 15.87 mm (5/8 inch) up from a point on the tread 77.8 mm (3 1/16 inch) from the back face of the wheel.

Table 3: Details of Worn Wheelsets in Configuration 2

Axle No.	Wheel ID	Hollow wear, mm	Flange wear, mm*
1	L1	No hollow	34.0
	R1	1.9	26.6
2	L2	No hollow	34.3
	R2	2.6	26.8
3	L3	1.3	30.5
	R3	No hollow	32.6
4	L4	1.0	29.6
	R4	No hollow	30.6

* Measured 15.87 mm (5/8 inch) up from a point on the tread 77.8 mm (3 1/16 inch) from the back face of the wheel.

Tests were run in the counterclockwise direction on the TTT. Data was recorded from T40 to T12 for all test runs. Data presented in this report is from section T18 to T12. This section has welded rail and wood ties and at the time of writing is TTC's standard high-speed stability test section for freight cars. There is a switch in the first 500 feet of the zone. Rail friction was measured to confirm the coefficient of friction was greater that 0.4 for all tests.

The lowest test speed for each wheel profile configuration was 30 mph. The test speed was increased on each subsequent run until car body accelerations exceeded Chapter XI limits.

4.0 RESULTS

4.1 Empty High-Speed Stability Simulations

Table 4 lists the results for simulations of an empty bulkhead flatcar. Appendix A contains typical graphs showing the car-body lateral accelerations and lead axle lateral displacements.

Table 4: Empty Bulkhead Flatcar Simulation Results

	Speed at Onset of Hunting		
Wheelset	**Car Body Hunting**	**Axle Hunting**	**Flange-to-Flange Oscillations**
New AAR 1B NF on new AREMA 136-RE rail	65 mph	60 mph	55 mph
Moderately Worn AAR 1B WF on new AREMA 136-RE rail	50 mph	50 mph	50 mph
Hollow wheel with mismatched wheel diameters on tangent worn rail	>70 mph	70 mph	Hugs one rail at 70 mph
Hollow wheel with flange wear on tangent worn rail	>65 mph – simulation does not complete at 70 mph	60 mph	Hugs one rail but can swap to the other rail at 65 mph
Hollow wheel with no flange wear on TTC's TTT rail	>70 mph	55 mph	Hugs one rail at 70 mph

The results show that the bulkhead flat hunts at 50 mph with the moderately worn wide flange wheel and at 65 mph with the new wheel. The hollow-worn wheels hug one rail or the other and do not have flange-to-flange oscillations in the speed range simulated.

The results for simulations of an empty RCV are shown in Table 5. Appendix B contains typical graphs showing the car-body lateral accelerations and lead axle lateral displacements.

Table 5: Empty RCV Results

	Speed at Onset of Hunting		
Wheelset	**Car Body Hunting**	**Axle Hunting**	**Flange-to-Flange oscillations**
New AAR 1B NF on new AREMA 136-RE rail	>90 mph	70 mph	50 mph
Moderately Worn AAR 1B WF on new AREMA 136-RE rail	>90 mph	55 mph	50 mph
Hollow wheel with mismatched wheel diameters on tangent worn rail	>90 mph	70 mph	Hugs one rail at 90 mph
Hollow wheel with flange wear on tangent work rail	>90 mph	65 mph	Hugs the rail but can swap at 90 mph
Hollow wheel with no flange wear on TTC's TTT rail	>90 mph	75 mph	Hugs one rail at 90 mph

These RCV results show a unique feature of that vehicle. Although the axles show flange-to-flange oscillations at relatively low speeds with the new and moderately worn wheels, the car body remains stable up to 90 mph. The hollow-worn wheels followed the same pattern as with the bulkhead flatcar. As the axle follows one rail or the other, the axle acceleration increases with speed so that the criteria for the onset of axle hunting occurs between 65 and 75 mph.

4.2 Loaded High-Speed Stability Simulations

Table 6 lists the results from simulations of a loaded bulkhead flatcar. Appendix C contains typical graphs showing the car-body lateral accelerations and lead axle lateral displacements.

Table 6: Loaded Bulkhead Flatcar Results

	Speed At Onset of Hunting			Maximum Truck-side L/V	Minimum Rail Roll Moment (in-kips)*
Wheelset	**Car Body Hunting**	**Axle Hunting**	**Flange-to-Flange Oscillations**		
New AAR 1B NF on new AREMA 136-RE rail	70	70	65	0.29	14
Moderately Worn AAR 1B WF on new AREMA 136-RE rail	55, accelerations fall at >55	55, acceleration s fall at >55	55, accelerations fall at >55	0.16	73
Hollow wheel with mismatched wheel diameters on tangent worn rail	>70	>70	Hugs one rail	0.24	169
Hollow wheel with flange wear on tangent worn rail	>70	65	Hugs one rail, can switch sides	0.36	-118
Hollow wheel with no flange wear on TTC's TTT rail	>70	>70	Hugs one rail	0.27	158

* Low rail roll moments are associated with increased rail rollover risk.

The loaded bulkhead flatcar results show that hunting was only noticeable with the moderately worn AAR1B wide flange wheel. This profile shows data consistent with the onset of hunting at 55 mph but then accelerations fall below the onset level at 65 and 70 mph. The hollow worn wheel with flange wear shows the highest truck side L/V and the lowest rail rollover moment.

Table 7 lists the results for simulations of a loaded RCV. Appendix D contains typical graphs of the car-body lateral accelerations and lead axle lateral displacements.

Table 7: Loaded RCV Results

Wheelset	Speed At Onset of Hunting			Maximum Truck-side L/V	Minimum Rail Roll Moment (in-kips)*
	Car Body Hunting	Axle Hunting	Flange-to-Flange Oscillations		
New AAR 1B NF on new AREMA 136-RE rail	90	75	60	0.21	41
Moderately Worn AAR 1B WF on new AREMA 136-RE rail	65	60	55	0.24	33
Hollow wheel with mismatched wheel diameters on tangent worn rail	>90	75	Hugs one rail	0.17	44
Hollow wheel with flange wear on tangent work rail	>90	75	Hugs one rail, can switch sides	0.20	42
Hollow wheel with no flange wear on TTC's TTT rail	>90	75	Hugs one rail	0.37	61

* Low rail roll moments are associated with increased rail rollover risk.

The loaded RCV model shows the same type of behavior seen in the empty RCV model. Flange-to-flange oscillations are seen at 60 and 55 mph with the new and moderately worn wheels, respectively. The car body remains stable with the new wheel but exceed the onset criteria at 65 mph with the moderately worn wheel.

The highest truck side L/V ratio occurred on the hollow wheel with very little flange wear, but it did not exceed the Chapter XI criteria of 0.6. The lowest rail rollover moment occurred on the moderately worn wheel, but it would not tend to roll the rail outward of the field corner. Rail rollover moments for the RCV should not be directly compared to the bulkhead flat moments since they are not normalized for wheel loads. Wheel loads on the bulkhead flat are about 2.5 times greater than the RCV, so it is expected that the bulkhead flat would have higher moments than the RCV.

4.3 Curving Simulations

Table 8 shows the results for simulations of a loaded bulkhead flat car.

Table 8: Loaded Bulkhead Flat Car Results

Wheelset	Maximum Wheel L/V	Maximum Axle Sum L/V	Maximum Truck-side L/V	Minimum Rail Roll Moment (in-kips)*
New AAR 1B NF on new AREMA 136-RE rail	0.37	0.68	0.17	209
Moderately Worn AAR 1B WF on new AREMA 136-RE rail	0.41	0.69	0.18	196
Hollow wheel with mismatched wheel diameters on tangent worn rail	0.68	1.12	0.45	98
Hollow wheel with flange wear on tangent work rail	0.64	1.05	0.44	115
Hollow wheel with no flange wear on TTC's TTT rail	0.32	0.60	0.16	131

* Low rail roll moments are associated with increased rail rollover risk.

The loaded bulkhead flatcar curving simulations show that the hollow-worn wheels tend to produce the highest single wheel, axle sum, and truck side L/V ratios although none of the values exceed Chapter XI criteria. The hollow-worn wheels also produced lower rail rollover moments although all wheels tended to produce roll to the inside of the outside rail corner.

Table 9 lists the results for simulations of a loaded RCV.

Table 9: Loaded RCV Results

Wheelset	Maximum Wheel L/V	Maximum Axle Sum L/V	Maximum Truck-side L/V	Minimum Rail Roll Moment (in-kips)*
New AAR 1B NF on new AREMA 136-RE rail	0.40	0.74	0.17	77
Moderately Worn AAR 1B WF on new AREMA 136-RE rail	0.39	0.56	0.13	68
Hollow wheel with mismatched wheel diameters on tangent worn rail	0.84	1.26	0.31	47
Hollow wheel with flange wear on tangent work rail	0.78	1.18	0.29	48
Hollow wheel with no flange wear on TTC's TTT rail	0.38	0.65	0.18	47

* Low rail roll moments are associated with increased rail rollover risk.

Loaded RCV simulations showed the same trends as the loaded bulkhead flatcar. Hollow-worn wheels produced higher single wheel, axle sum, and truck-side L/V ratios, and lower rail roll moments, although none exceeded the established criteria.

4.4 Empty Bulkhead Flat Test Results

4.4.1 Vehicle Characterization Test

The characterization test was performed as described in Section 3.2. Results from this type of test are used to calculate the mass moments of inertia of the body. The natural frequencies for the rigid body modes of vibration were measured and are shown in Table 10. The test data is compared to results from an eigenvalue model of the vehicle. There is good agreement between the test and model results.

Table 10: Characterization Test Results

	Natural Frequencies of Rigid Body Mode	
Rigid Body Mode of Vibration	Characterization Test	Eigenvalue Solution for Linearized NUCARS Model
Bounce	3.75 Hz	3.75 Hz
Yaw	2.23 Hz	2.43 Hz
Pitch	3.80 Hz	3.80 Hz
Upper center roll	3.07 Hz	3.20 Hz
Lower center roll	1.78 Hz	1.71 Hz

The car body inertias used to obtain these results in the eigenvalue model and in the empty bulkhead flat car modeling are:

- Roll: 570,000 lb-s^2/in
- Pitch: 13,800,000 lb-s^2/in
- Yaw: 13,650,000 lb-s^2/in
- Center of gravity height of car body: 58 inches

4.4.2 Warp Stiffness Test

The warp stiffness test was performed as described in Section 3.3. Results of the tests without and with friction wedges are shown in Figures 14 and 15 respectively. A linear regression was performed on the data between ±5mrad for the data without wedges and ±3mrad for the data with wedges. The resulting lines are shown on the plots. The stiffness shown is the average of the slopes and the warp friction moment is one-half the difference between the y intercepts of the lines.

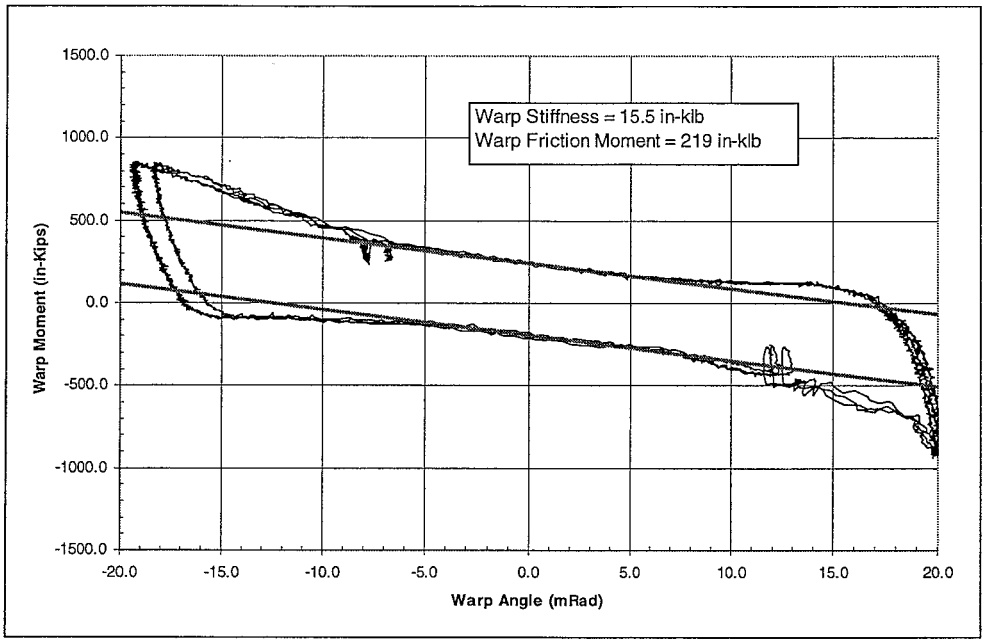

Figure 14: Empty Car Warp Test without Friction Wedges

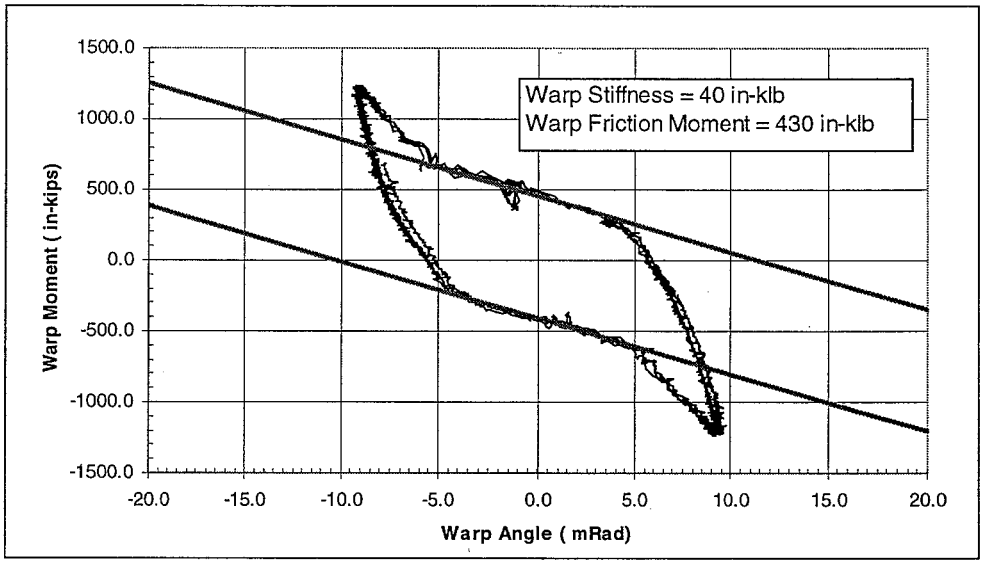

Figure 15: Empty Car Warp Test with Friction Wedges

NUCARS validation simulations were initially performed using the warp stiffness from the test with friction wedges installed. In this condition, the model did not hunt. A series of simulations was then undertaken to find what warp stiffness produced a critical speed similar to that found in the high-speed stability test.

4.4.3 Truck Rotation Test

The center-plate friction test was performed as described in Section 3.4. The car was tested in the empty condition. Figure 16 shows the results from the test.

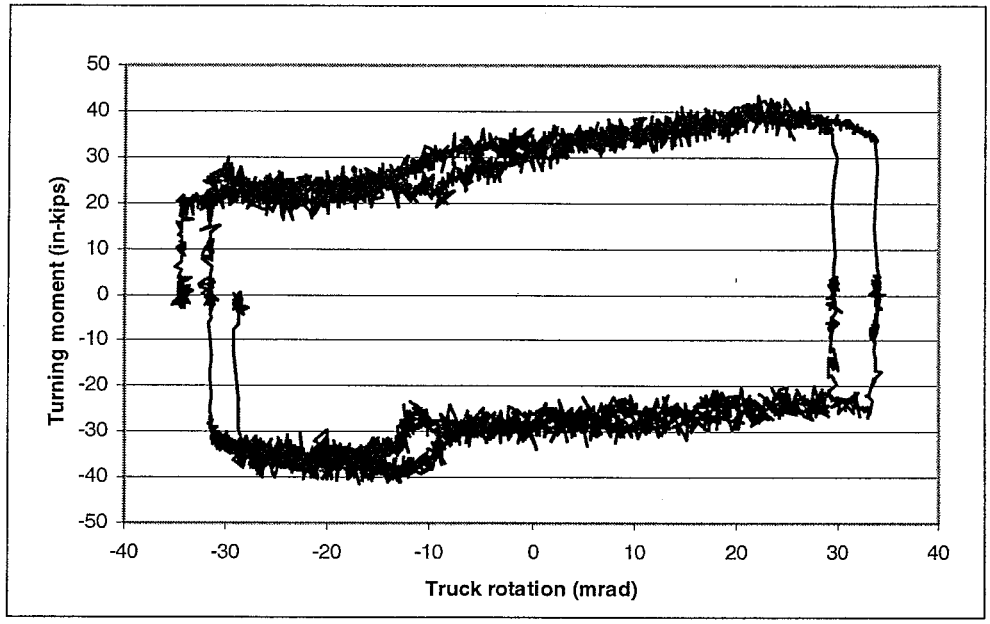

Figure 16: Results of the Truck Rotation Test on TTPX 81550

The NUCARS system file used to model the bulkhead flat approximates a center plate with four line-friction elements located 8 inches from the center of the bolster. To match the NUCARS model with the turning moment seen in the truck rotation test, the following equation was used.

$$\frac{W_{CarBody}}{2} R_{CenterPlate} \mu = M \qquad (1)$$

The car body weight is 81,200 lbs – 9,700 lbs/truck * 2 trucks = 61,800 lbs.

The radius of the center plate is 8 inches.

The turning moment from Figure 16 is about 30,000 in-lbs.

This gives a NUCARS model coefficient of friction of $\mu = 0.12$.

In practice, the vehicle weight is not supported solely on the edges of the center plate, but is distributed more evenly over the plate. Therefore, the actual coefficient of friction in the center plate is likely to be higher than the calculated value for use in the NUCARS model. That is, considering equation 1, the effective value of R is less than 8 inches, leading to an increase in μ.

4.4.4 High-Speed Tangent Track Stability Test Results

The high-speed stability tests were performed on September 19, 2001, with AAR1B wheels and September 21, 2001, with hollow-worn wheels in Configuration 1 and Configuration 2 (refer to Tables 2 and 3). Figure 17 is a plot of the maximum standard deviation of car-body lateral acceleration over 2000 feet of track. It shows the following results:

- With AAR1B wheels, the vehicle shows a rapid increase in lateral acceleration at about 50-55 mph.
- Rapid increase in acceleration is also seen with the worn wheels installed, but the critical speed has fallen to 45-50 mph. In addition, the worn wheels show a higher standard deviation of acceleration than the AAR1B wheels at speeds below 50 mph.
- Accelerations for the worn wheels at 50 mph are similar to those from the AAR1B wheels at 60 mph.
- Configuration 1 (diagonally hollow-worn wheels in a truck) worn wheel results are very similar to the Configuration 2 (in-line hollow-worn wheels in a truck) worn wheel results. At least for the hollow-worn wheels used in this study, their distribution appears to have little effect on lateral acceleration.

The corresponding results from the NUCARS simulations are shown in Figure 18. Comparing the NUCARS and test results:

- The NUCARS results for the AAR1B wheels are similar in form to the test results, though two differences are apparent. First, the NUCARS simulations show a rapid increase in acceleration at speeds of 45-50 mph (50-55 mph in the test results). Second, the maximum accelerations predicted by NUCARS (about 0.25 g) are lower than the maximal found in the tests (about 0.35 g).
- The NUCARS results for the worn wheels appear at first sight to show a difference from the test results, but there are similarities. First, instead of showing a relatively sudden increase in acceleration (45-50 mph in the tests), the NUCARS results appear to show a gradual increase in acceleration from 30 mph upwards. However, like the test results, the worn wheel model results clearly show higher accelerations at low speeds, unlike the AAR1B wheel model results. Second, also like the test results, the worn wheel model results show accelerations similar to the AAR1B wheels at higher speeds.

- As with the test results, the NUCARS simulations indicate that the configuration of the axles in the vehicle has little effect on vehicle stability in tangent track.

In summary, TTCI believes that the agreement between the test and model results is encouraging, and gives confidence that NUCARS simulations can be used to analyze the effect of hollow wheel profiles on vehicle stability.

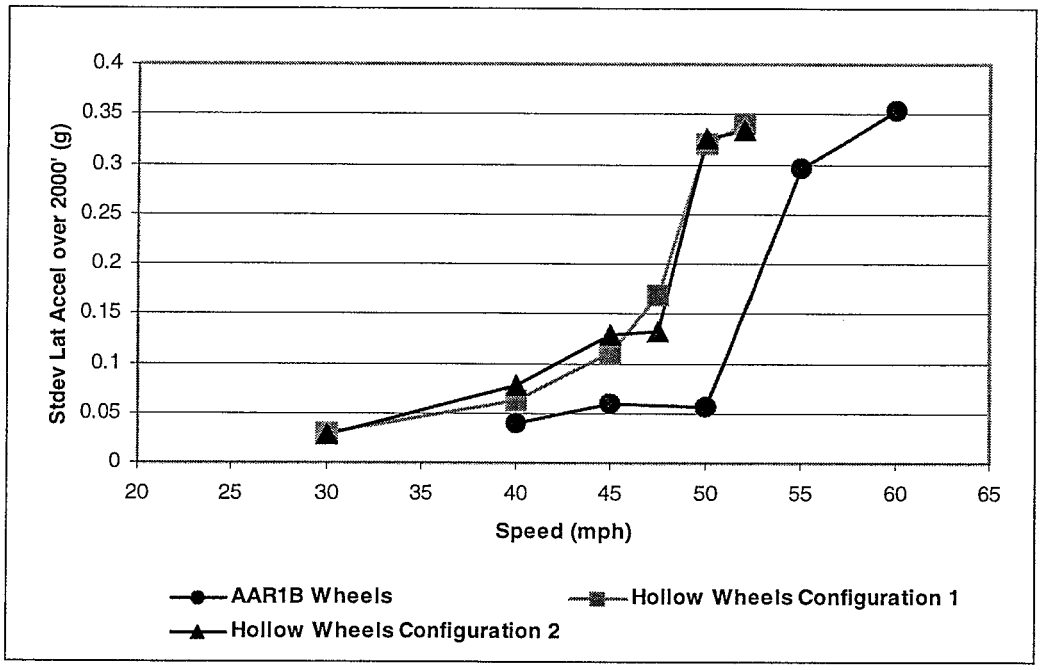

Figure 17. Results of the Track Tests using Vehicle TTPX 81550 with Worn and Hollow-Worn Wheels

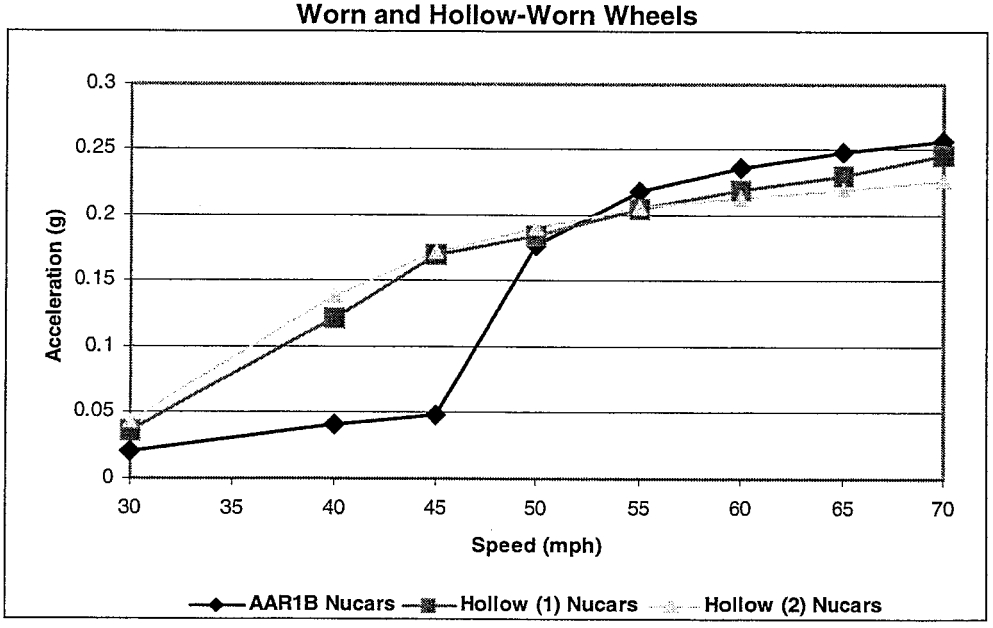

Figure 18. NUCARS Simulations of the Track Tests

5.0 DISCUSSION AND CONCLUSIONS

5.1 Vehicle Stability in Tangent Track

Both the modeling and the tests indicate that hollow wear decreases the speed at which vehicle hunting* is likely to start, and increases the standard deviation of lateral car body acceleration at speeds below the onset of hunting. However, the loaded tangent track simulations do not indicate that hollow-worn wheels necessarily lead to high L/V forces (refer to Tables 6 and 7).

A more detailed analysis of the NUCARS output indicates that the vehicle instabilities produced by hollow-worn wheels may be different from those produced by non-hollow-worn wheels (see Figures 19 and 20).

Figure 19 shows output for new wheels on new rails. The graph shows the position of the left- and right-hand rails and the lateral position of the lead axle at speeds of 30 mph (black line) and 70 mph (red line), as a function of distance along the tangent track. At 30 mph, the axle wanders around the track centerline. At 70 mph (above the onset speed for hunting), the axle moves from flange contact to flange contact with a well-defined sinusoidal pattern. This is the classic form of hunting and is promoted by the type of RRD graph shown in Figure 4.

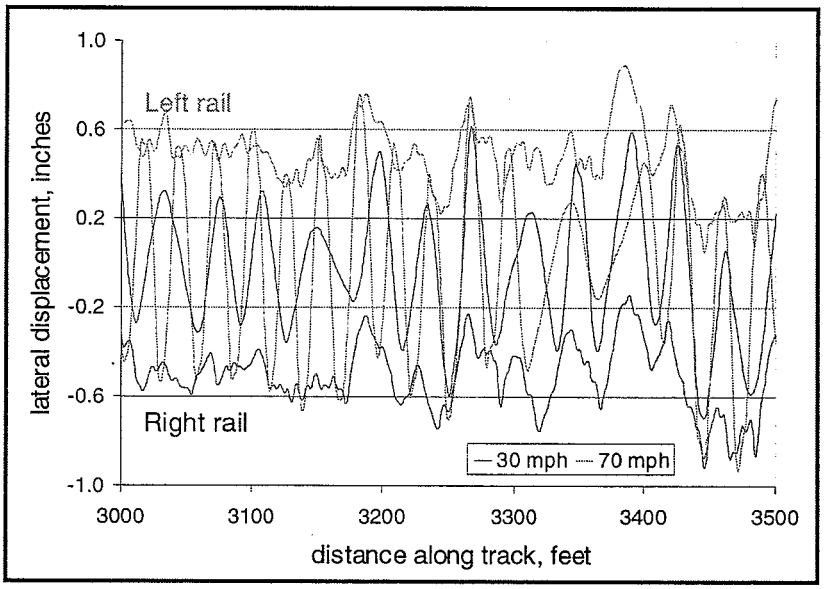

Figure 19: Example NUCARS Output for New Wheels on New Rail

* A sudden increase in standard deviation of lateral car body acceleration.

In contrast, Figure 20 shows the same type of output for a vehicle with 3-mm hollow-worn wheels. Classic hunting is not seen. Rather, at both speeds the wheelset tends to move to the left or right rail, and then runs against the rail until lateral impact from the laterally rough track causes it to move to the other rail. While it is running against the rail, the axle tends to oscillate in yaw, producing the lateral accelerations shown in Figures 17 and 18. In a sense, this oscillation against a rail is a form of hunting, but it is rather different from classical hunting. It is promoted by the type of RRD graph shown in Figure 7.

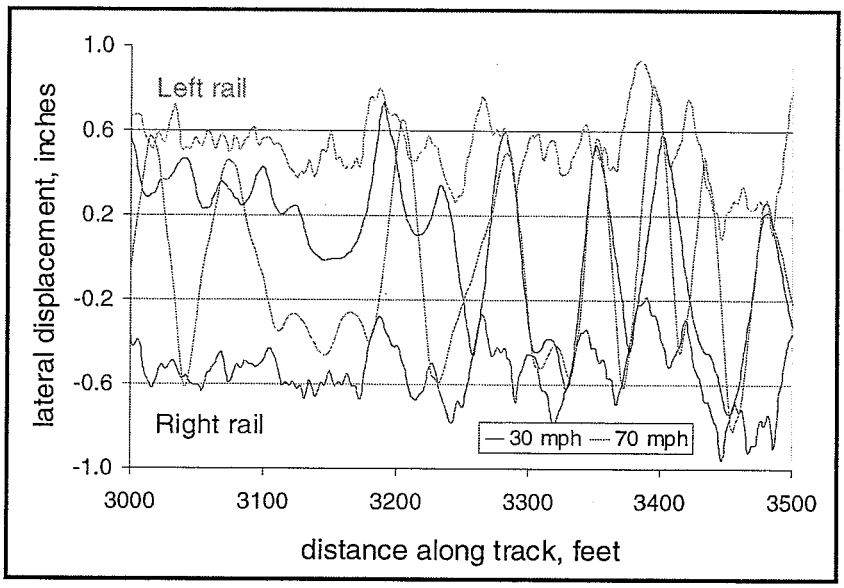

Figure 20: Example NUCARS Output for Hollow-Worn Wheels on New Rail

Results from this project, and the associated AAR SRI project, imply that vehicle stability depends critically on the interaction between wheel and rail geometries. The geometry parameters that influence interaction include:

- Detailed transverse wheel profiles, not just the degree of hollow wear.
- Detailed transverse rail profiles, though these likely have a lesser effect than the wheel profiles.
- Diameter difference at the tread between the two wheels on the axle. This has a major effect on the way the axle runs along the rail.
- The amount of flange wear on the wheelset, which influences the flangeway clearance.
- The amount of gage face wear on the rails, and the track gage, both of which influence flangeway clearance.

The way these geometry parameters interact to influence stability can be considered using the RRD graph examples shown in Figure 21 and discussion that follows.

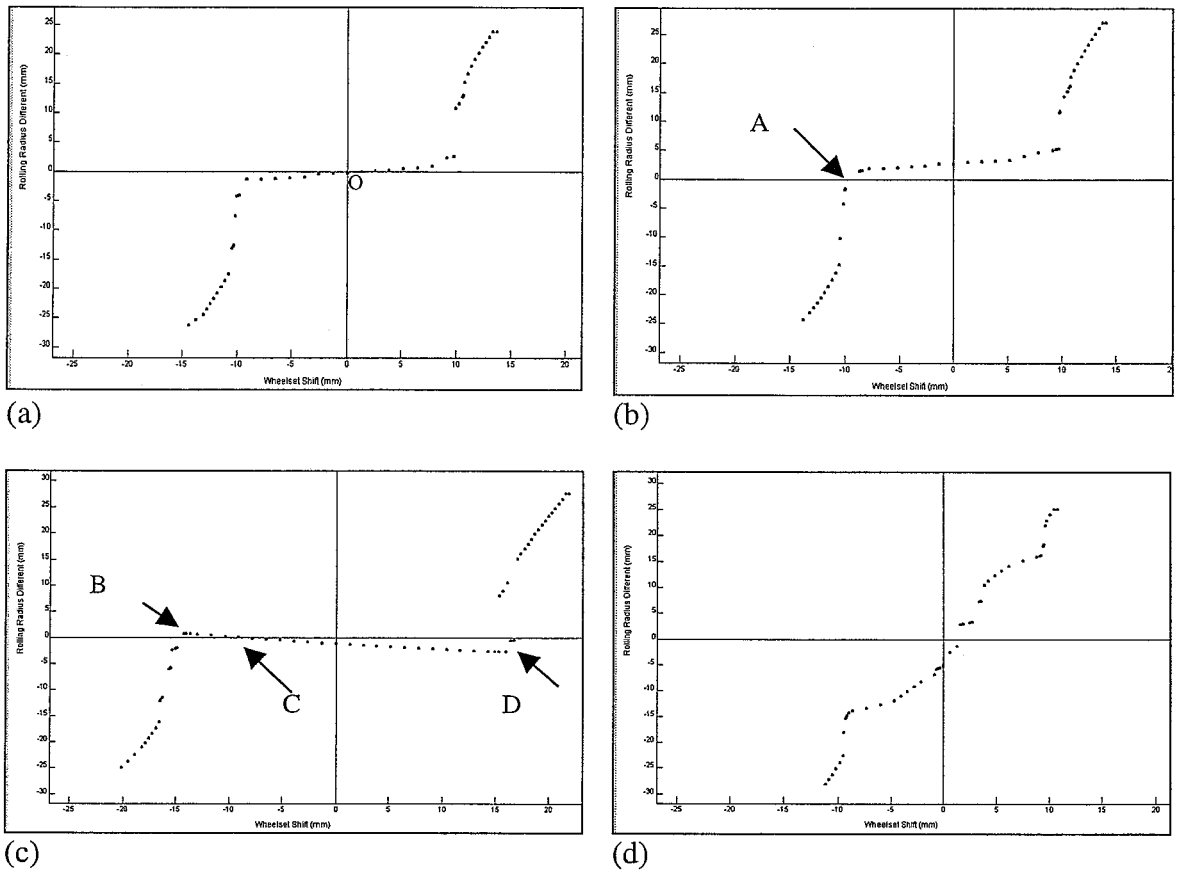

Figure 21: Examples of RRD graphs. Y-axis shows Rolling Radius Difference (right wheel minus left wheel). X-axis shows Wheelset Lateral Shift

Classical hunting: Classical hunting can occur when the RRD graph looks like that in Figure 21a. This graph, typical of new wheels on new rails, is centered around the origin (O) and has a positive slope. In this common graph, when the wheelset is perturbed and shifts to the right, the right wheel radius increases and causes the wheelset to steer back towards the track center, which it overshoots. This sets up a lateral oscillation about the track centerline. For a wheelset constrained in the vehicle, these oscillations are expected to decay at low speeds. However, as the speed is increased, the decay rate falls until, at a specific speed, the damping goes to zero and lateral movement is constrained only by contact of the wheel flanges on the rails. This is termed hunting (refer to Figure 19).

For a given vehicle/bogie, the speed at which hunting starts depends on the effective conicity (C_E), which is defined as one-half the slope of the center part of the RRD graph. Analysis of a single wheelset restrained by springs to a frame indicates that the critical speed at which the damping becomes zero is inversely proportional to the square root of the effective conicity. [2] Hence, the speed at which hunting starts is expected to fall as the slope of the RRD graph rises. To test this prediction for freight trucks, TTCI has undertaken hunting simulations of an empty coal hopper running on tangent track with different wheel/rail combinations. The results, shown in Figure 22, confirm that hunting speed falls as effective conicity increases.

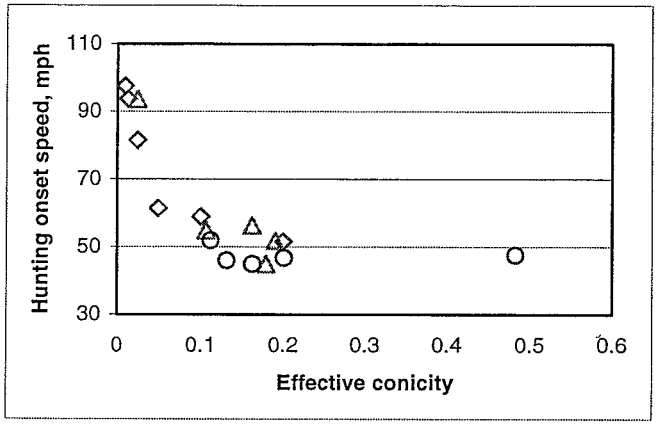

Figure 22: NUCARS Simulations of the Effect of Effective Conicity on Hunting Onset Speed

Offset running: RRD graph 21b is similar to that in 21a, but is offset vertically because of a small difference in wheel tread radii. The wheel radii are now equal at point A, which is at a negative (left) lateral shift of 10 mm. Hence, with this sort of RRD graph, the wheelset will run offset towards one rail, close to flange contact. At point A, the local conicity is very high, and this is likely to cause the wheelset to oscillate in yaw against the rail. Point A is the only stable point on this graph, and thus the wheelset will rarely move (if ever) into flange contact on the other rail.

Offset running with "rebound": RRD graph 21c shows a negative central slope, typical of a wheelset with hollow-worn wheels and some degree of flange wear (or increased flangeway clearance). This wheelset has three lateral shift positions that give equal wheel radii (points B, C and D). Points B and D are stable, but point C is unstable in that any perturbation from C will cause the wheelset to approach B and D. This wheelset will therefore move to flange contact with one rail, but will "rebound" to the other rail given sufficient lateral force from a lateral track irregularity. (To cause "rebound" the force must be sufficient to move the wheelset past point C.) This is the type of behavior seen in Figure 20. As with normal offset running, the local conicity at points B and D is high, causing the wheelset to oscillate in yaw against the rail.

Abnormal high effective conicity: RRD graph 21d shows an abnormally high effective conicity. It can occur when the wheelset has hollow-worn wheels, but when the flangeway clearance is small. This can occur if flange wear is minimal, the track gage is tight, or the back-to-back spacing is small. It tends to be associated with wheel/rail contact like that Figure 8 shows, where contact is concentrated on the gage corner of both rails. This high conicity can lead to hunting at reduced speeds, but, if large enough, it can cause the wheelsets to stay at the track centerline with little lateral deviation. (To some extent the RRD slope can be thought of as a spring whose strength is proportional to the slope. Positive slopes pull the wheelset back to the

centerline. Negative slopes push the wheelset towards the rails. Thus, a very high positive slope passing through the origin can prevent the wheelset from deviating laterally from the track centerline.) Finally, Figures 21c and 21d are both caused by hollow-worn wheels. The difference in the two graphs is principally due to the different amount of flangeway clearance the wheelset sees. The wheelset in 21c shows high flange wear and therefore large flangeway clearance. The wheelset in 21d shows minimal flange wear and thus less flangeway clearance. Figure 21c can be transformed to 21d simply by reducing the flangeway clearance, by tightening track gage. The reverse is also true. Figure 21d can be transformed to 21c by decreasing track gage.

As discussed in Section 5.2, it may be possible to estimate wheelset behavior, and therefore to some extent vehicle behavior, by considering the form of the RRD graph. Generating these RRD graphs is straightforward.

5.2 Truck-Side L/V Ratios

The maximum truck-side L/V ratios predicted for loaded vehicles (bulkhead flatcar and RCV) are shown in Tables 6 and 7 for tangent track, and Figures 8 and 9 for curved track. In all cases, for the wheelsets modeled, these maximum L/V ratios are relatively low, varying from 0.16 to 0.37, and unlikely to produce a flange-climb derailment risk. It should be noted, however, that the wheelsets modeled did not have severely hollow-worn wheels (the most hollow wheel was only 2.6 mm hollow and had a non-hollow mating wheel). It is possible that wheels with more severe hollow wear would have given higher L/V ratios. This needs further study.

5.3 Rail Roll Moments

The rail roll moments shown for loaded vehicles are shown in Tables 6 and 7 for tangent track, and Figures 8 and 9 for curved track. These moments are calculated as Figure 12 illustrates, and are the moments produced about the outside corner of the rail by the predicted lateral forces and wheel/rail contact positions. Positive moments tend to roll the rail inwards; negative moments tend to roll the rail outwards. The presence of a negative moment does not imply that rail rollover will occur since the fastening system works to prevent rollover. The support offered by the fastening system will depend critically on the system (spikes, elastic, etc.) and on the integrity of the ties. Hence, no critical value of rail roll moment can be offered in this preliminary study.

However, the rail roll moment negative (-118 inch-kips) is only seen in one case. This occurs for the loaded bulkhead flatcar equipped with hollow-worn wheels with flange wear running in tangent track. This is understandable, since the hollow-worn wheels tend to produce higher lateral forces, and promote offset running (to rail A), and the higher amount of flange wear allows the hollow wheel false flange to contact the field side of the other rail (rail B). Both effects act together to produce a negative rail roll moment. The rail roll moment for the corresponding RCV case is positive, but low, with a value of +42 inch-kips. The RCV, however, gives lower lateral forces, as shown by the difference in the truck-side L/V ratios (0.36 for the bulkhead flat car, 0.20 for the RCV).

5.4 Identifying Inappropriate Wheel Profiles

The ideal wheelset should give the form of RRD graph shown in Figure 21a when matched against the rails over which it passes. This helps ensure that the wheelset runs centrally in tangent track and steers adequately in curves. Since the RRD graph has a small positive slope, it is unlikely to cause hunting at low speeds. The positive slope also implies that the wheels are not significantly hollow — reducing the risk of high rail rollover moments from loaded vehicles in curved track. New wheels with identical diameters on new rail will give the type of graph shown in Figure 21a, but most other wheelset/rail pair combinations will deviate from this ideal behavior. Small deviations from ideal behavior are likely to be acceptable.

This work indicates, however, that certain combinations of wheel/rail profiles can give unwanted vehicle stability and high rail roll moments. Both of these can adversely affect safety. The surest way of identifying inappropriate wheel profiles is through their effect on the RRD graph. Inappropriate profiles will lead to RRD graphs that have one or more of the following attributes:

- A negative central slope. This indicates the presence of hollow-worn wheels and can cause the wheelset to hug the rails. It can also lead to negative rail roll moment – especially when the central slope covers a wide range of lateral wheelset shift (implies large flangeway clearance).

- A vertical displacement. This indicates differential tread wear of the two wheels. It: causes the wheelset to hug one of the rails and can lead to negative rail roll moment.

- An abnormally high central slope. This indicates low flangeway clearance because of tight track gage, high back-to-back spacing, and low flange wear. It may lead to low hunting speed.

At present, with current knowledge, these attributes are still qualitative; more work is needed to provide quantification. However, TTCI believes that the analytical approach adopted in the current study can form the basis for further work.

Software is available to calculate RRD graphs rapidly and efficiently for any combinations of wheelsets and rail pairs. The software developed by TTCI to achieve this is called WRTOL.[3] At present, the software is designed to test a single rail pair against multiple wheelsets, and is capable, for example, of analyzing the interaction between 150 wheelsets and a single rail pair in less than 25 seconds. The software works well with hand-measured profiles, and early indications are that RRD graph calculation can also be achieved using automatically measured digital profiles. The capability exists, therefore, for the automatic assessment of measured wheel profiles given a range of typical rail pair profiles. Many railroads currently use automatic methods to measure rail profiles at speed, and similar systems to measure wheel profiles are currently in trial.

Given the large number of wheelsets in the North American population, RRD graph analysis would need to be computer-based. TTCI believes that simple rules on which computer decisions can be based are readily achievable. These rules might include consideration of the:

- central slope of the RRD graph,
- number of times the RRD graph crosses the X-axis, the lateral shift position at each crossing, and the local slope of the RRD graph at each crossing, and
- lateral shift range between the two-wheel/rail flange contacts.

Some examples illustrate how these calculated parameters can be used.

First, suppose that the central slope is small but positive (e.g., 0.1), and that the single crossing point occurs at a lateral shift of 2 mm. In this case, the RRD graph is similar to that shown in Figure 4 for new wheels on new rails. The wheelset would be expected to perform adequately on the rails used in the calculation.

Second, suppose that the central slope is very close to zero, and that the single crossing is at a lateral shift of –15 mm. This RRD graph is similar to that shown in Figure 6. In this case, the

wheelset will run in tangent track against one of the rails (oscillating in yaw), and will rarely if ever, reach the other rail.

Third, suppose that the central slope is negative and that there are three crossing points (refer to Figure 7). In this case, the wheelset in tangent will rebound randomly between the two rails, oscillating in yaw against each rail.

While the RRD graph may be the best way to judge the effect of wheel and rail profile on vehicle performance, it is possible, at least initially, that the railroad industry will still need to relate wheel profile parameters to performance. TTCI believes this may be possible using the following scheme:

1. Define the wheelset profile parameters of interest. These may include the hollow wear on each wheel, the flange wear on each wheel, and the tapeline radius on each wheel.
2. Define a wheelset database (e.g., the North American database described in reference 1) and a rail pair database. Subsets of the rail pair database may include tangent rails, mild-curve rails, and severe curve rails.
3. For all the wheelsets, generate a graph linking the defined parameters; e.g., axis 1 may be left wheel hollow wear, axis 2 may be right wheel hollow wear and so on.
4. Match each wheelset against the rail pairs in the rail pair database; calculate the RRD graph and the associated parameters.
5. Based on the RRD graph rules, determine whether the wheelset is "good" or "bad," and mark the wheelset accordingly on the graph generated in No. 3 above.
6. Examine the graph for clusters of wheelsets judged to be bad, and determine the wheelset parameters common to the bad wheelsets.
7. Set simply measurable wheel wear limits based on these common parameters.

For example only, Figure 23 illustrates the results of such a process, assuming a simple 2-dimensional wheelset parameter graph (left wheel hollow depth and total flange wear). These parameters are taken from the wheelset database described in reference 1. Two regions of bad wheelset performance are indicated by the colored ovals. The blue oval indicates an area where high effective conicity is likely — the wheel is hollow, but the wheelset has little flange wear.

The gold oval indicates an area where a negative RRD central slope is likely and where high rail roll moments may occur — the wheel is hollow, but the wheelset shows high flange wear.

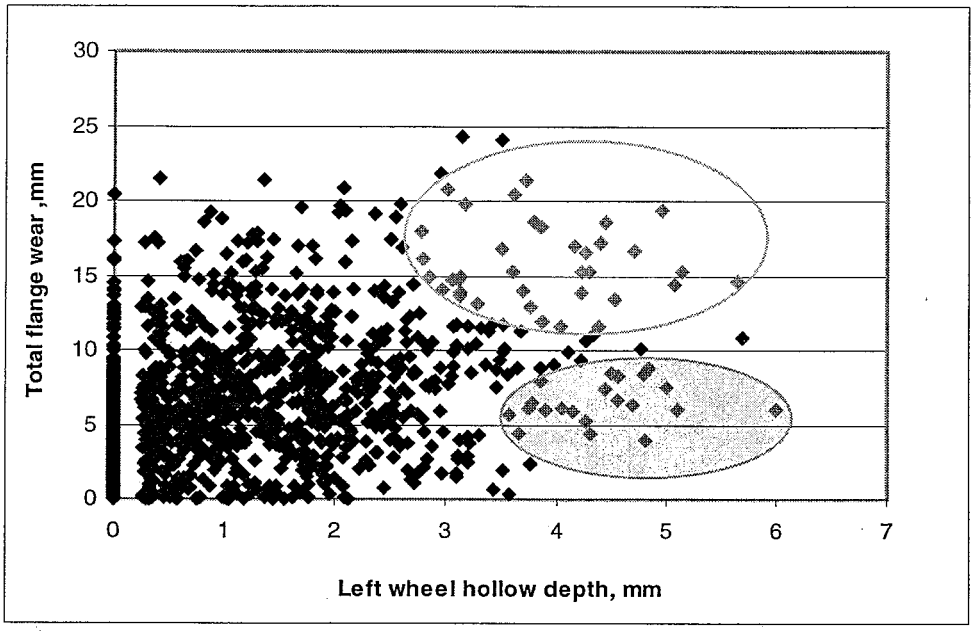

Figure 23: Illustration of Identification of Inappropriate Wheel Profiles

6.0 SUGGESTIONS FOR FURTHER WORK

This study, and the associated AAR SRI project, has led to a much better understanding of the effect of hollow wear on vehicle stability and safety. The studies have also identified areas where knowledge of wheel profiles is deficient, and areas where further work is needed to further improve understanding of the effects of hollow-worn wheels on railroad safety. Hence, below is a list of suggestions for further work.

6.1 Improved Knowledge of Wheel Profiles

- Careful measurements of the diameter of new and worn wheels at the tape line and flange tip are needed to verify if using the flange, as a diameter reference is appropriate. This is important since the relative diameter of the wheels is critical to the makeup of the RRD graph. It is suggested that such a project would entail measurements of samples of new wheels at a wheel shop and worn wheels in service.
- Further work is needed to establish confidence in using as-measured wheel profiles or to determine ways of rotating measured wheel profiles to the some assumed correct rotation. This could be achieved by comparing profile results from single-headed and twin-headed Miniprof™ machines.

- Work is also needed to establish whether rail roll (under the action of lateral forces) and wheel profile rotation (caused by axle bending) are effects that need to be included in either WRTOL™* or NUCARS analysis.

6.2 Improved Quantification of Hollow Wheel Effects

TTCI believes that these further studies ideally need to be undertaken once the work described in Section 6.1 has been satisfactorily completed.

- The study needs to be extended to include wheels with larger amounts of hollow wear, and to include wheelsets with both wheels hollow.
- The study has identified wheel/rail conditions that can lead to very high positive conicity. Such very high conicity may cause hunting at low speeds or may possibly cause the wheelset to deviate negligibly from its stable position (equal wheel rolling radius) in tangent or curved track. Work is needed to determine how probable these very high conicities are and the vehicle stability concerns they pose.
- The rail roll moment calculations have been done assuming no restraint from the fastening system. It would be useful to undertake tests to establish the ranges of restraint offered by common fastening systems, to give better knowledge of the amount of rail roll moment a rail can withstand without giving risk of derailment.
- Work is needed to develop a set of quantitative rules for judging the appropriateness of wheel and rail profiles based on the RRD graph (refer to Section 5.4). Once these rules are available, wheel profiles from the North American wheel database should be matched with measured tangent rail profiles to establish the range of RRD graphs in service and the probabilities of the different types of vehicle stability described in Section 5.1. The study could also be extended to considered curved-track rail profiles.

* Trademark of Transportation Technology Center, Inc.

REFERENCES

1. E. Parker and K. J. Sawley, "North American Wheel Profile Survey," Association of American Railroads, Transportation Technology Center, Report R-920, June 1998.
2. A. H. Wickens, "Steering and Stability of the Bogie: Vehicle Dynamics and Suspension Design," *Proc Instn Mech Engrs*, Vol 205, 1991, pp 109-122.
3. K. J. Sawley, "Wheel/Rail Profile Maintenance," *World Congress on Railway Research*, Köln, Germany, November 2001.

APPENDICES

The following four appendices give sample NUCARS™ results for the tangent track, empty and loaded bulkhead flatcar, and RCV simulations. In the pages that follow, for each condition (type of car, empty or loaded, type of wheelset), the following graphs are given:

1. Car-body acceleration versus distance – low speed.
2. Car-body acceleration versus distance – high speed.
3. Lead axle lateral displacement – low speed.
4. Lead axle lateral displacement – high speed.

The wheelset descriptions contained in the appendices refer to the wheelsets described in Table 1 of the main report, which is also shown below.

Wheelset	Wheel Filename		Hollow Wear, mm	Flange Wear,* mm
1	AAR1B Narrow Flange	Left	0	0
		Right	0	0
2	Moderately worn AAR1B Wide Flange (2NED)	Left	0	0.03
		Right	0	0.14
3	Hollow worn wheelset with wheel radius mismatch (11NED)	Left	0.61	2.59
		Right	0.37	2.83
4	Hollow worn wheelset with flange wear (21NED)	Left	2.93	8.49
		Right	3.01	8.99
5	Hollow worn wheelset with minimal flange wear (3-6#22)	Left	4.06	1.55
		Right	3.93	1.12

* Wear loss at the flange gage point

APPENDIX A

EMPTY BULKHEAD FLATCAR
HIGH-SPEED STABILITY PLOTS

New AAR1B Wheels (Narrow Flange)

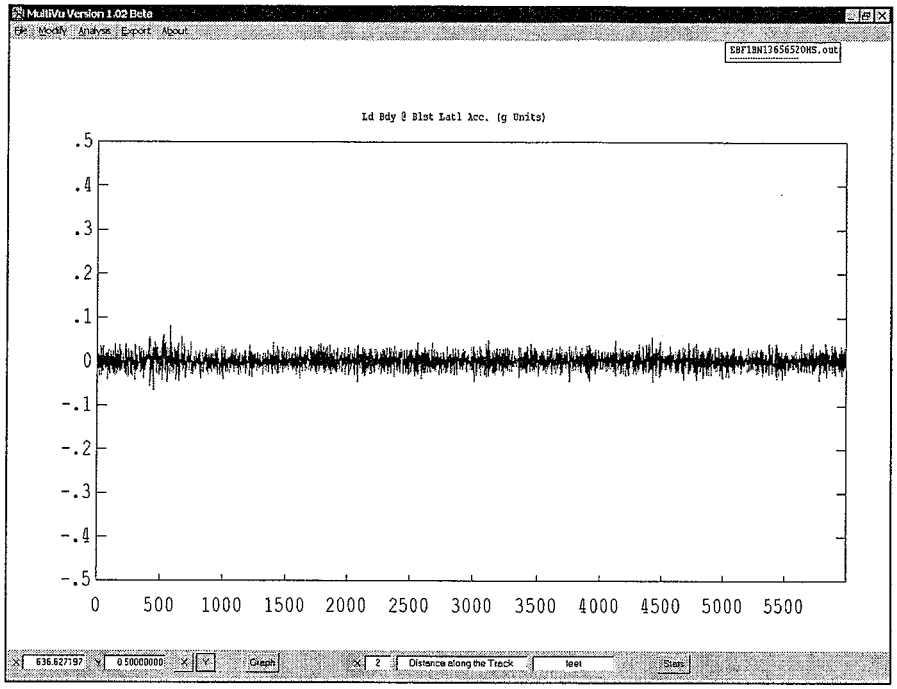

Figure A1. 20 mph, Car-body acceleration versus distance (empty bulkhead flat, AAR1B narrow flange wheel on AREMA 136-RE rail, 10-inch crown radius, 1:40 cant, 56.5-inch gage)

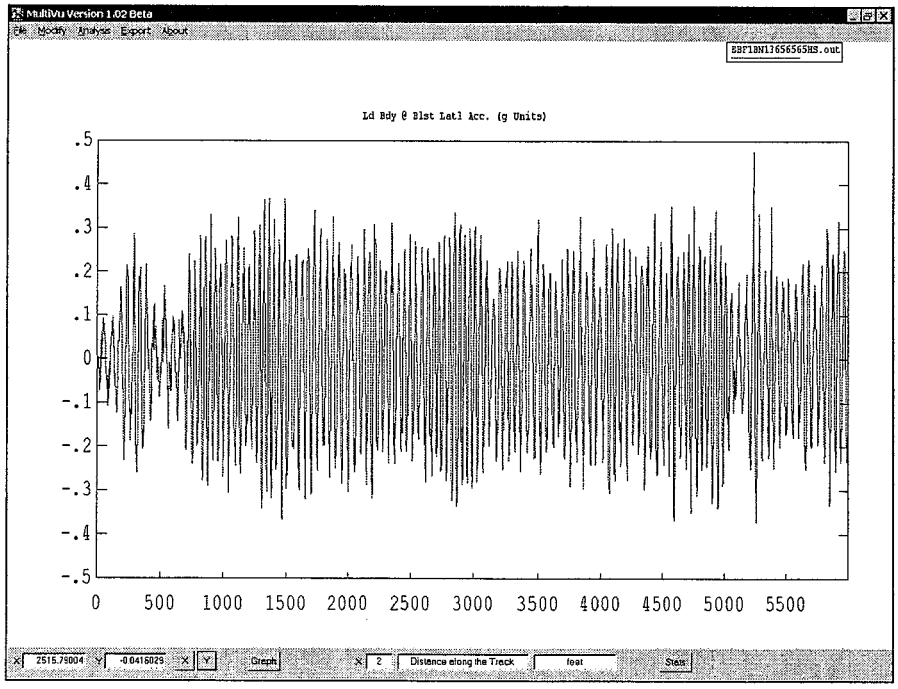

Figure A2. 65 mph, Car-body acceleration versus distance (empty bulkhead flat, AAR1B narrow flange wheel on AREMA 136-RE rail, 10-inch crown radius, 1:40 cant, 56.5-inch gage)

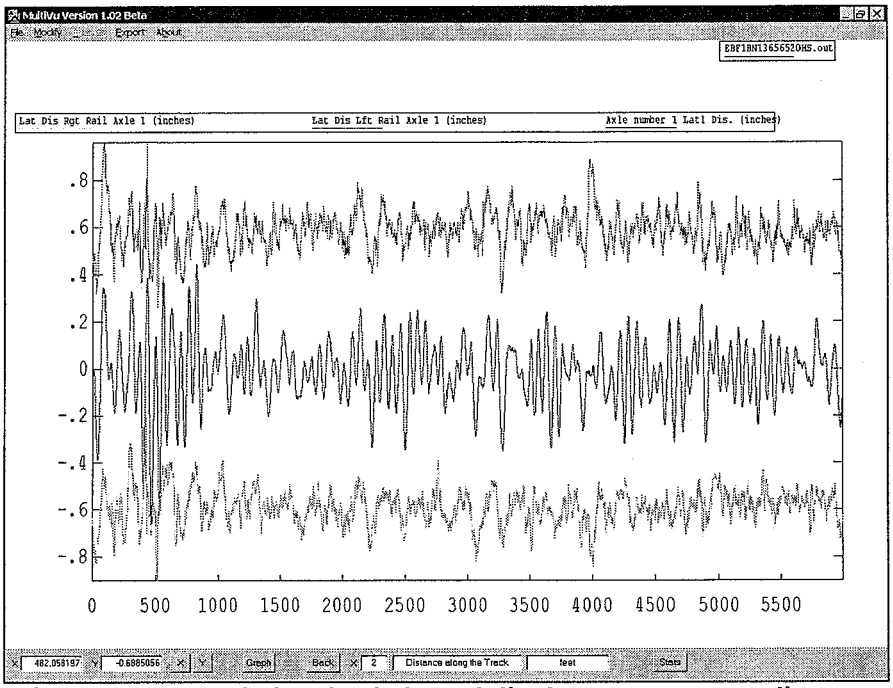

Figure A3. 20 mph, Lead axle lateral displacement versus distance (empty bulkhead flat, AAR1B narrow flange wheel on AREMA 136-RE rail, 10-inch crown radius, 1:40 cant, 56.5-inch gage)

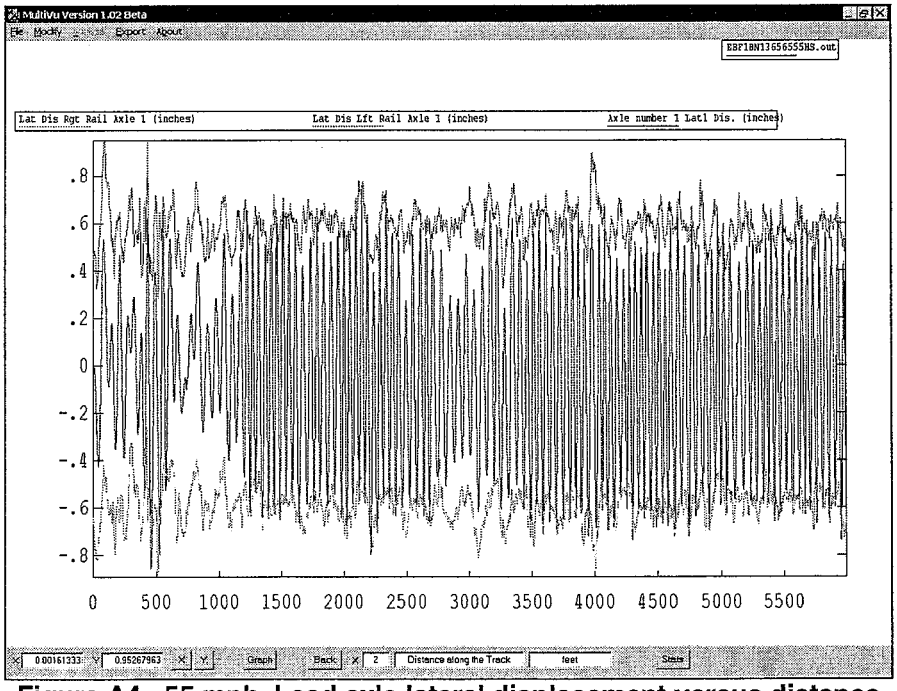

Figure A4. 55 mph, Lead axle lateral displacement versus distance (empty bulkhead flat, , AAR1B narrow flange wheel on AREMA 136-RE rail, 10-inch crown radius, 1:40 cant, 56.5-inch gage)

Moderately Worn AAR1B Wheels (Wide Flange)

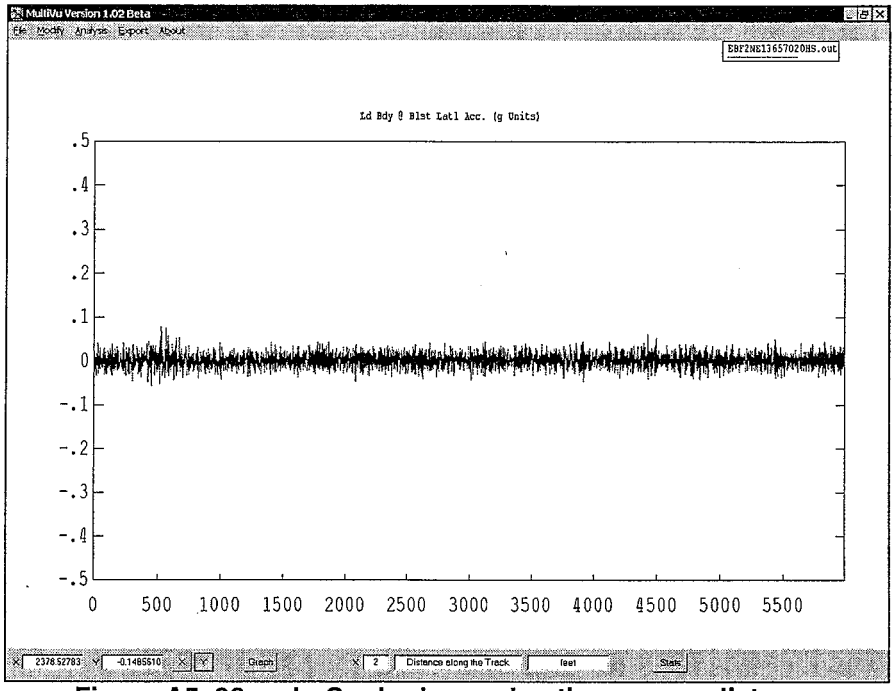

Figure A5. 20 mph, Car-body acceleration versus distance (empty bulkhead flat, moderately worn AAR1B wide flange wheel on AREMA 136-RE rail, 10-inch crown radius, 1:40 cant, 57.0-inch gage)

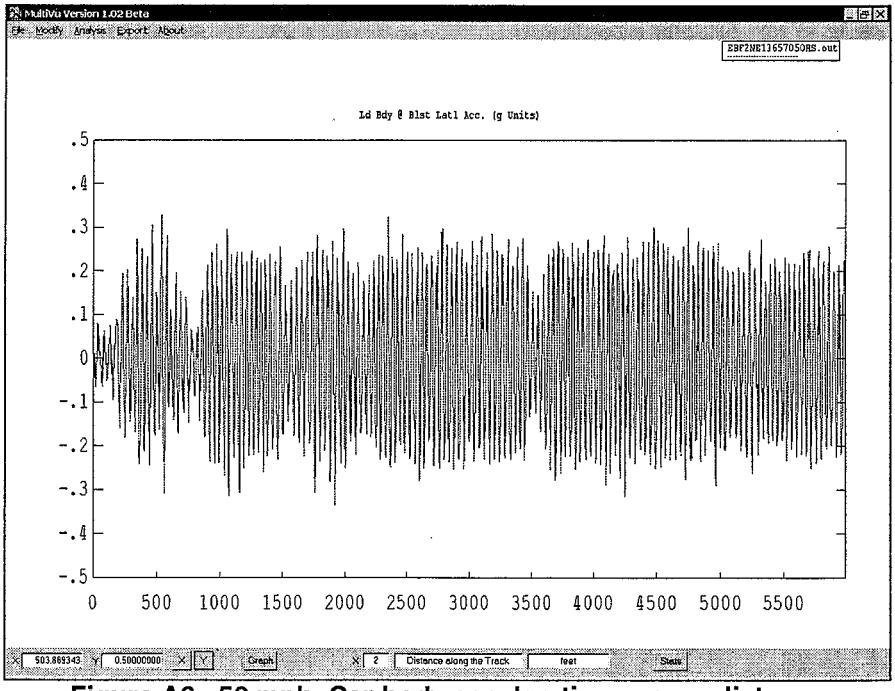

Figure A6. 50 mph, Car-body acceleration versus distance (empty bulkhead flat, moderately worn AAR1B wide flange wheel on AREMA 136-RE rail, 10-inch crown radius, 1:40 cant, 57.0-inch gage)

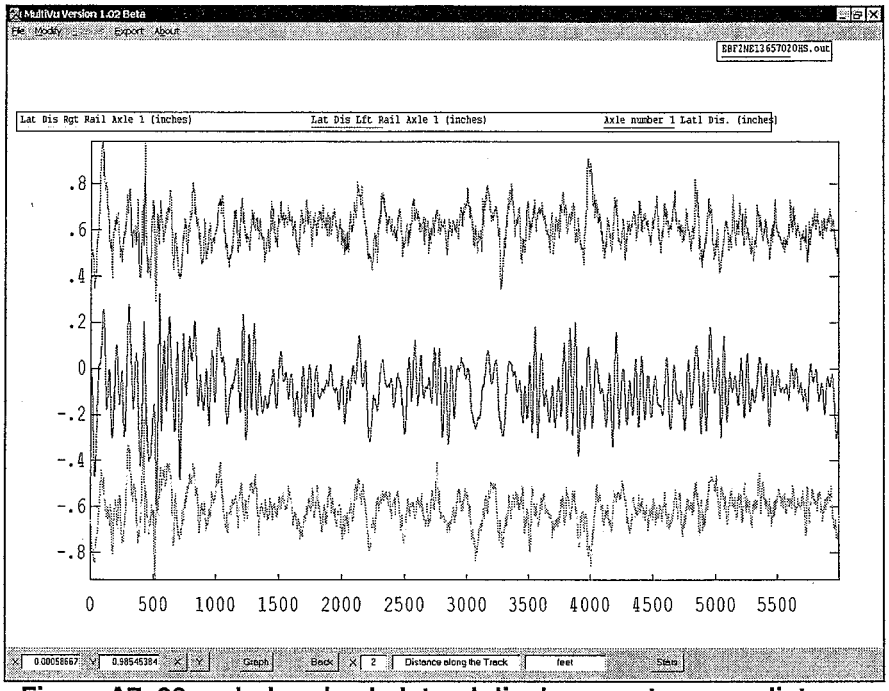

Figure A7. 20 mph, Lead axle lateral displacement versus distance (empty bulkhead flat, moderately worn AAR1B wide flange wheel on AREMA 136-RE rail, 10-inch crown radius, 1:40 cant, 57.0-inch gage)

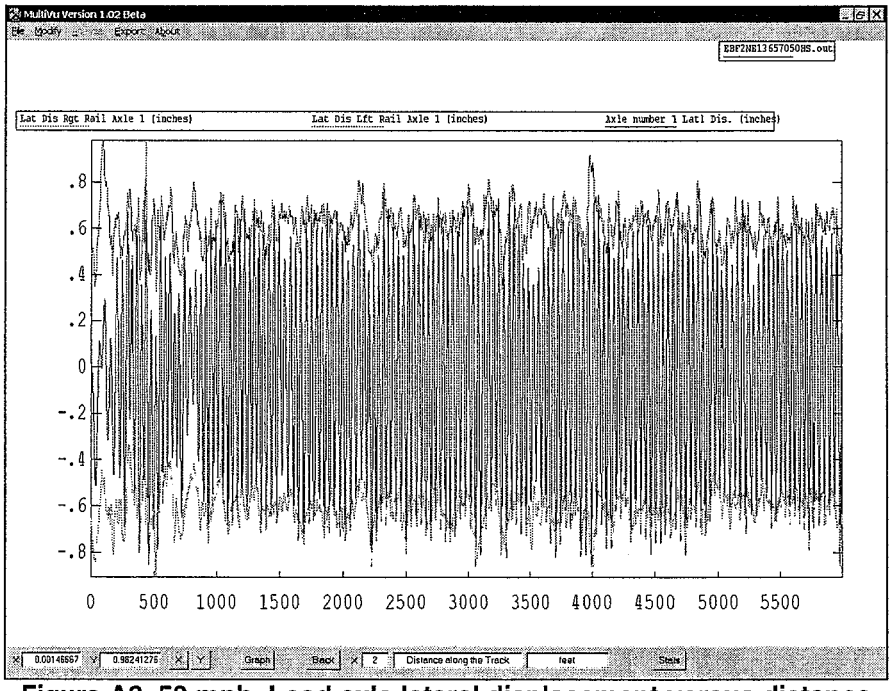

Figure A8. 50 mph, Lead axle lateral displacement versus distance (empty bulkhead flat, moderately worn AAR1B wide flange wheel on AREMA 136-RE rail, 10-inch crown radius, 1:40 cant, 57.0-inch gage)

Hollow Worn Wheelset with Wheel Radius Mismatch

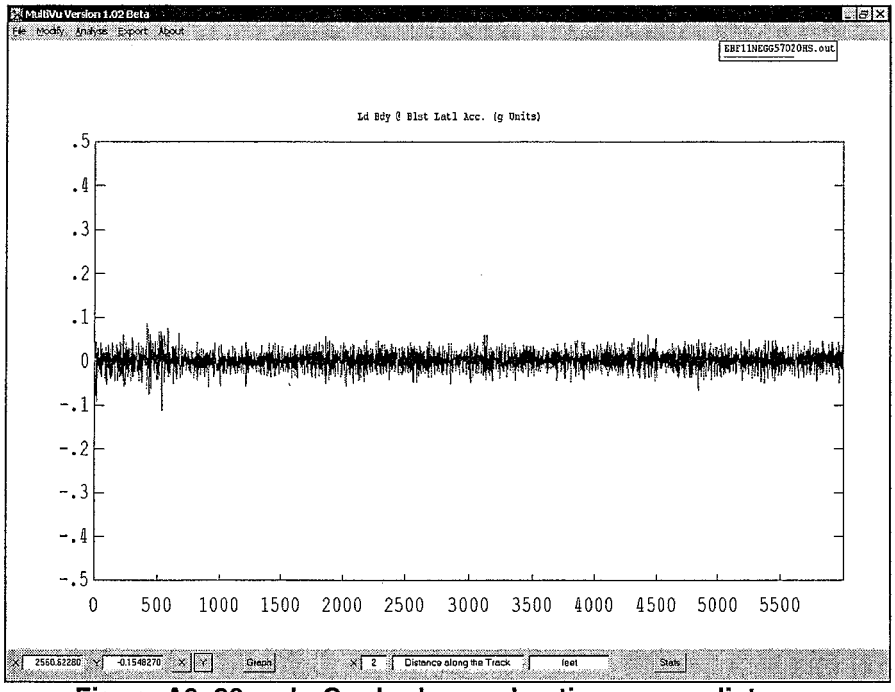

Figure A9. 20 mph, Car-body acceleration versus distance (empty bulkhead flat, , hollow worn wheel with wheel radius mismatch on tangent worn rail at 57.0-inch gage)

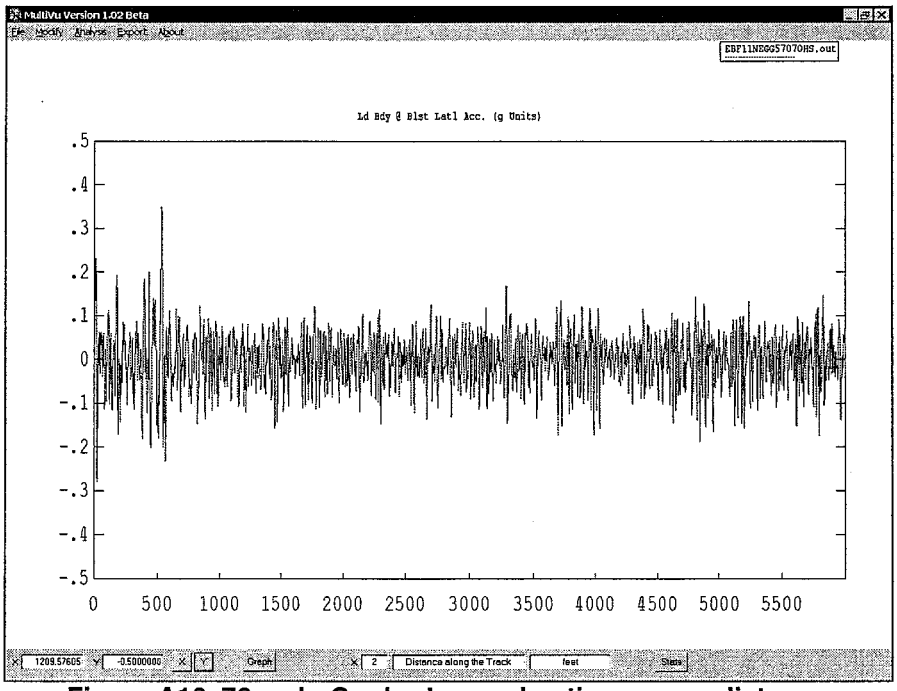

Figure A10. 70 mph, Car-body acceleration versus distance (empty bulkhead flat, hollow worn wheel with wheel radius mismatch on tangent worn rail at 57.0-inch gage)

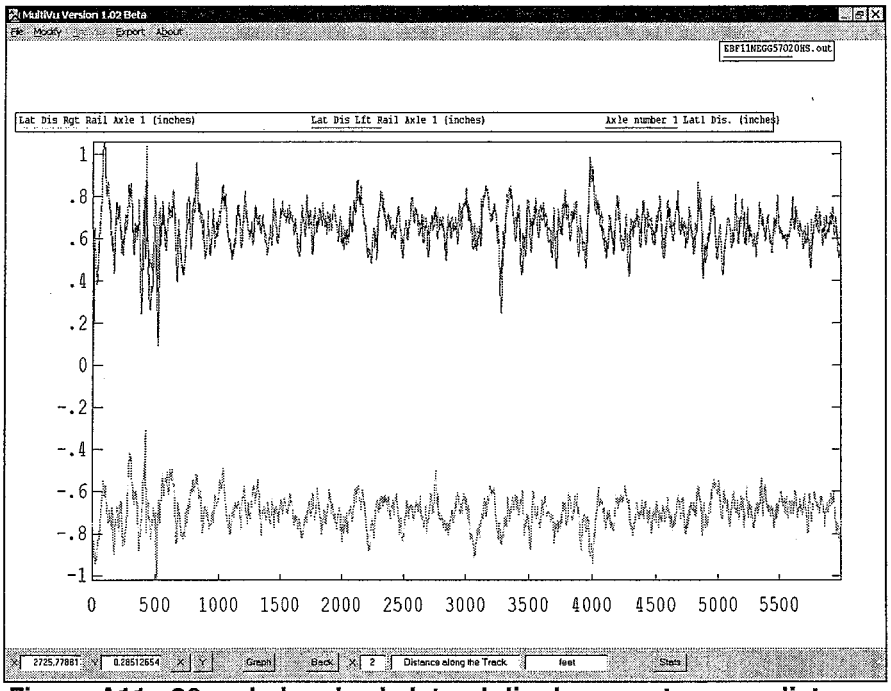

Figure A11. 20 mph, Lead axle lateral displacement versus distance (empty bulkhead flat, hollow worn wheel with wheel radius mismatch on tangent worn rail at 57.0-inch gage)

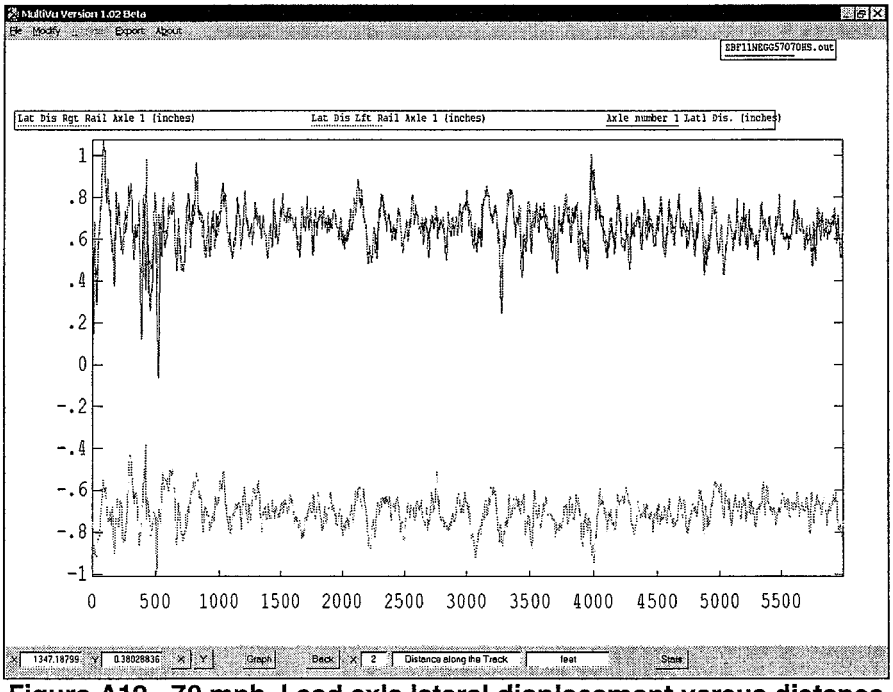

Figure A12. 70 mph, Lead axle lateral displacement versus distance (empty bulkhead flat, hollow worn wheel with wheel radius mismatch on tangent worn rail at 57.0-inch gage)

Hollow Worn Wheelset with Flange Wear

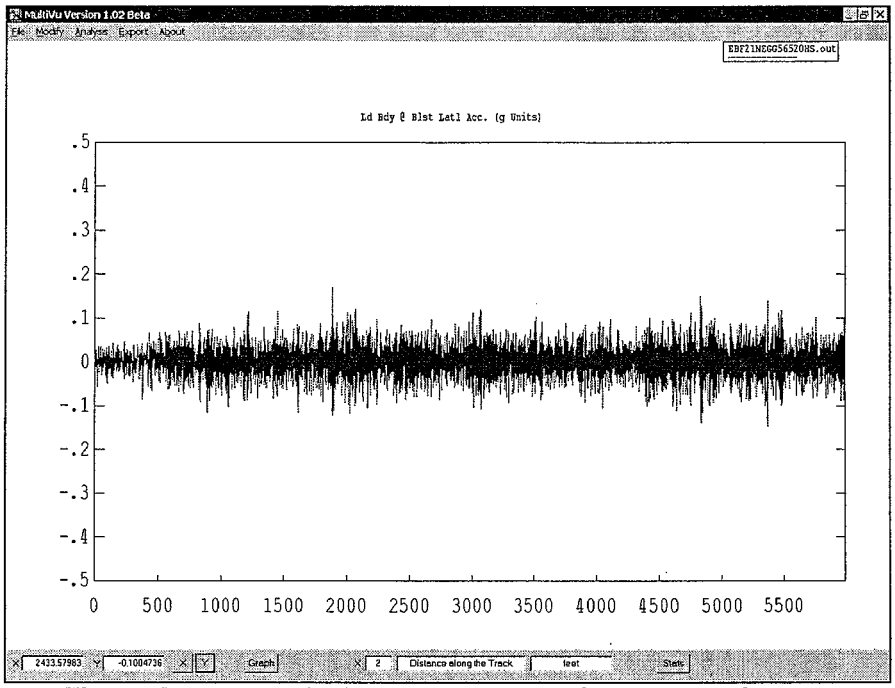

Figure A13. 20 mph, Car-body acceleration versus distance (empty bulkhead flat, hollow worn wheel on tangent worn track at 56.5-inch gage)

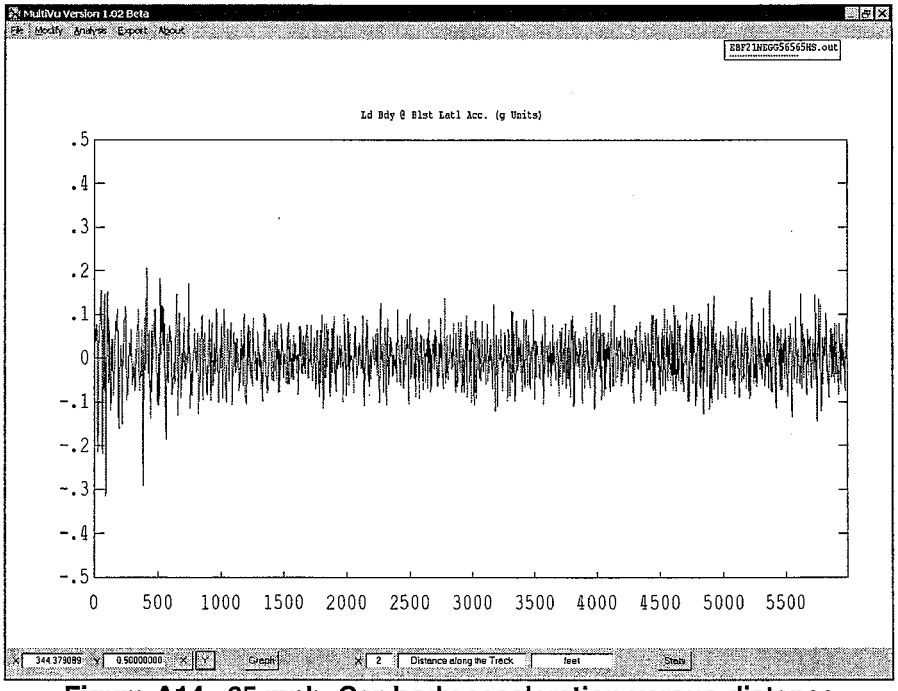

Figure A14. 65 mph, Car-body acceleration versus distance (empty bulkhead flat, hollow worn wheel on tangent worn track at 56.5-inch gage)

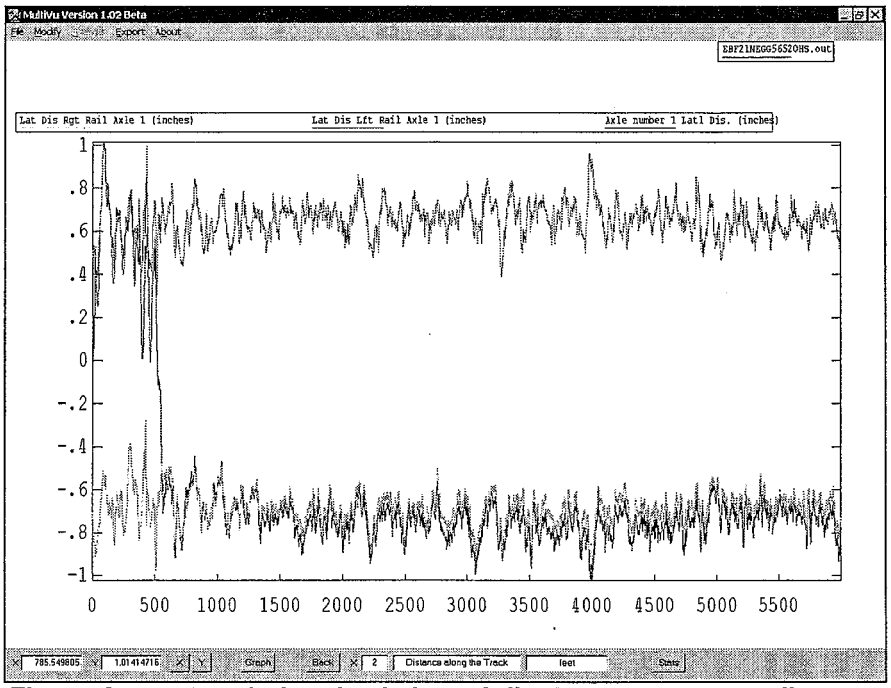

Figure A15. 20 mph, Lead axle lateral displacement versus distance (empty bulkhead flat, hollow worn wheel on tangent worn track at 56.5-inch gage)

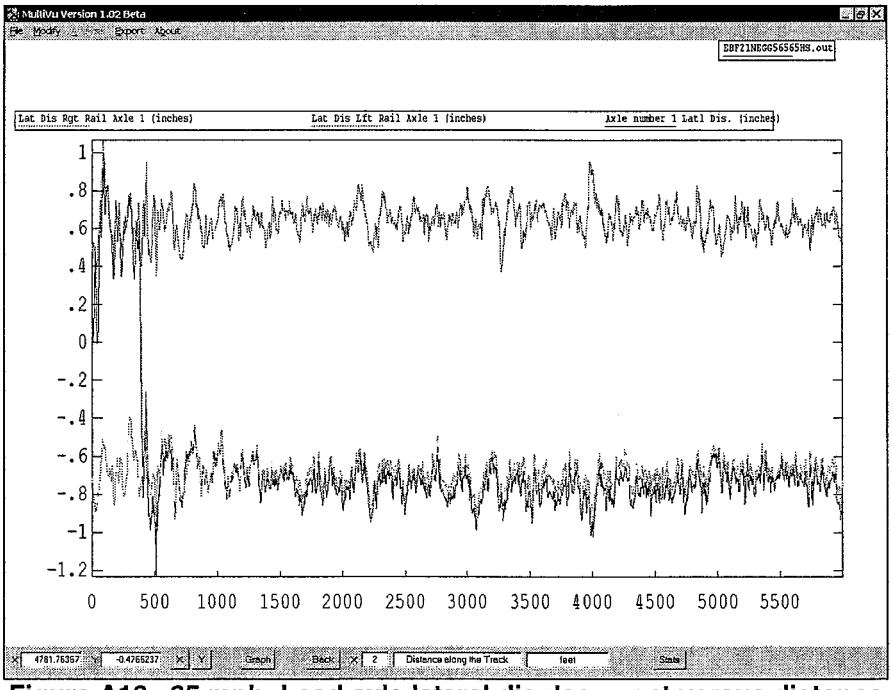

Figure A16. 65 mph, Lead axle lateral displacement versus distance (empty bulkhead flat, hollow worn wheel on tangent worn track at 56.5-inch gage)

Hollow Worn Wheelset with Minimal Flange Wear

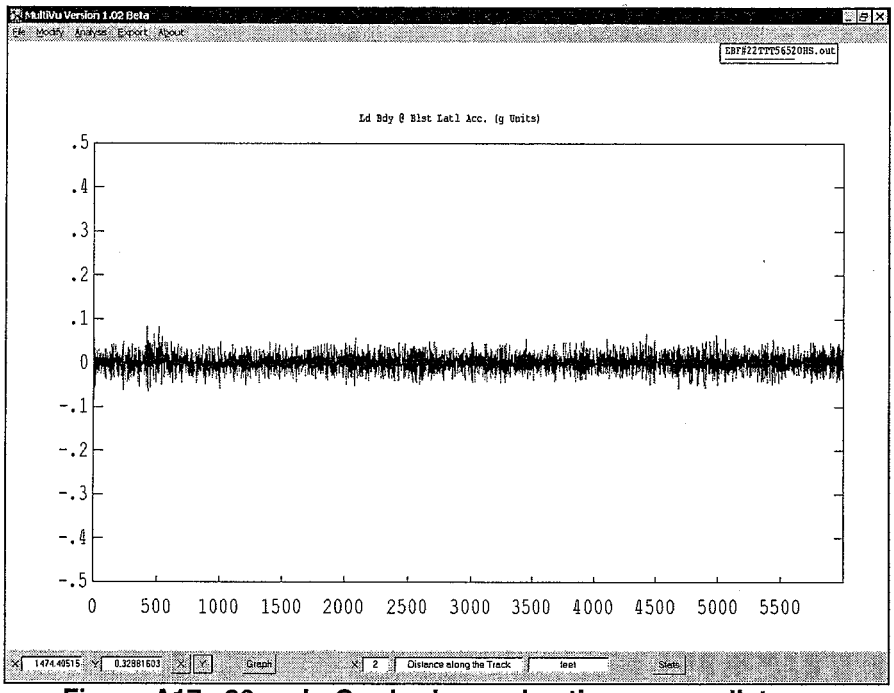

Figure A17. 20 mph, Car-body acceleration versus distance (empty bulkhead flat, hollow worn wheel with minimal flange wear on TTC's TTT at 56.5-inch gage)

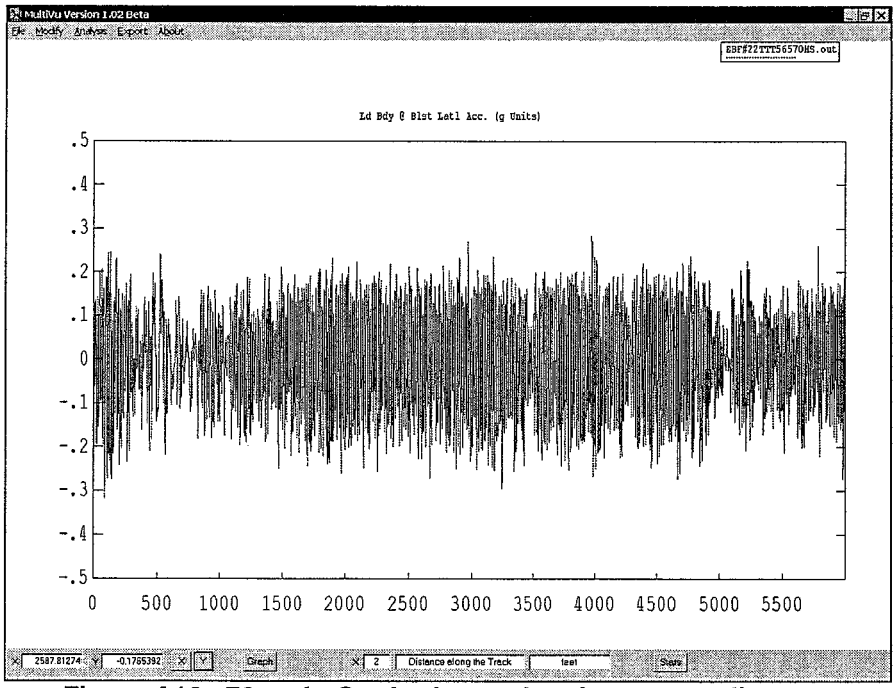

Figure A18. 70 mph, Car-body acceleration versus distance (empty bulkhead flat, hollow worn wheel with minimal flange wear on TTC's TTT at 56.5-inch gage)

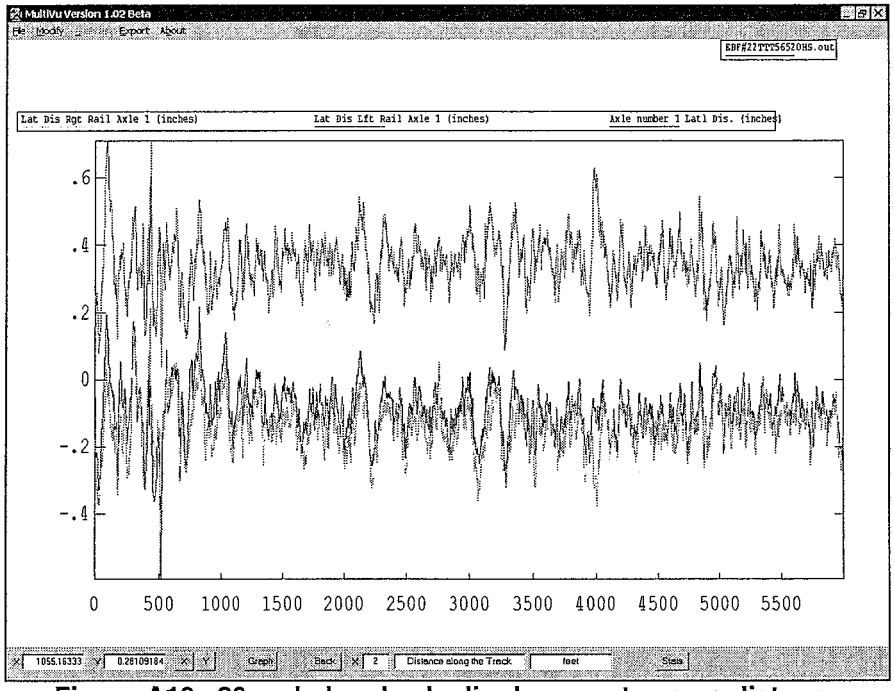

Figure A19. 20 mph, Lead axle displacement versus distance (empty bulkhead flat, lateral, hollow worn wheel with minimal flange wear on TTC's TTT at 56.5-inch gage)

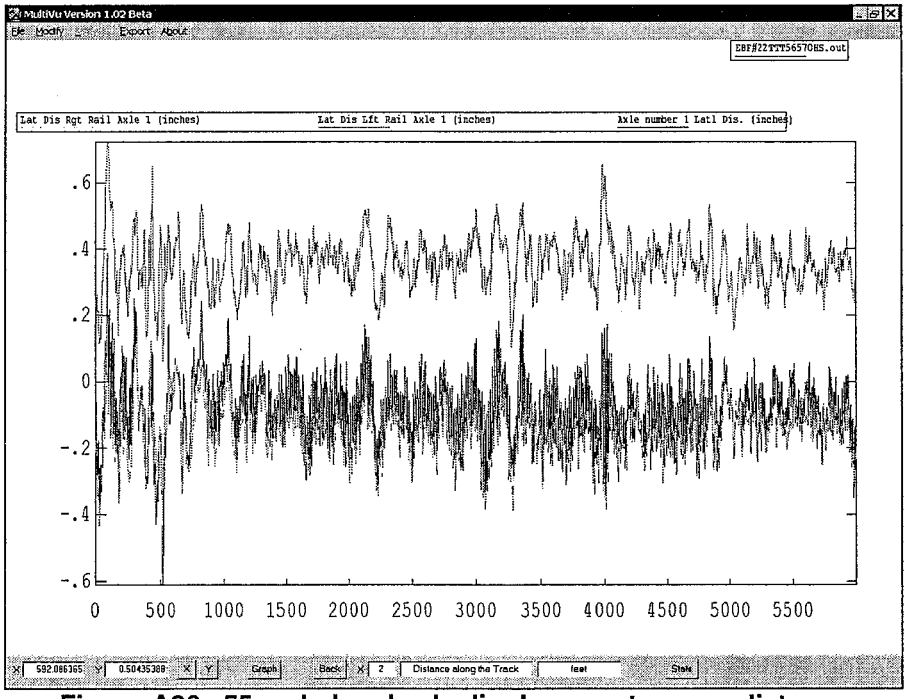

Figure A20. 55 mph, Lead axle displacement versus distance empty bulkhead flat, lateral, hollow worn wheel with minimal flange wear on TTC's TTT at 56.5-inch gage)

APPENDIX B

EMPTY RCV HIGH-SPEED STABILITY PLOTS

New AAR1B Wheels (Narrow Flange)

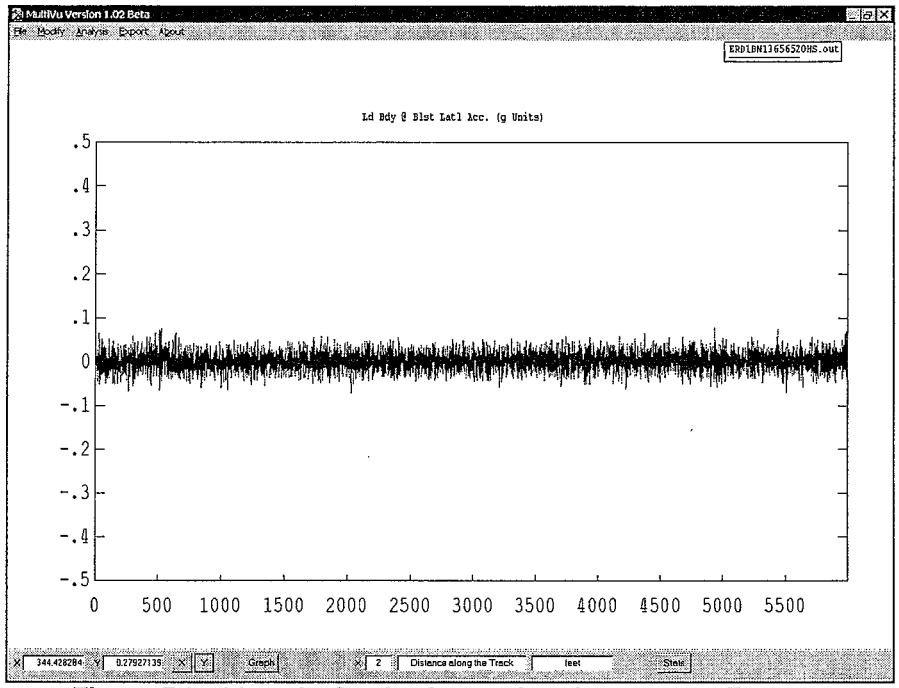

Figure B1. 20 mph, Car-body acceleration versus distance (empty RCV, AAR1B narrow flange wheel on AREMA 136-RE rail, 10-inch crown radius, 1:40 cant, at 56.5-inch gage)

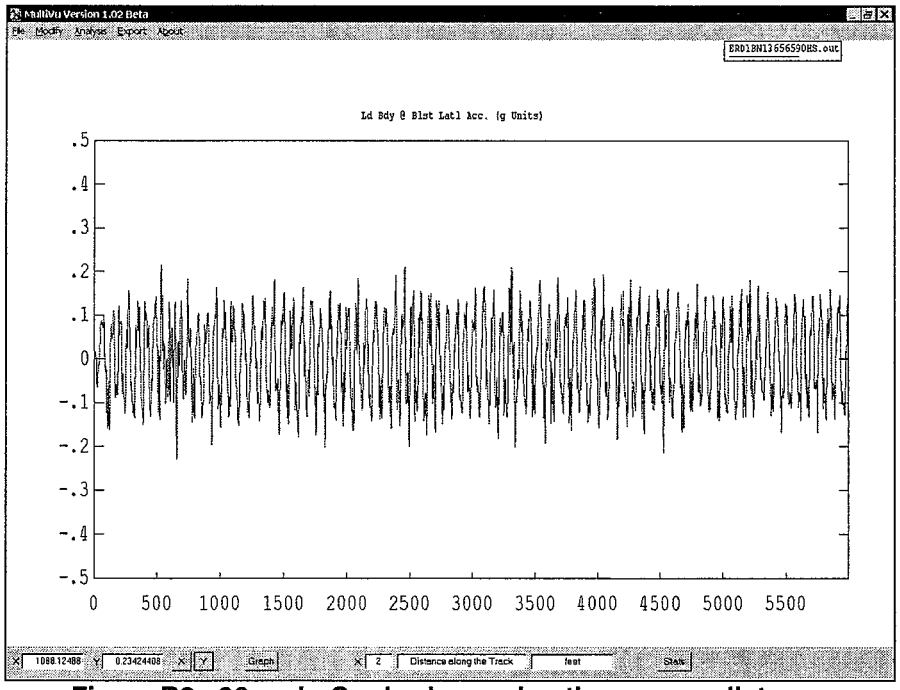

Figure B2. 90 mph, Car-body acceleration versus distance (empty RCV, AAR1B narrow flange wheel on AREMA 136-RE rail, 10-inch crown radius, 1:40 cant, at 56.5-inch gage)

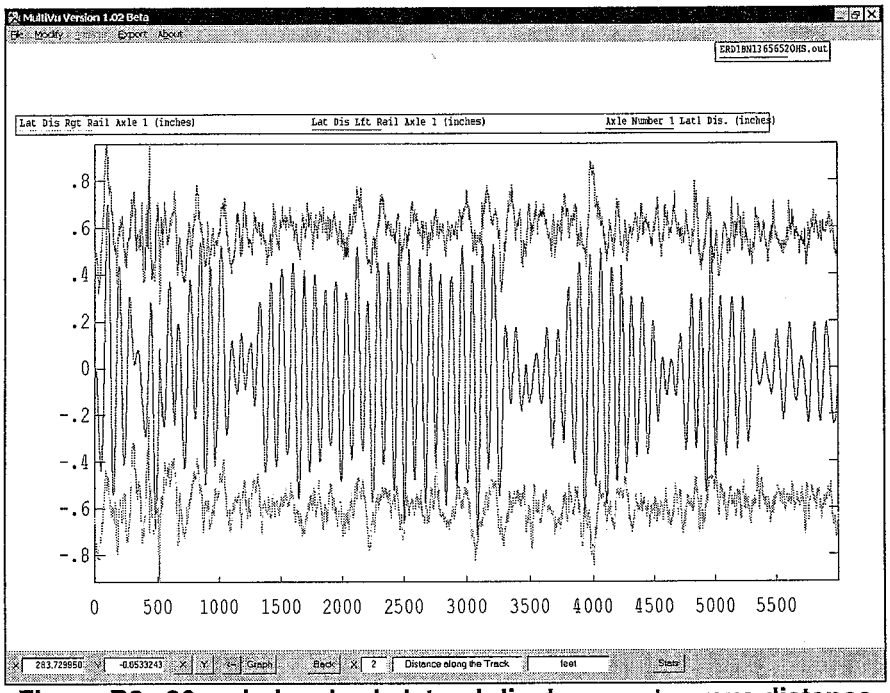

Figure B3. 20 mph, Lead axle lateral displacement versus distance (empty RCV, AAR1B narrow flange wheel on AREMA 136-RE rail, 10-inch crown radius, 1:40 cant, at 56.5-inch gage)

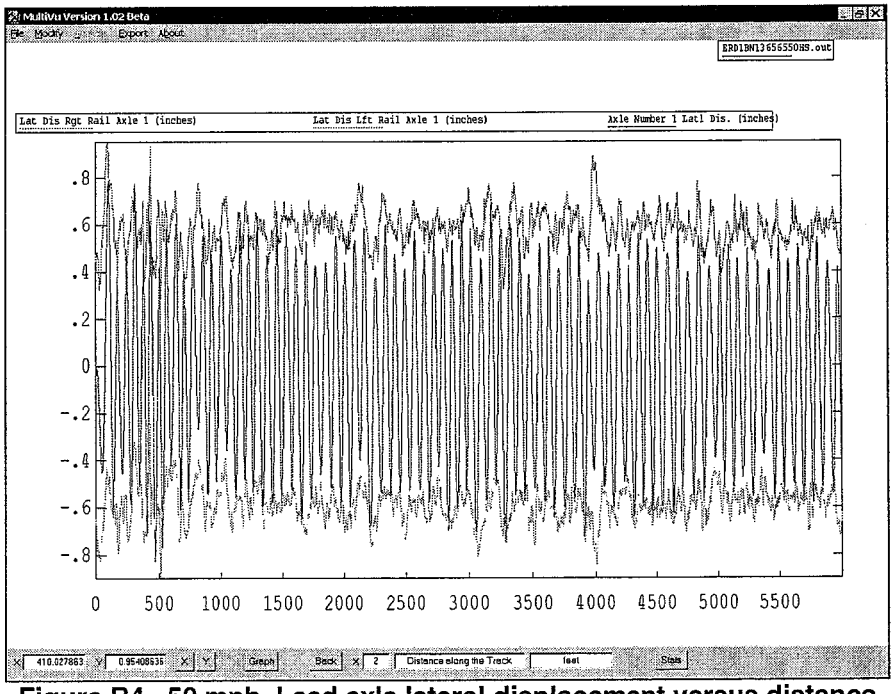

Figure B4. 50 mph, Lead axle lateral displacement versus distance (empty RCV, AAR1B narrow flange wheel on AREMA 136-RE rail, 10-inch crown radius, 1:40 cant, at 56.5-inch gage)

Moderately Worn AAR1B Wheels (Wide Flange)

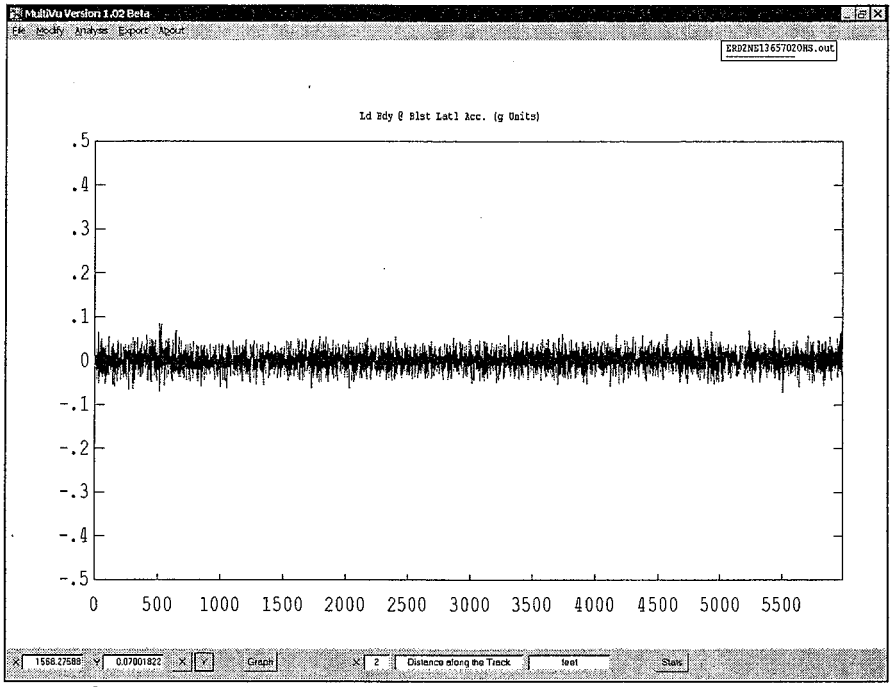

Figure B5. 20 mph, Car-body acceleration versus distance (empty RCV, moderately worn AAR1B wide flange wheel on AREMA 136-RE rail, 10-inch crown radius, 1:40 cant, at 57.0-inch gage)

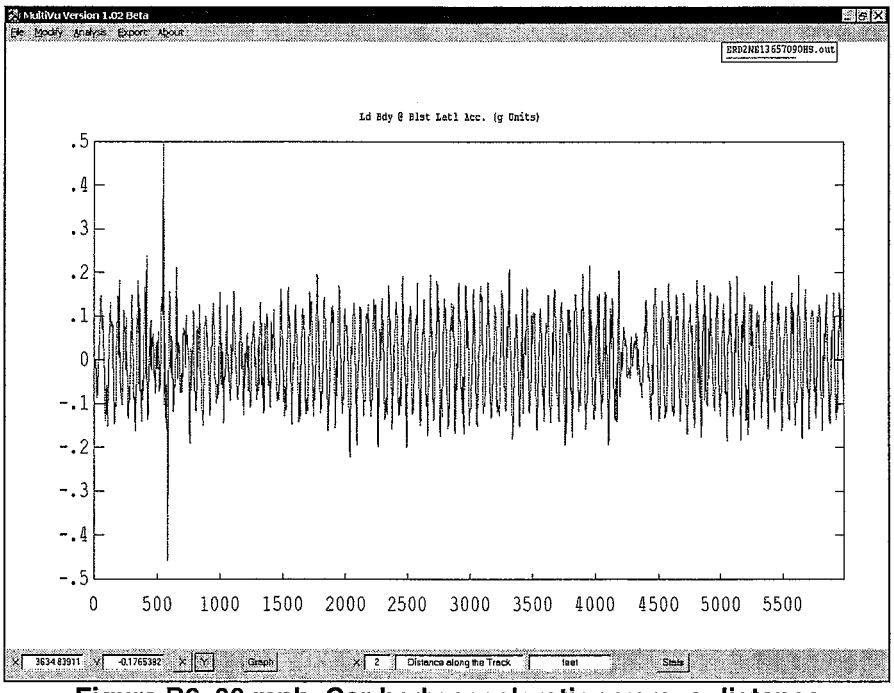

Figure B6. 90 mph, Car-body acceleration versus distance (empty RCV, moderately worn AAR1B wide flange wheel on AREMA 136-RE rail, 10-inch crown radius, 1:40 cant, at 57.0-inch gage)

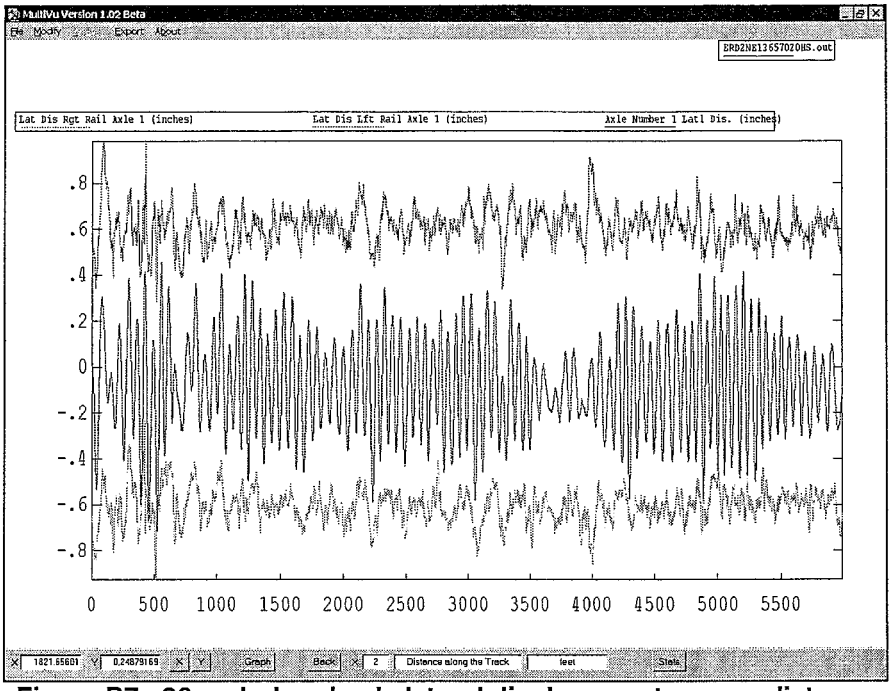

Figure B7. 20 mph, Lead axle lateral displacement versus distance (empty RCV, moderately worn AAR1B wide flange wheel on AREMA 136-RE rail, 10-inch crown radius, 1:40 cant, at 57.0-inch gage)

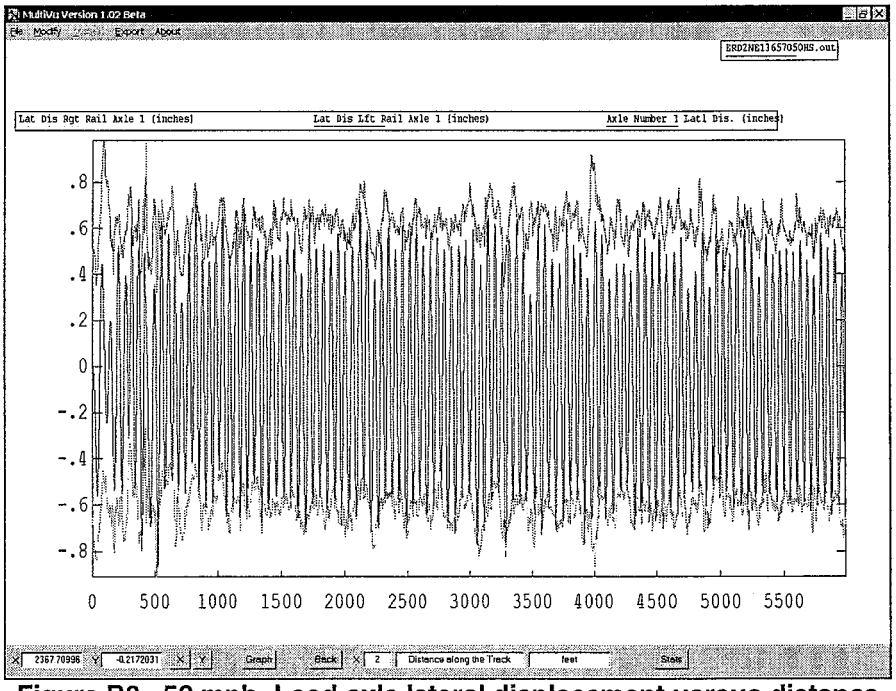

Figure B8. 50 mph, Lead axle lateral displacement versus distance (empty RCV, moderately worn AAR1B wide flange wheel on AREMA 136-RE rail, 10-inch crown radius, 1:40 cant, at 57.0-inch gage)

Hollow Worn Wheelset with Wheel Radius Mismatch

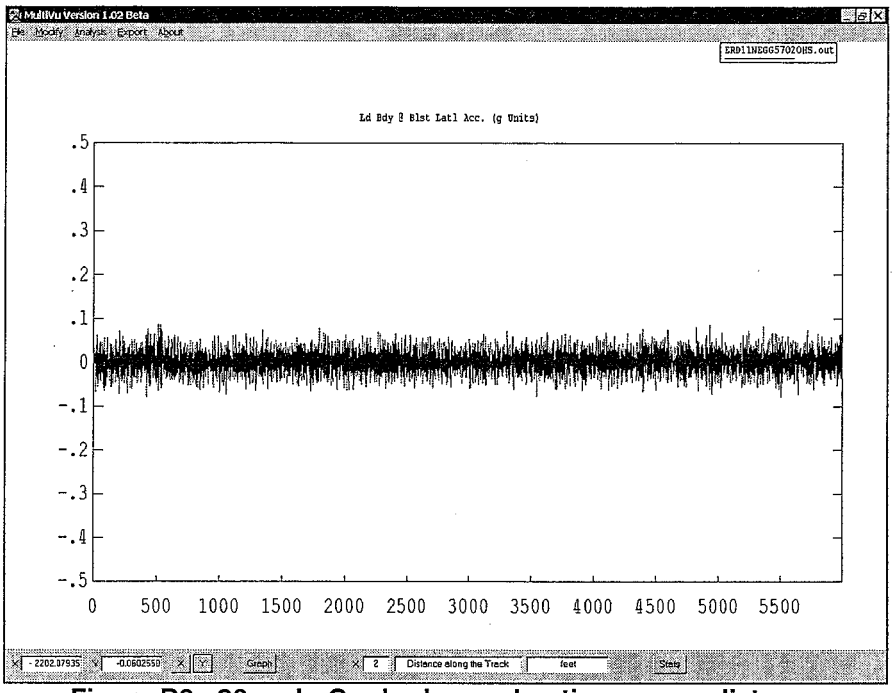

Figure B9. 20 mph, Car-body acceleration versus distance (empty RCV, hollow worn wheel with wheel radius mismatch on tangent worn rail at 57.0-inch gage)

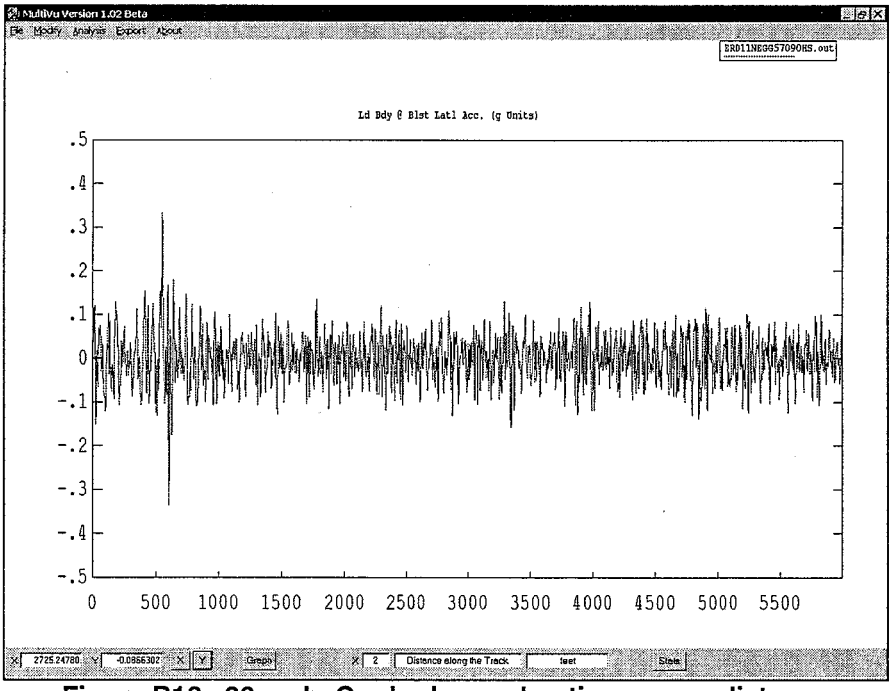

Figure B10. 90 mph, Car-body acceleration versus distance (empty RCV, hollow worn wheel with wheel radius mismatch on tangent worn rail at 57.0 inch-gage)

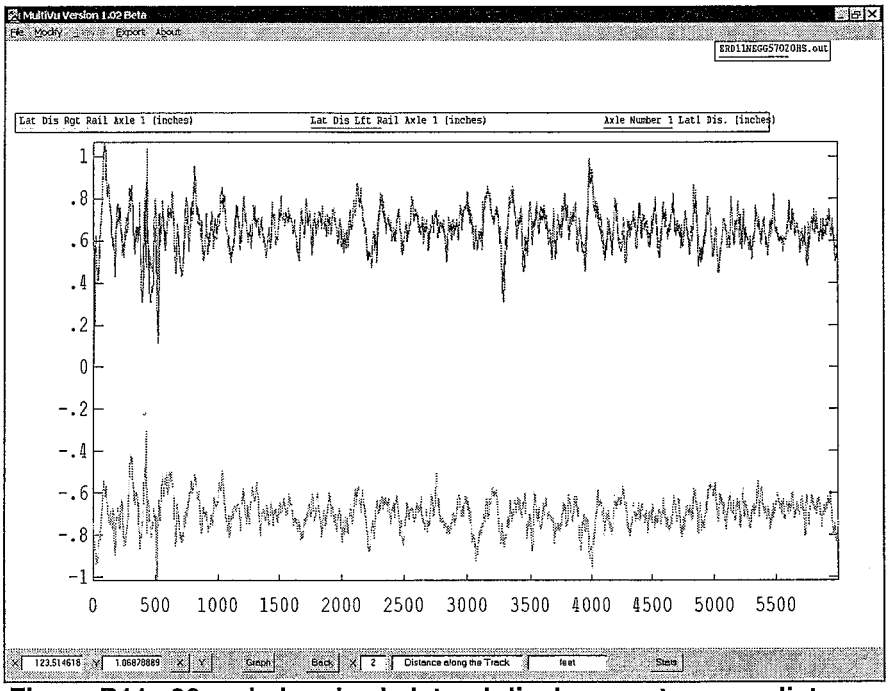

Figure B11. 20 mph, Lead axle lateral displacement versus distance (empty RCV, hollow worn wheel with wheel radius mismatch on tangent worn rail at 57.0 inch-gage)

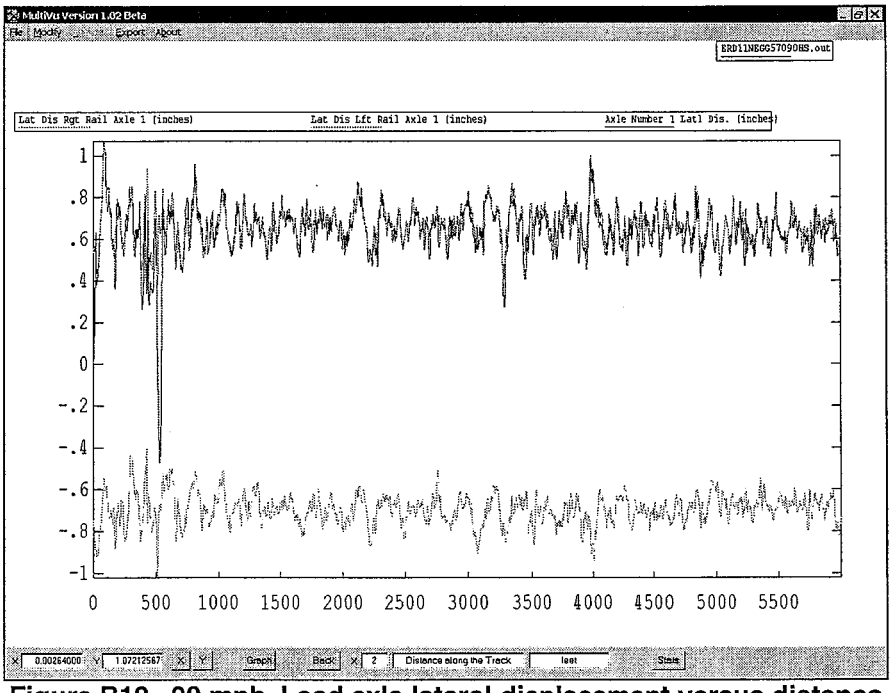

Figure B12. 90 mph, Lead axle lateral displacement versus distance (empty RCV, hollow worn wheel with wheel radius mismatch on tangent worn rail at 57.0-inch gage)

Hollow Worn Wheelset with Flange Wear

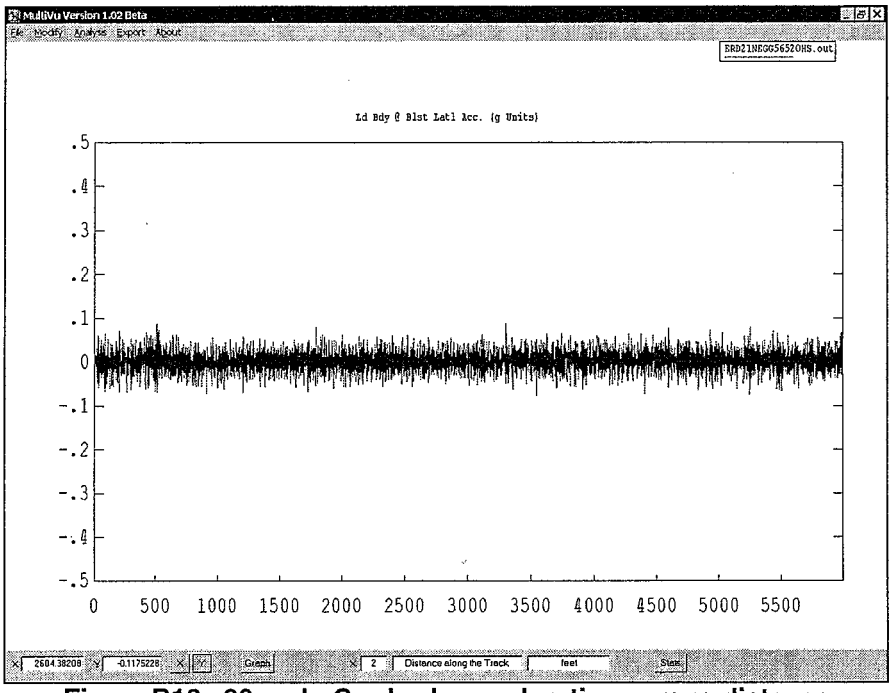

Figure B13. 20 mph, Car-body acceleration versus distance (empty RCV, hollow worn wheel on tangent worn track at 56.5-inch gage)

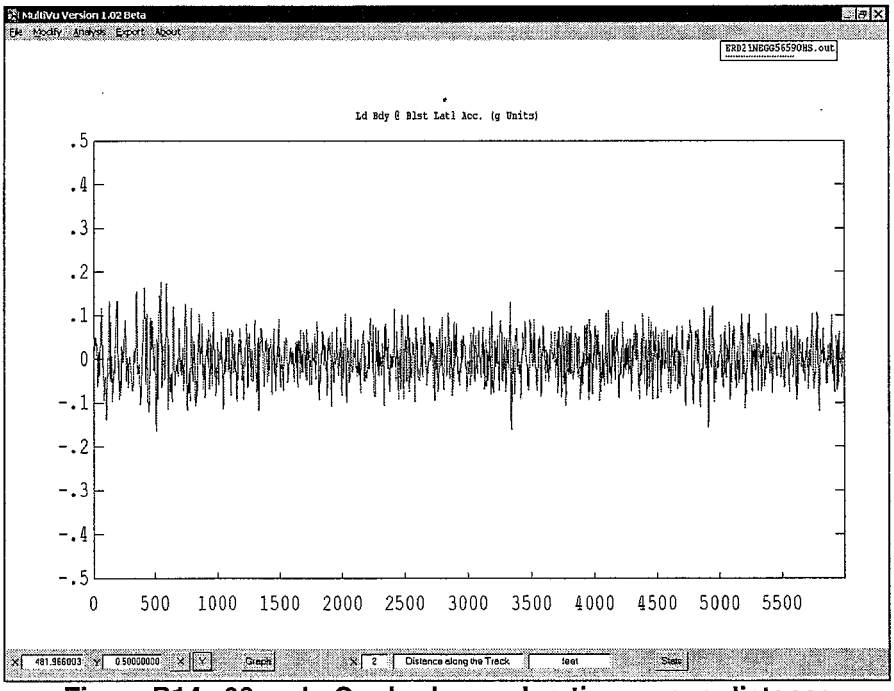

Figure B14. 90 mph, Car-body acceleration versus distance (empty RCV, hollow worn wheel on tangent worn track at 56.5-inch gage)

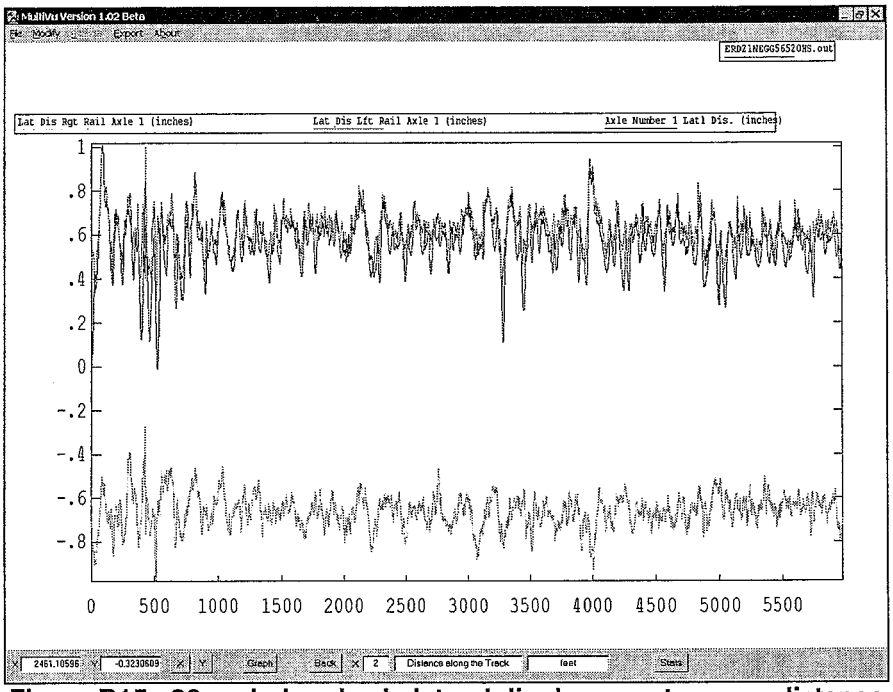

Figure B15. 20 mph, Lead axle lateral displacement versus distance (empty RCV, hollow worn wheel on tangent worn track at 56.5-inch gage)

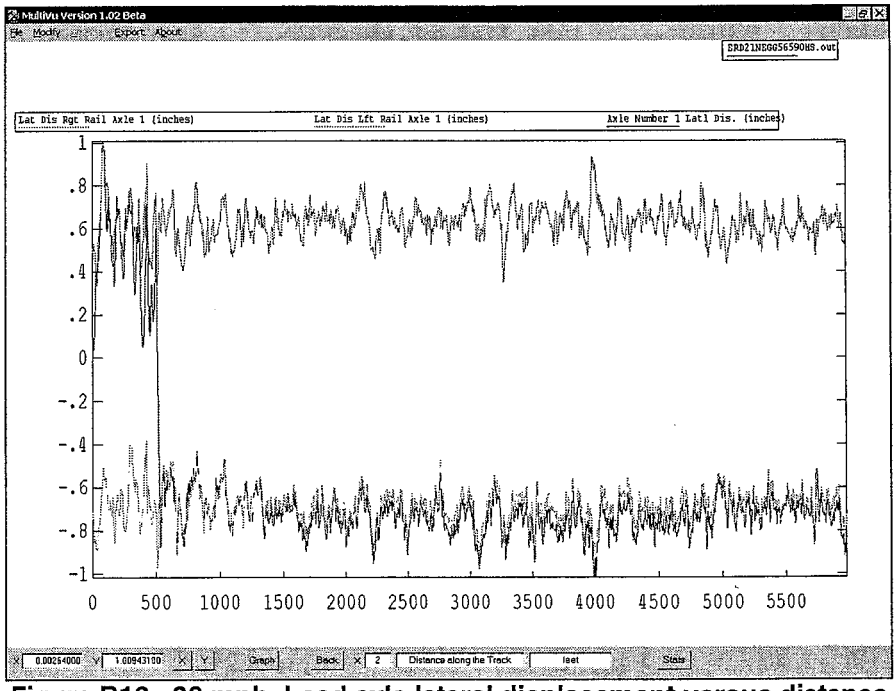

Figure B16. 90 mph, Lead axle lateral displacement versus distance (empty RCV, hollow worn wheel on tangent worn track at 56.5-inch gage)

Hollow Worn Wheelset with Minimal Flange Wear

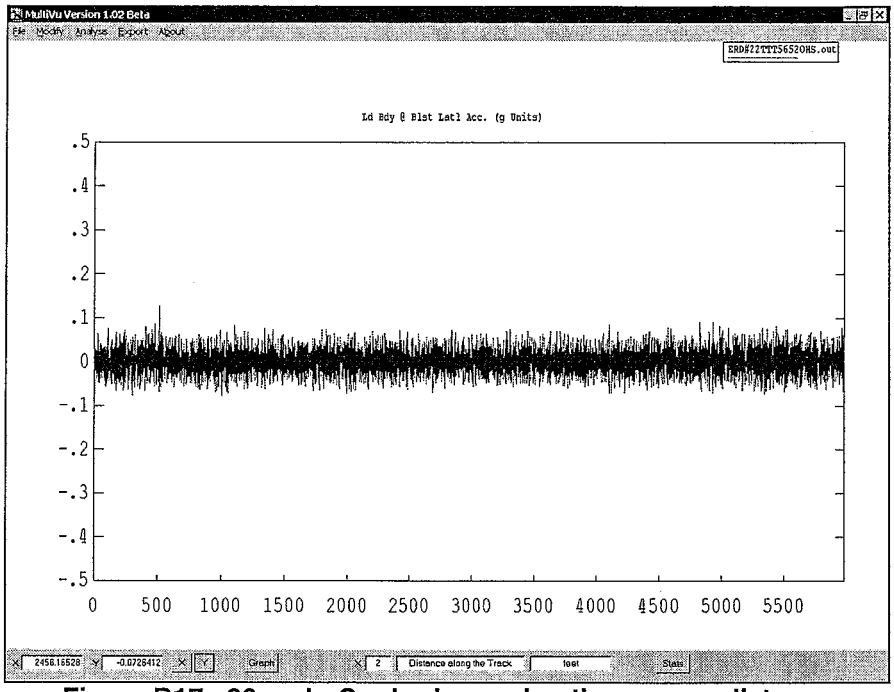

Figure B17. 20 mph, Car-body acceleration versus distance (empty RCV, hollow worn wheel with minimal flange wear on TTC's TTT at 56.5-inch gage)

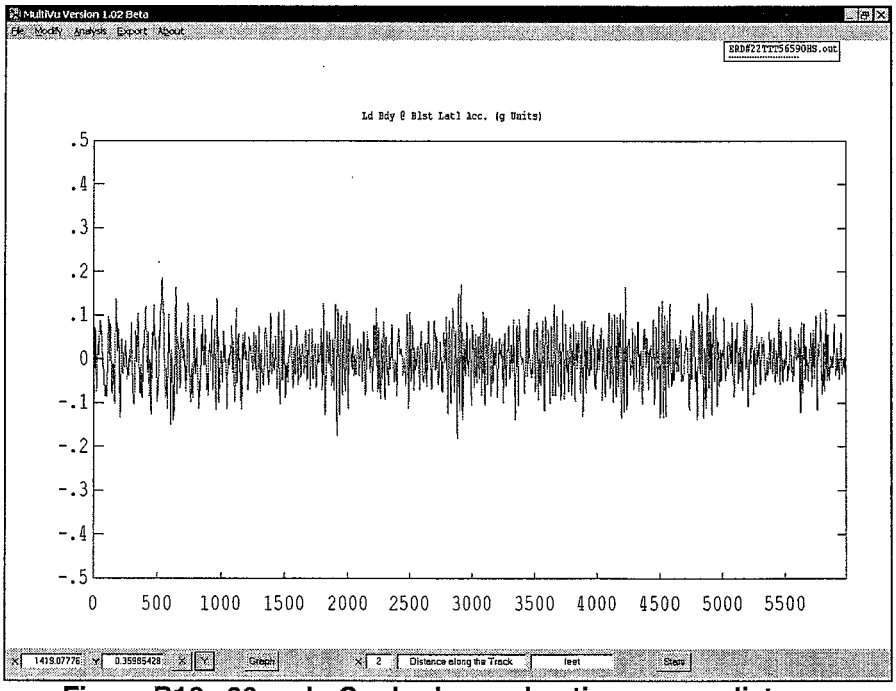

Figure B18. 90 mph, Car-body acceleration versus distance (empty RCV, hollow worn wheel with minimal flange wear on TTC's TTT at 56.5-inch gage)

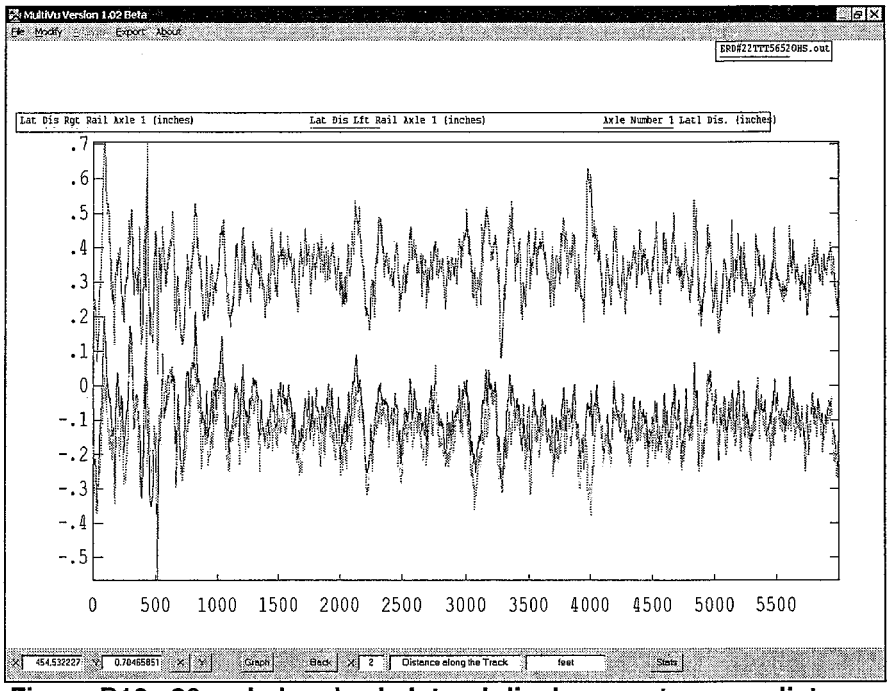

Figure B19. 20 mph, Lead axle lateral displacement versus distance (empty RCV, hollow worn wheel with minimal flange wear on TTC's TTT at 56.5-inch gage)

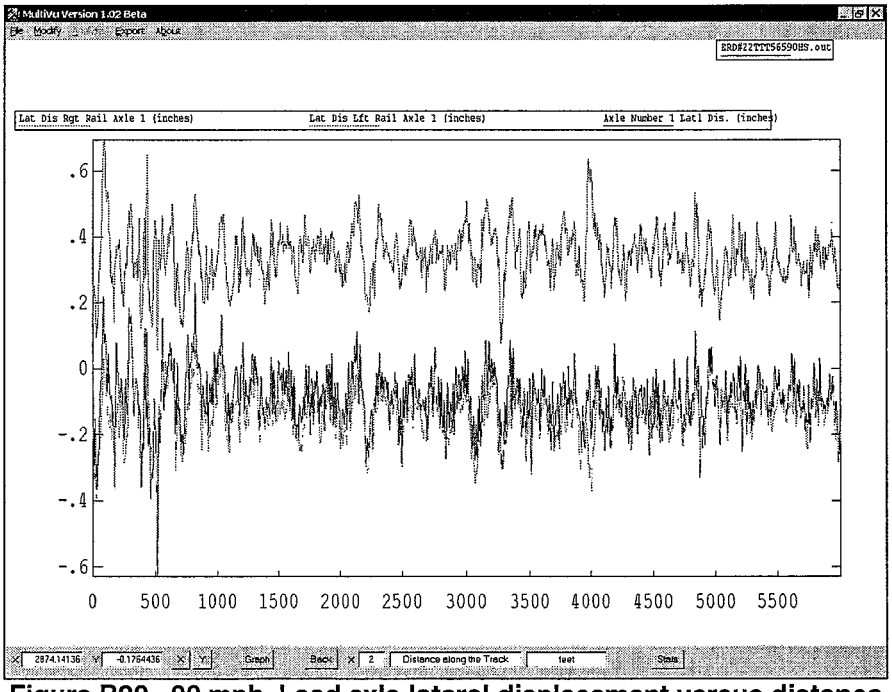

Figure B20. 90 mph, Lead axle lateral displacement versus distance (empty RCV, hollow worn wheel with minimal flange wear on TTC's TTT at 56.5-inch gage)

APPENDIX C

LOADED BULKHEAD FLATCAR
HIGH-SPEED STABILITY PLOTS

New AAR1B Wheels (Narrow Flange)

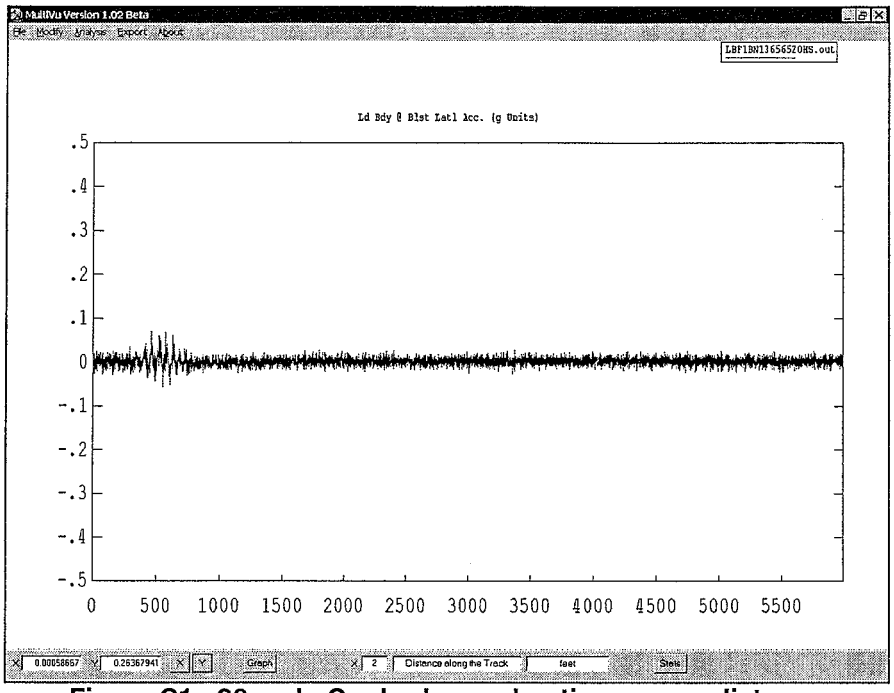

Figure C1. 20 mph, Car-body acceleration versus distance (loaded bulkhead flat, AAR1B narrow flange wheel on AREMA 136-RE rail, 10-inch crown radius, 1:40 cant, at 56.5-inch gage)

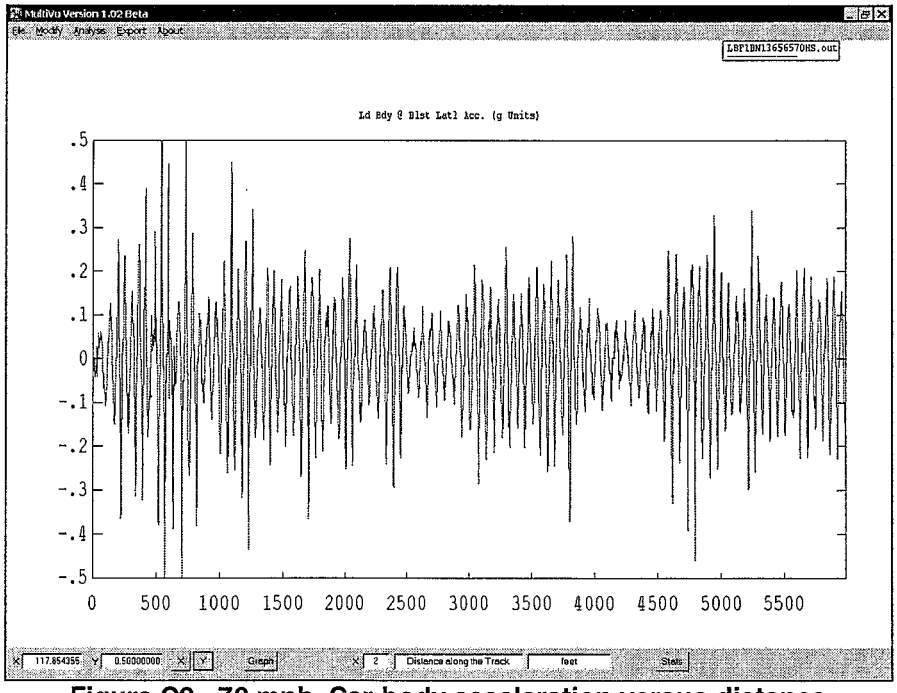

Figure C2. 70 mph, Car-body acceleration versus distance (loaded bulkhead flat, AAR1B narrow flange wheel on AREMA 136-RE rail, 10-inch crown radius, 1:40 cant, at 56.5-inch gage)

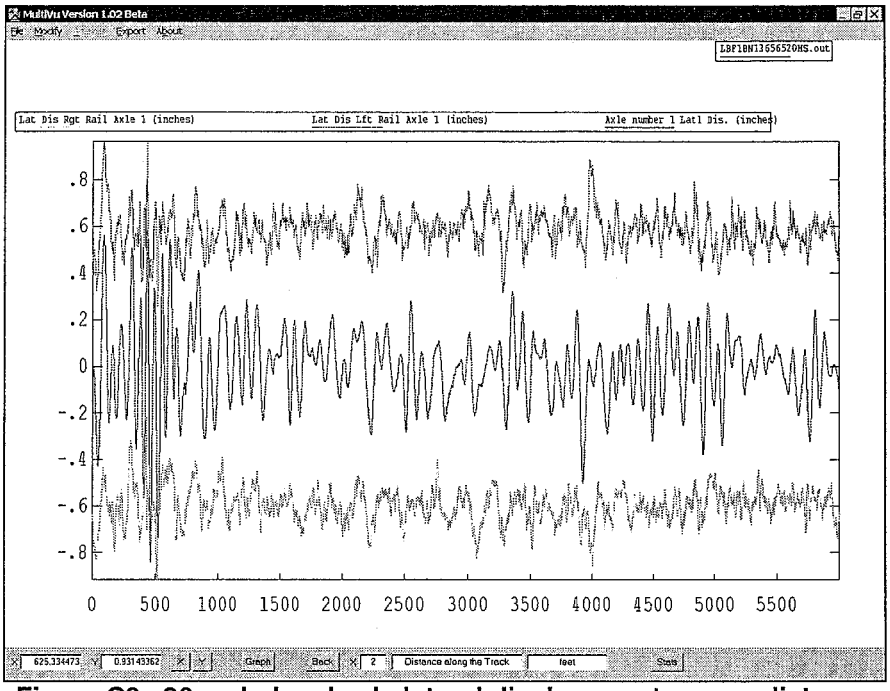

Figure C3. 20 mph, Lead axle lateral displacement versus distance (loaded bulkhead flat, AAR1B narrow flange wheel on AREMA 136-RE rail, 10-inch crown radius, 1:40 cant, at 56.5-inch gage)

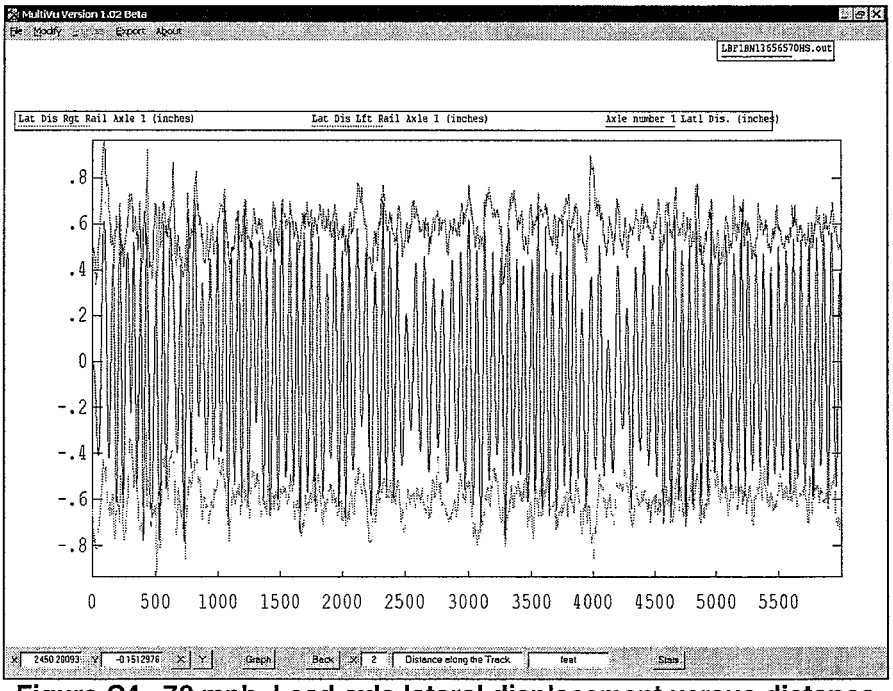

Figure C4. 70 mph, Lead axle lateral displacement versus distance (loaded bulkhead flat, AAR1B narrow flange wheel on AREMA 136-RE rail, 10-inch crown radius, 1:40 cant, at 56.5-inch gage)

Moderately Worn AAR1B Wheels (Wide Flange)

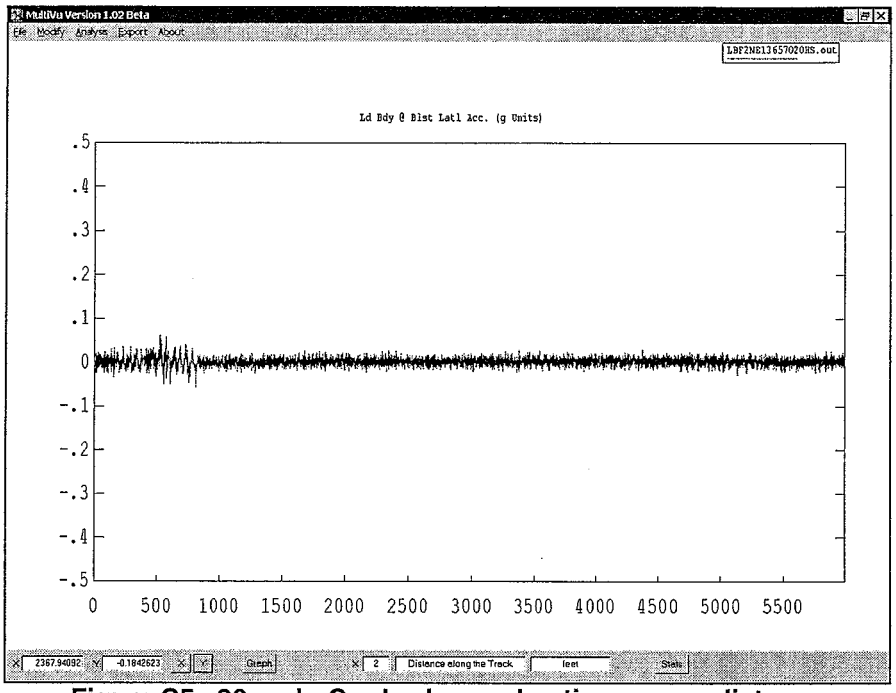

Figure C5. 20 mph, Car-body acceleration versus distance (loaded bulkhead flat, moderately worn AAR1B wide flange wheel on AREMA 136-RE rail, 10-inch crown radius, 1:40 cant, at 57.0-inch gage)

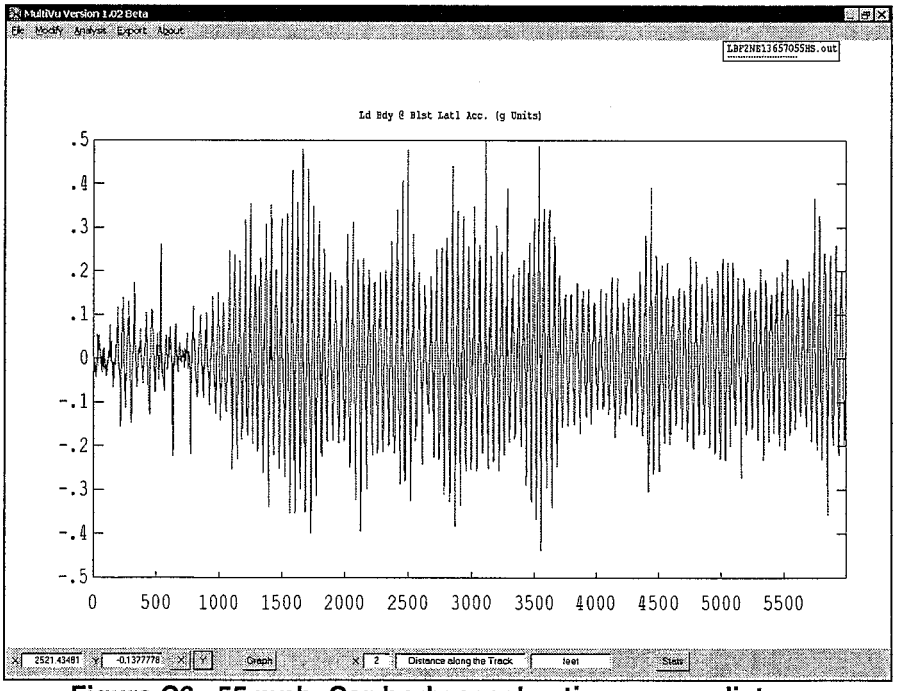

Figure C6. 55 mph, Car-body acceleration versus distance (loaded bulkhead flat, moderately worn AAR1B wide flange wheel on AREMA 136-RE rail, 10-inch crown radius, 1:40 cant, at 57.0-inch gage)

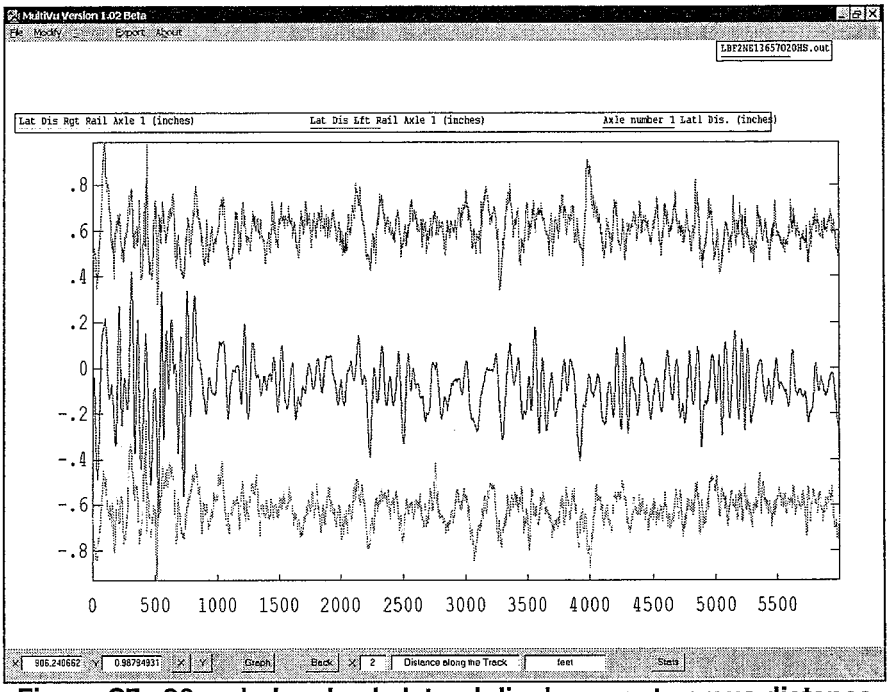

Figure C7. 20 mph, Lead axle lateral displacement versus distance (loaded bulkhead flat, moderately worn AAR1B wide flange wheel on AREMA 136-RE rail, 10-inch crown radius, 1:40 cant, at 57.0-inch gage)

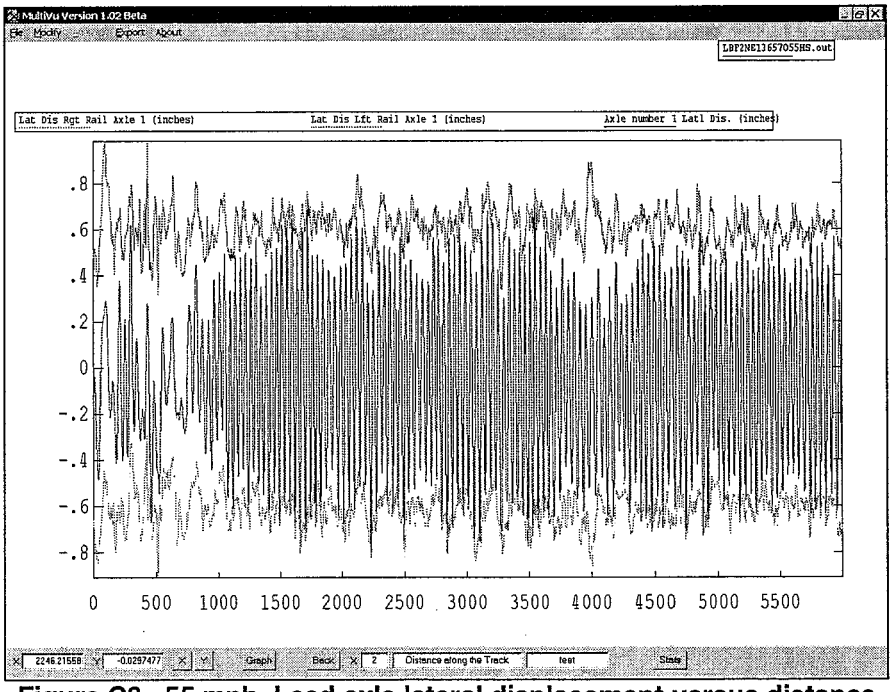

Figure C8. 55 mph, Lead axle lateral displacement versus distance (loaded bulkhead flat, moderately worn AAR1B wide flange wheel on AREMA 136-RE rail, 10-inch crown radius, 1:40 cant, at 57.0-inch gage)

Hollow Worn Wheelset with Wheel Radius Mismatch

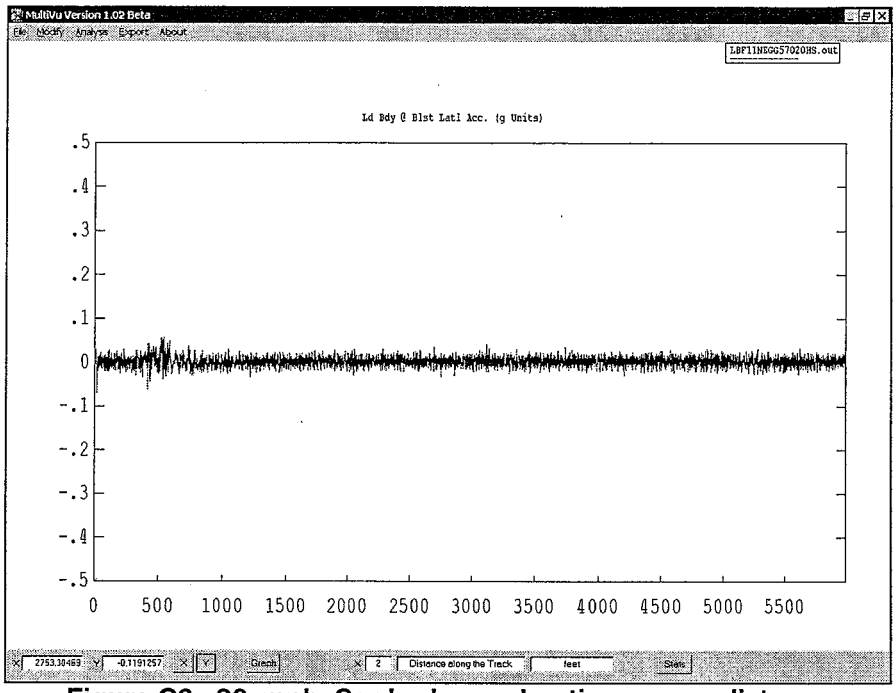

Figure C9. 20 mph, Car-body acceleration versus distance (loaded bulkhead flat, hollow worn wheel with wheel radius mismatch on tangent worn rail at 57.0-inch gage)

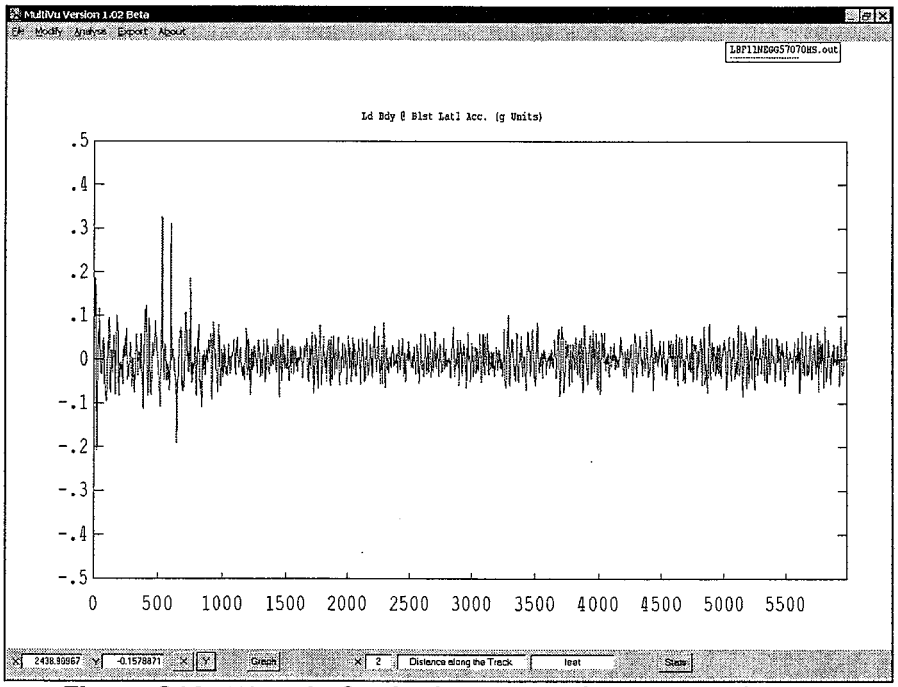

Figure C10. 70 mph, Car-body acceleration versus distance (loaded bulkhead flat, hollow worn wheel with wheel radius mismatch on tangent worn rail at 57.0-inch gage)

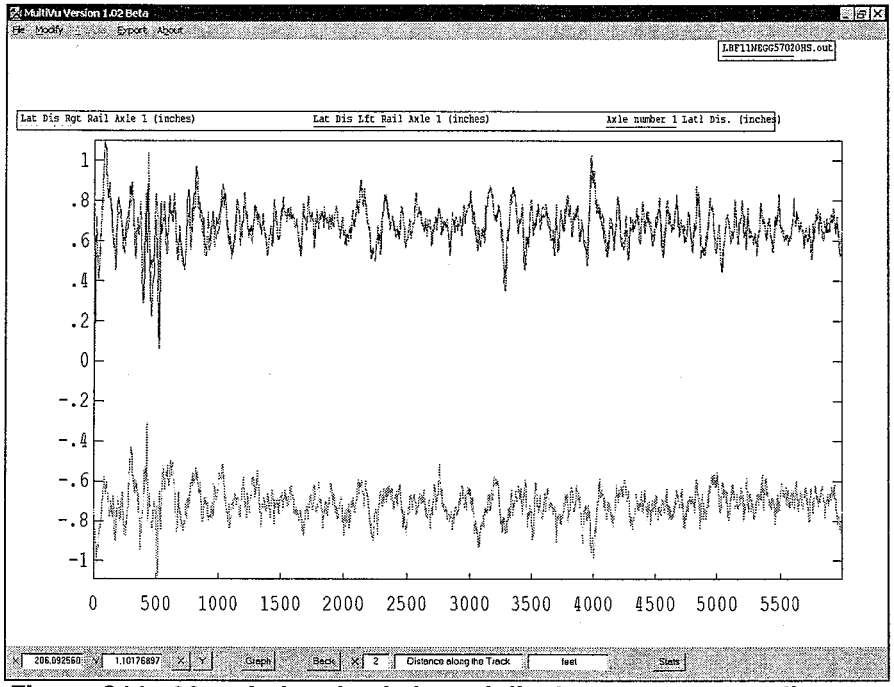

Figure C11. 20 mph, Lead axle lateral displacement versus distance (loaded bulkhead flat, hollow worn wheel with wheel radius mismatch on tangent worn rail at 57.0-inch gage)

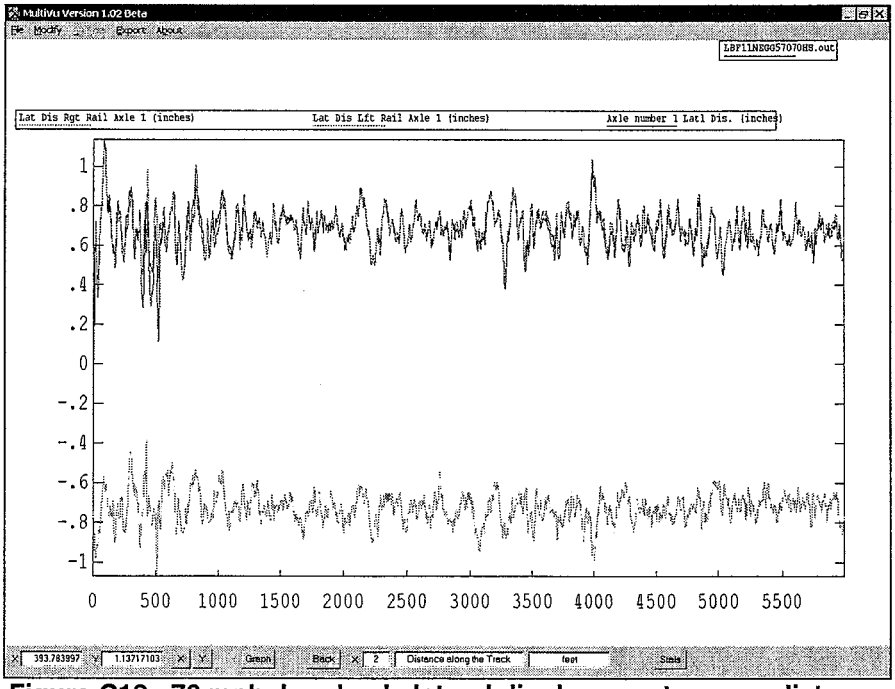

Figure C12. 70 mph, Lead axle lateral displacement versus distance (loaded bulkhead flat, hollow worn wheel with wheel radius mismatch on tangent worn rail at 57.0-inch gage)

Hollow Worn Wheelset with Flange Wear

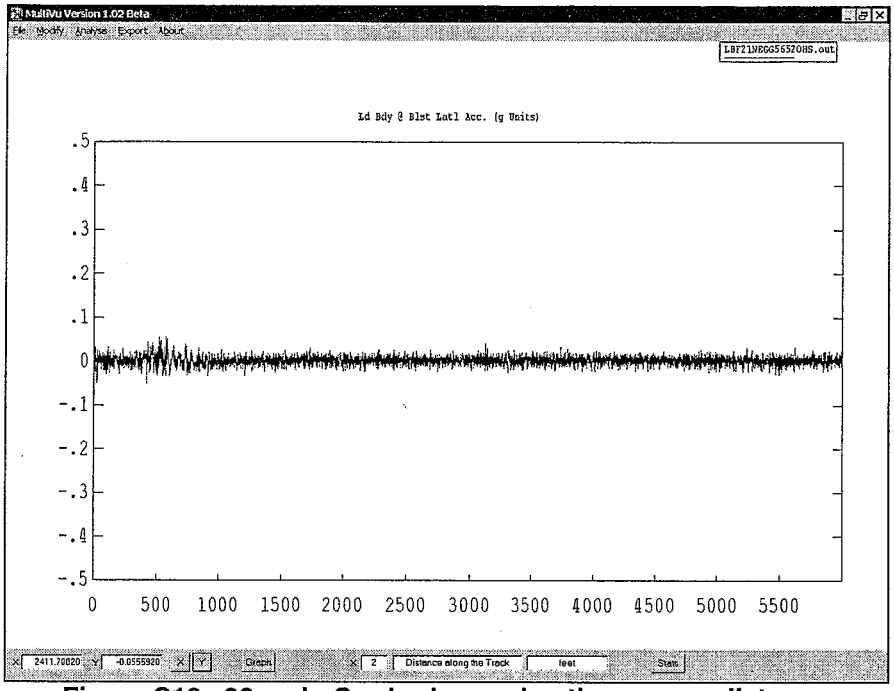

Figure C13. 20 mph, Car-body acceleration versus distance (loaded bulkhead flat, hollow worn wheel on tangent worn track at 56.5-inch gage)

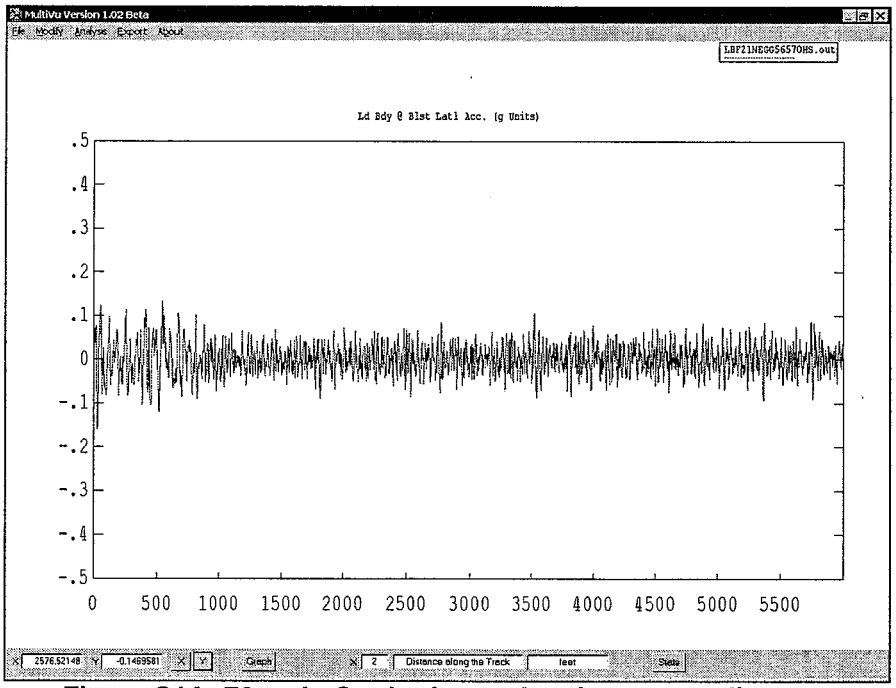

Figure C14. 70 mph, Car-body acceleration versus distance (loaded bulkhead flat, hollow worn wheel on tangent worn track at 56.5-inch gage)

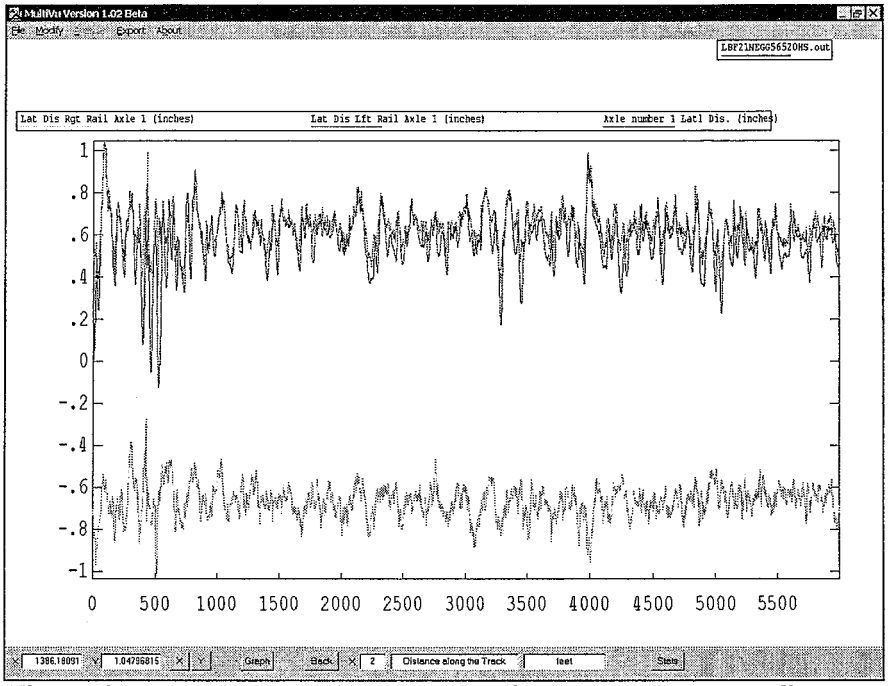

Figure C15. 20 mph, Lead axle lateral displacement versus distance (loaded bulkhead flat, hollow worn wheel on tangent worn track at 56.5-inch gage)

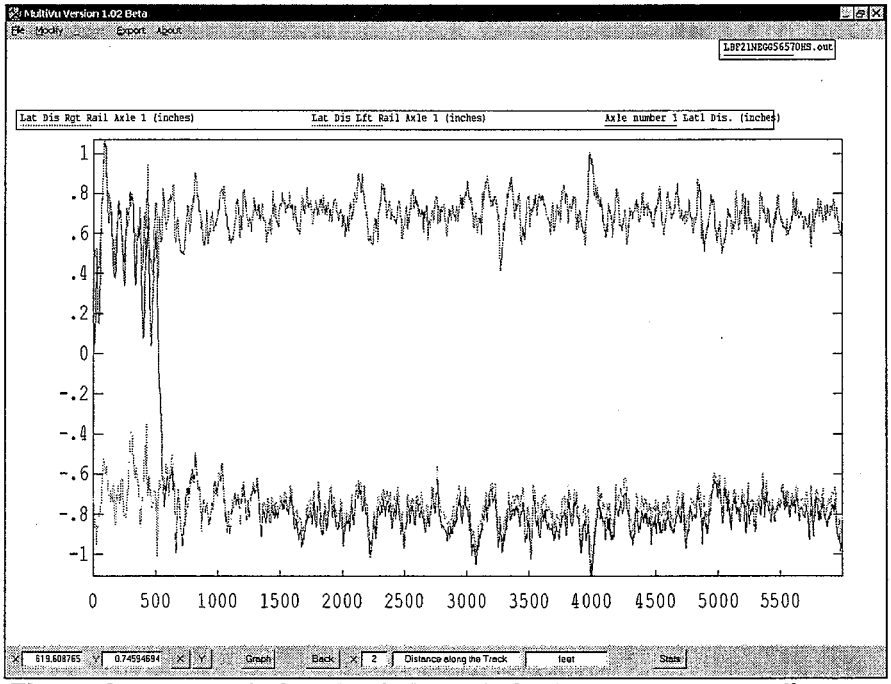

Figure C16. 70 mph, Lead axle lateral displacement versus distance (loaded bulkhead flat, hollow worn wheel on tangent worn track at 56.5-inch gage)

Hollow Worn Wheelset with Minimal Flange Wear

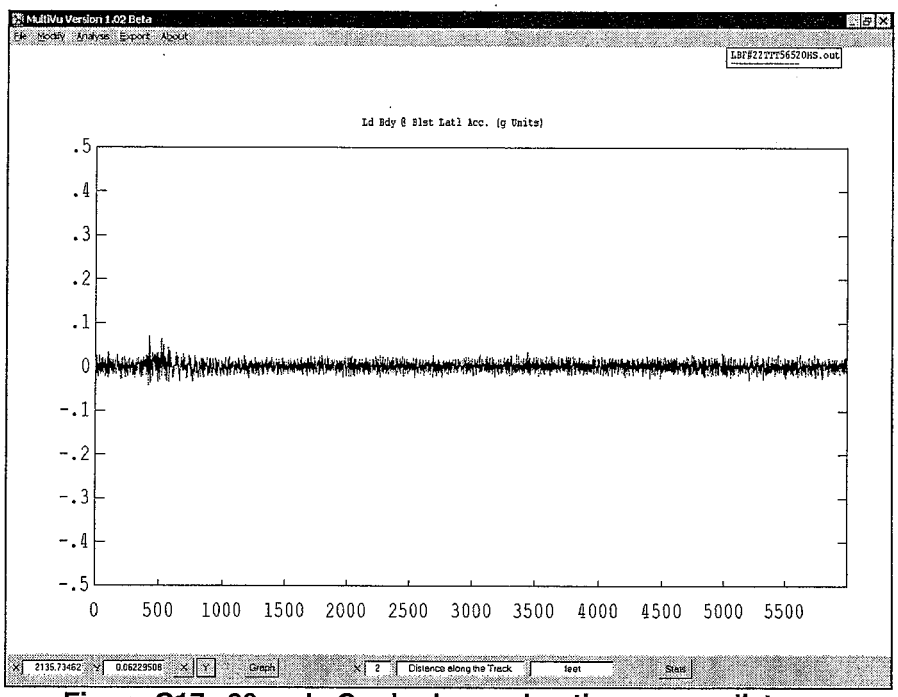

Figure C17. 20 mph, Car-body acceleration versus distance (loaded bulkhead flat, hollow worn wheel with minimal flange wear on TTC's TTT at 56.5-inch gage)

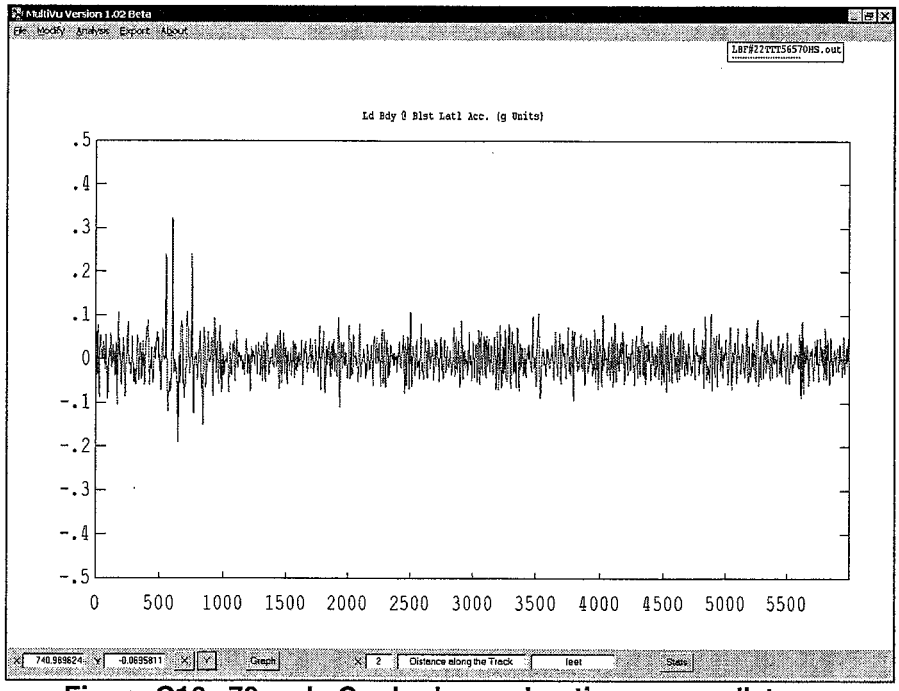

Figure C18. 70 mph, Car-body acceleration versus distance (loaded bulkhead flat, hollow worn wheel with minimal flange wear on TTC's TTT at 56.5-inch gage)

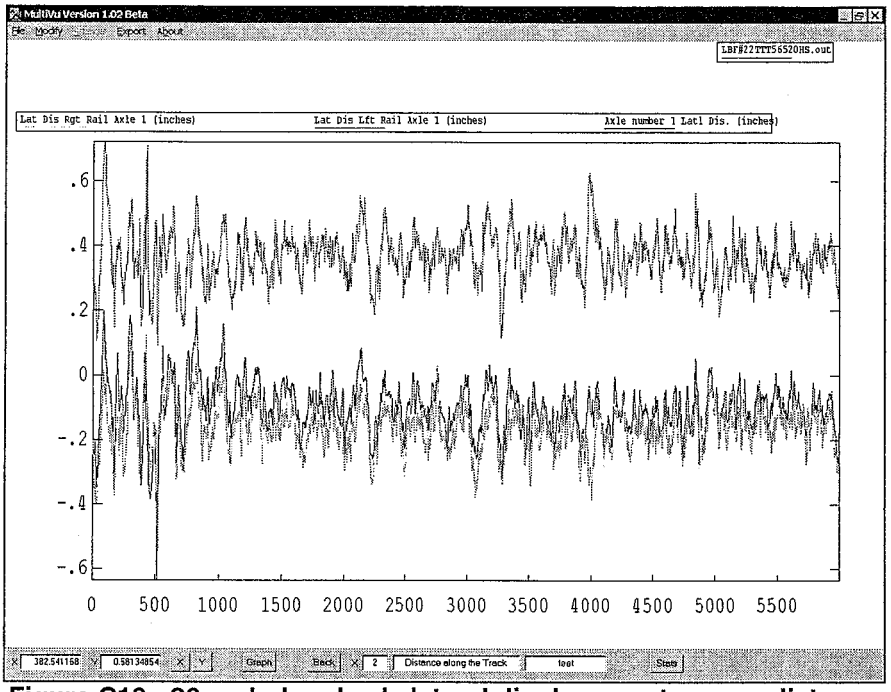

Figure C19. 20 mph, Lead axle lateral displacement versus distance (loaded bulkhead flat, hollow worn wheel with minimal flange wear on TTC's TTT at 56.5-inch gage)

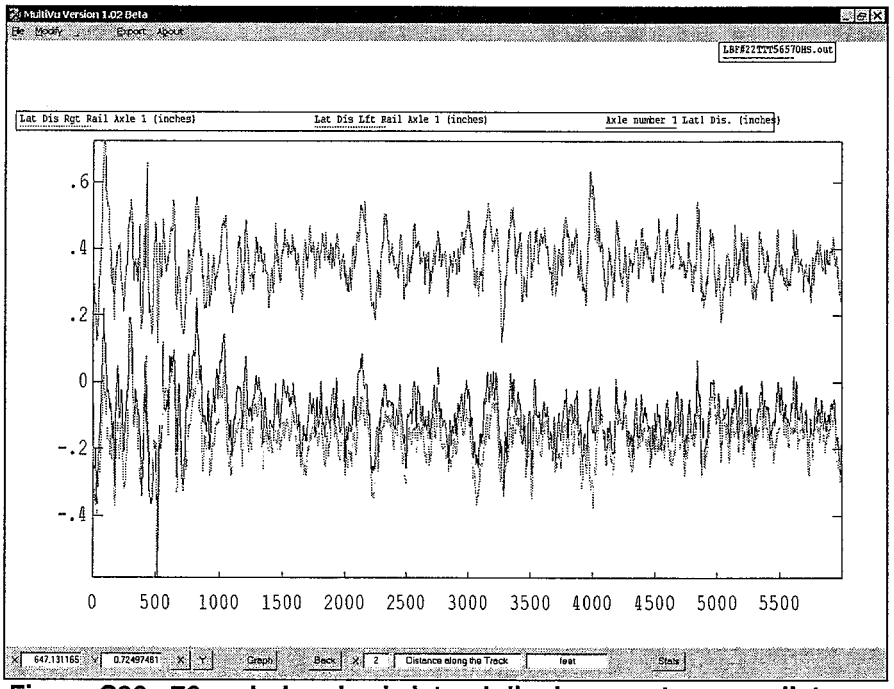

Figure C20. 70 mph, Lead axle lateral displacement versus distance (loaded bulkhead flat, hollow worn wheel with minimal flange wear on TTC's TTT at 56.5-inch gage)

APPENDIX D

LOADED RCV HIGH-SPEED STABILITY PLOTS

New AAR1B Wheels (Narrow Flange)

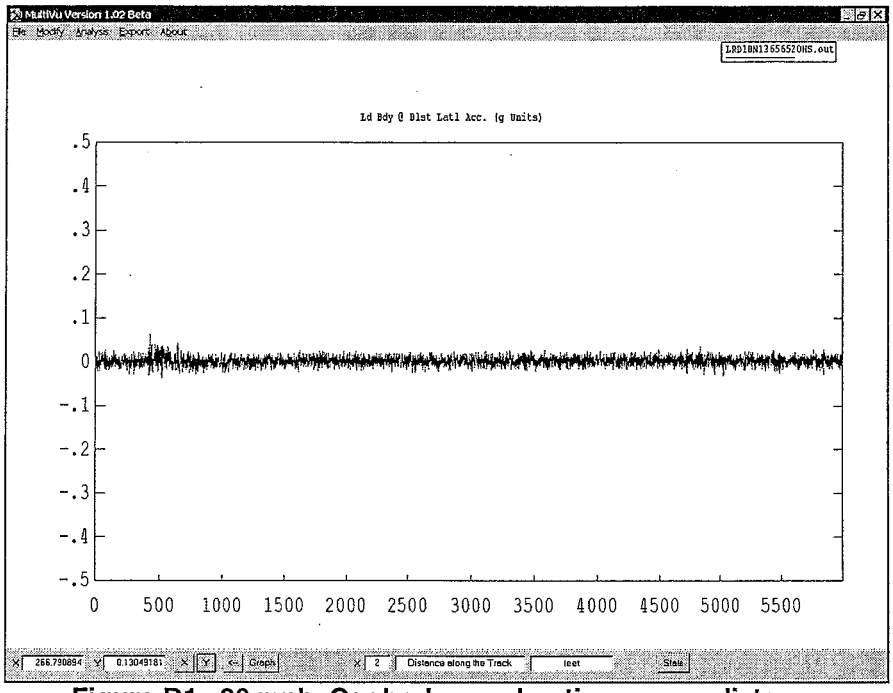

Figure D1. 20 mph, Car-body acceleration versus distance (loaded RCV, AAR1B narrow flange wheel on AREMA 136-RE rail, 10-inch crown radius, 1:40 cant, at 56.5-inch gage)

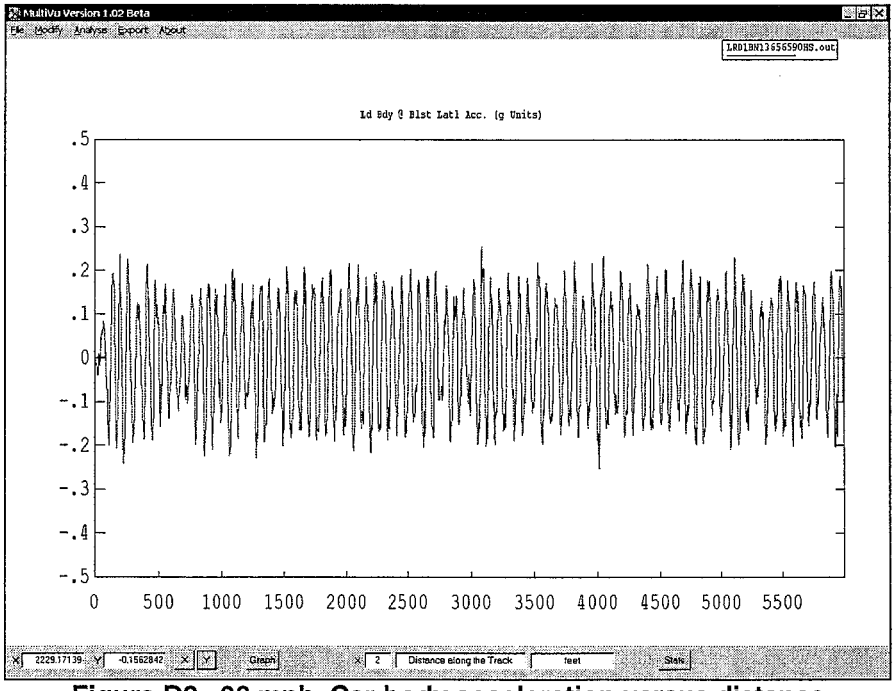

Figure D2. 90 mph, Car-body acceleration versus distance (loaded RCV, AAR1B narrow flange wheel on AREMA 136-RE rail, 10-inch crown radius, 1:40 cant, at 56.5-inch gage)

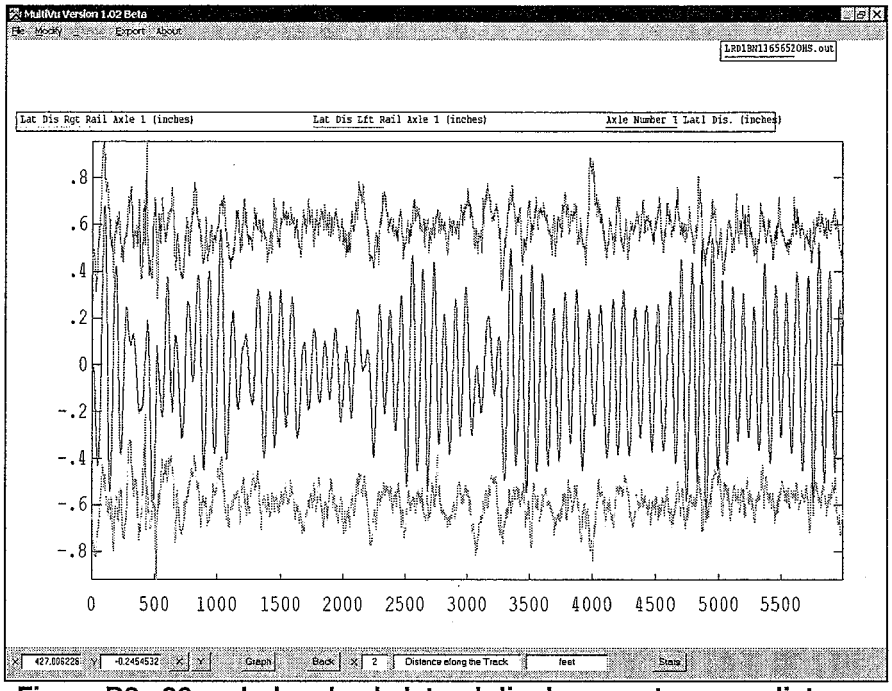

Figure D3. 20 mph, Lead axle lateral displacement versus distance (loaded RCV, AAR1B narrow flange wheel on AREMA 136-RE rail, 10-inch crown radius, 1:40 cant, at 56.5-inch gage)

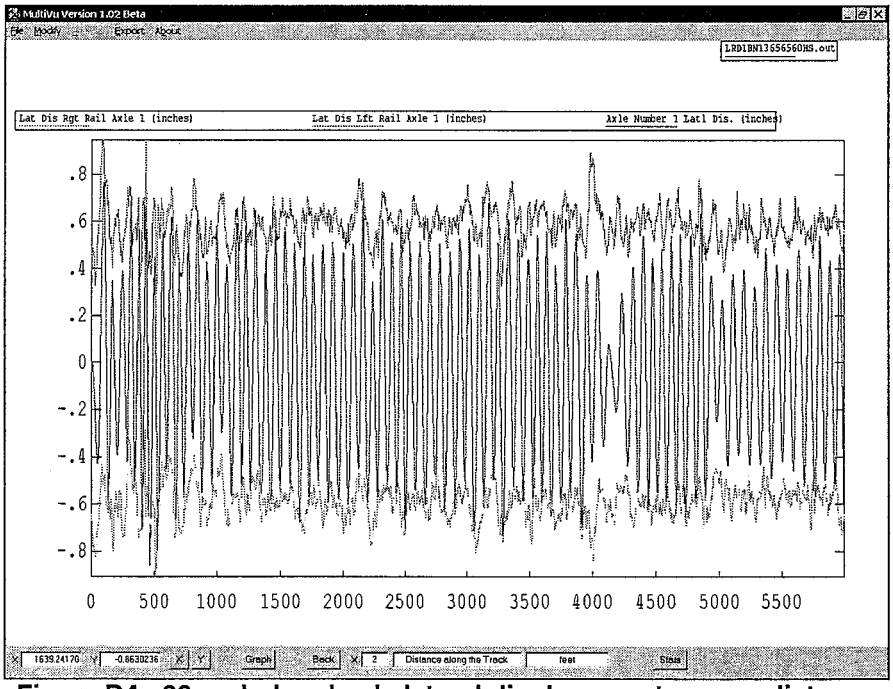

Figure D4. 60 mph, Lead axle lateral displacement versus distance (loaded RCV, AAR1B narrow flange wheel on AREMA 136-RE rail, 10-inch crown radius, 1:40 cant, at 56.5-inch gage)

Moderately Worn AAR1B Wheels (Wide Flange)

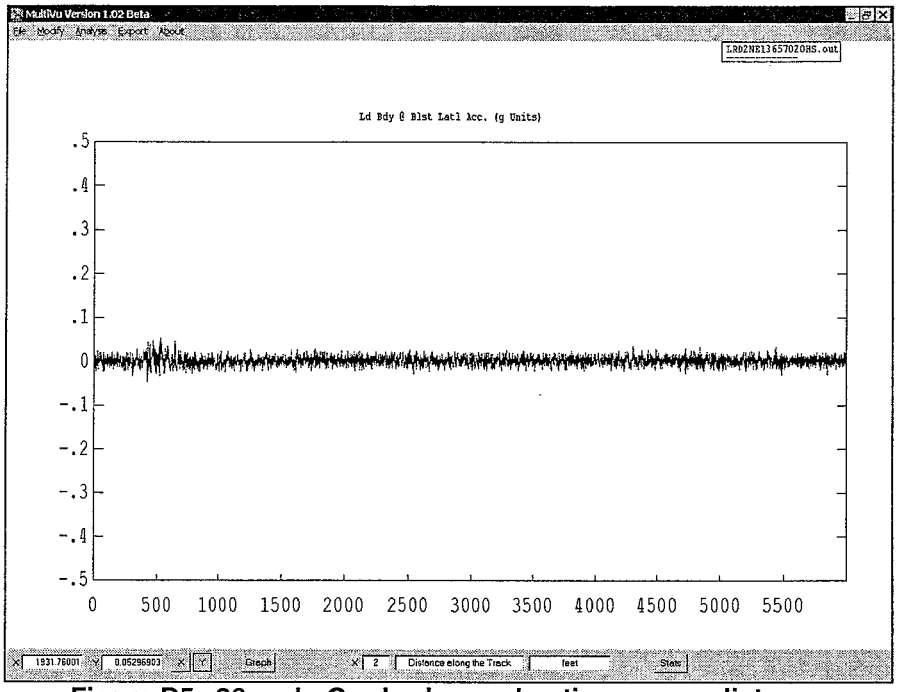

Figure D5. 20 mph, Car-body acceleration versus distance (loaded RCV, moderately worn AAR1B wide flange wheel on AREMA 136-RE rail, 10-inch crown radius, 1:40 cant, at 57.0-inch gage)

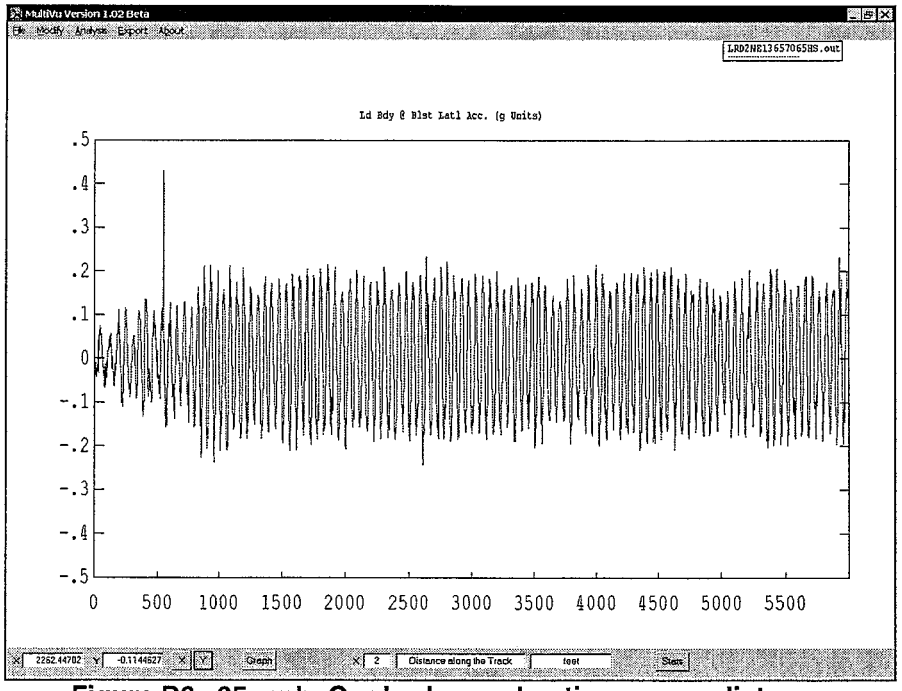

Figure D6. 65 mph, Car-body acceleration versus distance (loaded RCV, moderately worn AAR1B wide flange wheel on AREMA 136-RE rail, 10-inch crown radius, 1:40 cant, at 57.0-inch gage)

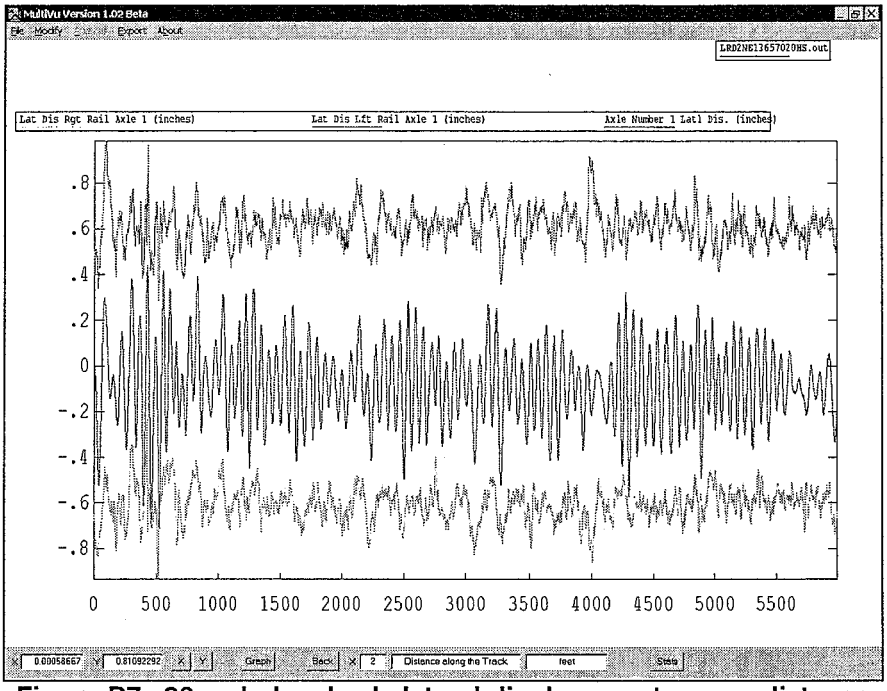

Figure D7. 20 mph, Lead axle lateral displacement versus distance (loaded RCV, moderately worn AAR1B wide flange wheel on AREMA 136-RE rail, 10-inch crown radius, 1:40 cant, at 57.0-inch gage)

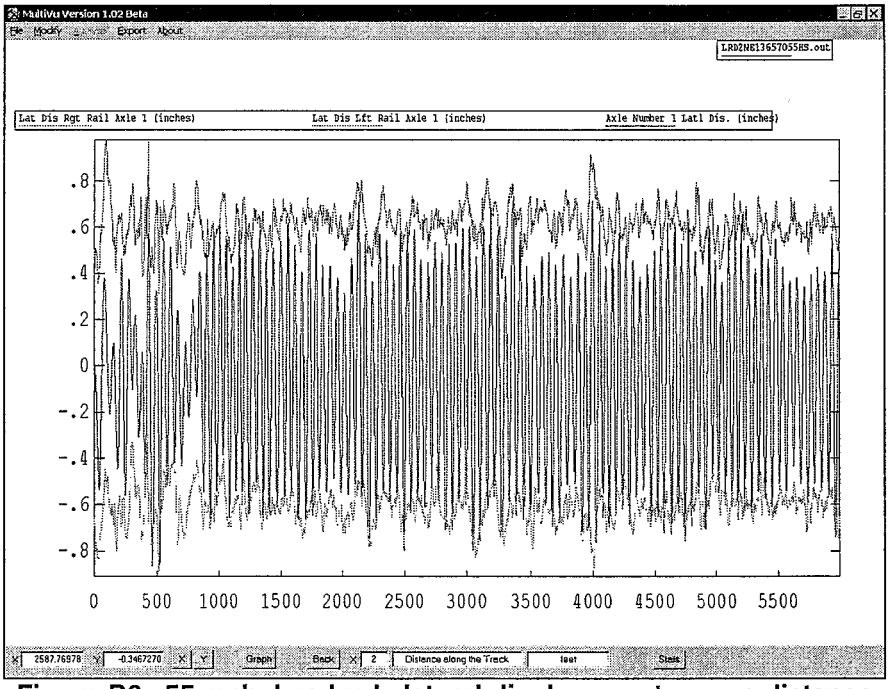

Figure D8. 55 mph, Lead axle lateral displacement versus distance (loaded RCV, moderately worn AAR1B wide flange wheel on AREMA 136-RE rail, 10-inch crown radius, 1:40 cant, at 57.0-inch gage)

Hollow Worn Wheelset with Wheel Radius Mismatch

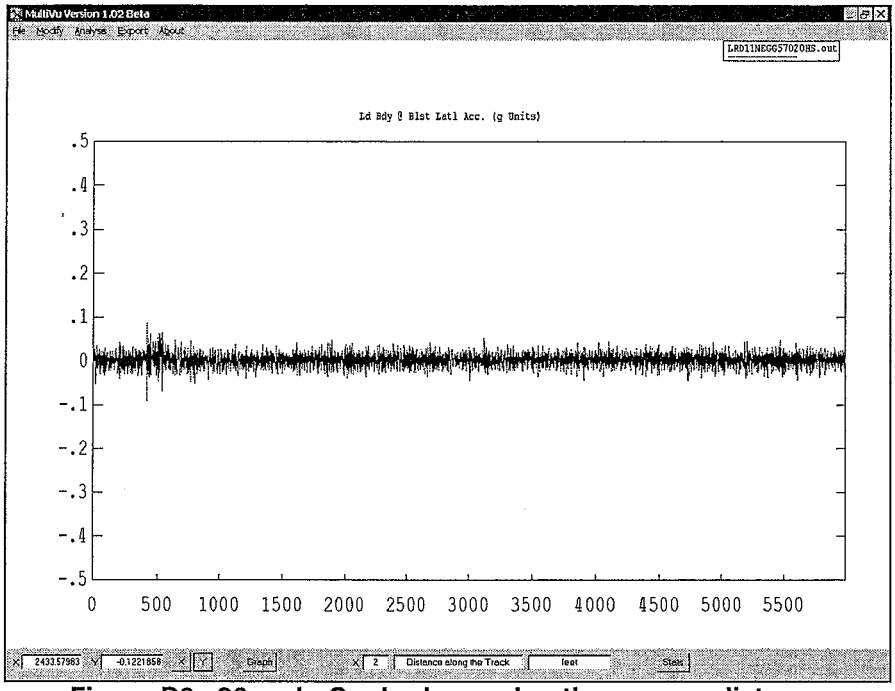

Figure D9. 20 mph, Car-body acceleration versus distance (loaded RCV, hollow worn wheel with wheel radius mismatch on tangent worn rail at 57.0-inch gage)

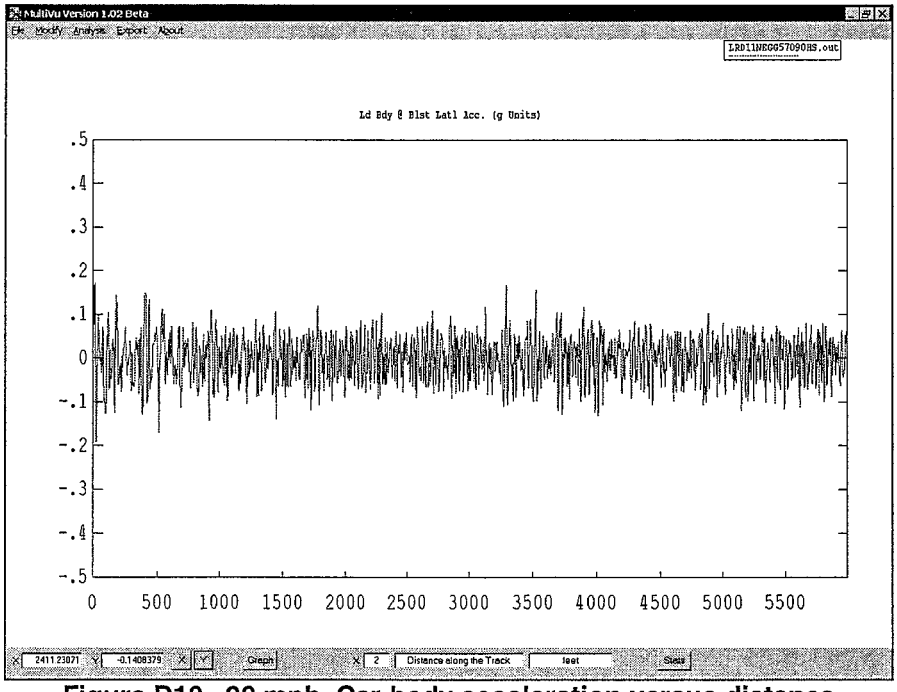

Figure D10. 90 mph, Car-body acceleration versus distance (loaded RCV, hollow worn wheel with wheel radius mismatch on tangent worn rail at 57.0-inch gage)

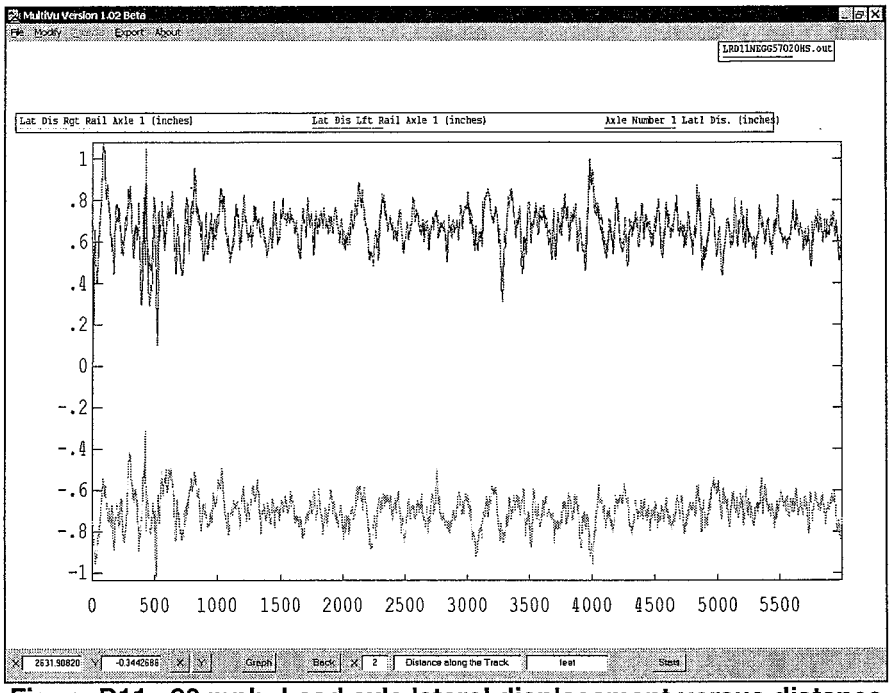

Figure D11. 20 mph, Lead axle lateral displacement versus distance (loaded RCV, hollow worn wheel with wheel radius mismatch on tangent worn rail at 57.0-inch gage)

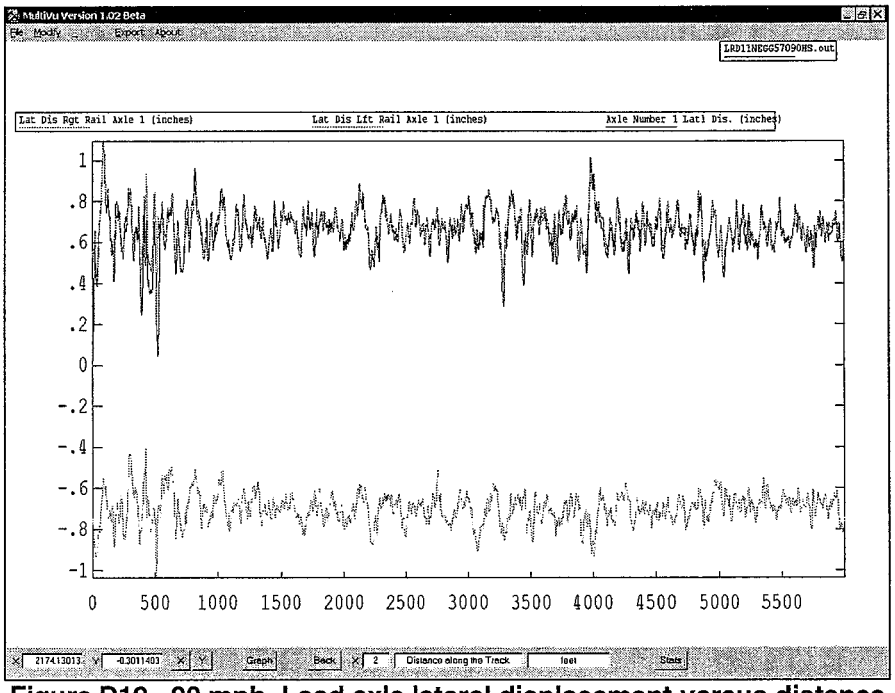

Figure D12. 90 mph, Lead axle lateral displacement versus distance (loaded RCV, hollow worn wheel with wheel radius mismatch on tangent worn rail at 57.0-inch gage)

Hollow Worn Wheelset with Flange Wear

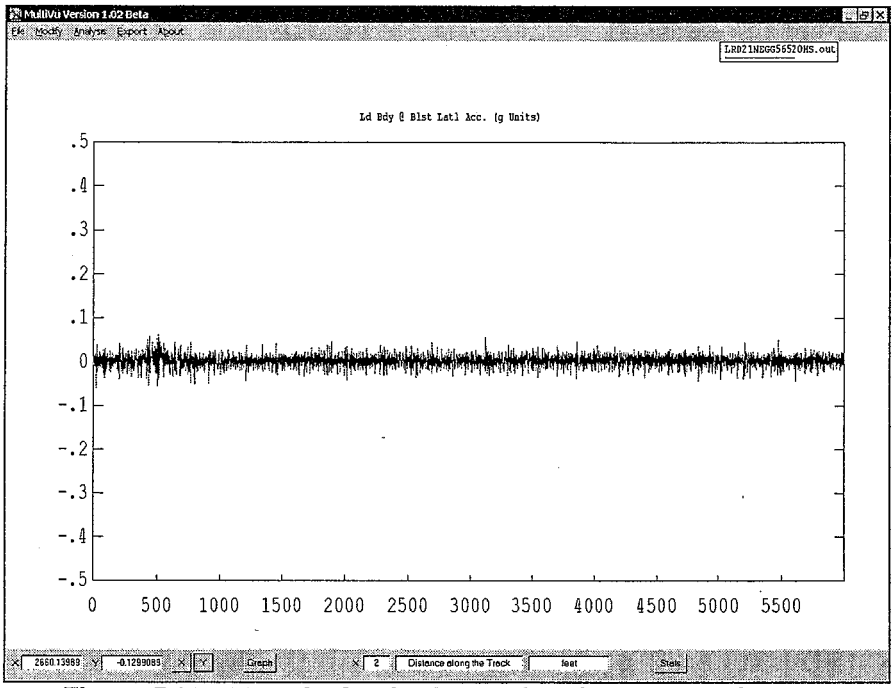

Figure D13. 20 mph, Car-body acceleration versus distance (loaded RCV, hollow worn wheel on tangent worn track at 56.5-inch gage)

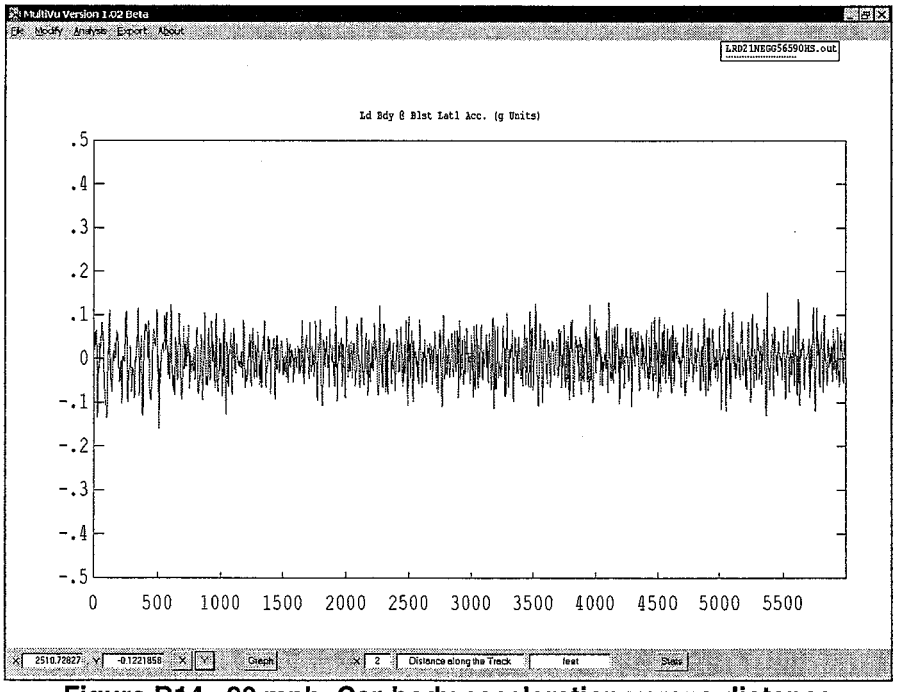

Figure D14. 90 mph, Car-body acceleration versus distance (loaded RCV, hollow worn wheel on tangent worn track at 56.5-inch gage)

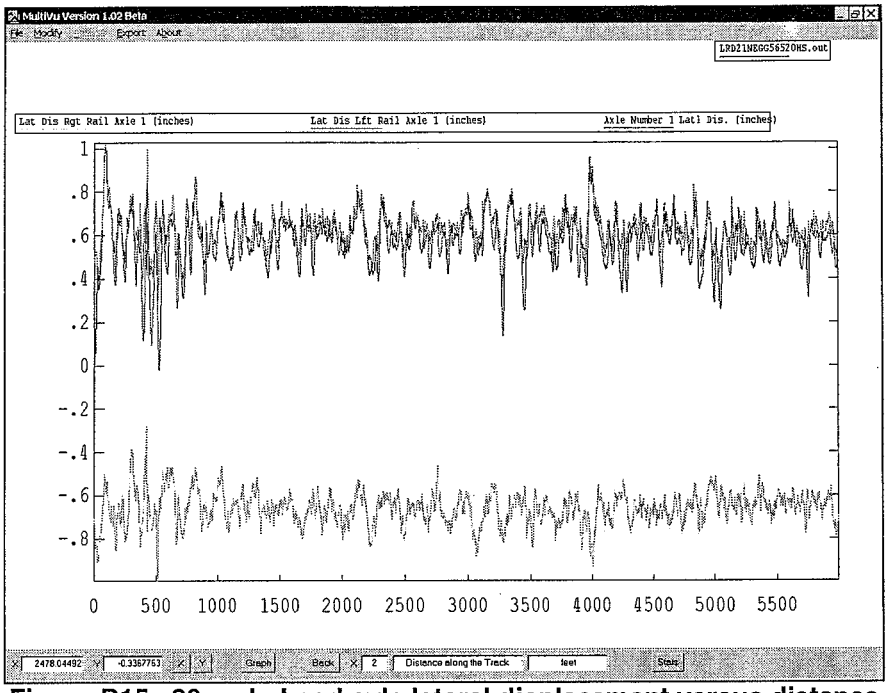

Figure D15. 20 mph, Lead axle lateral displacement versus distance (loaded RCV, hollow worn wheel on tangent worn track at 56.5-inch gage)

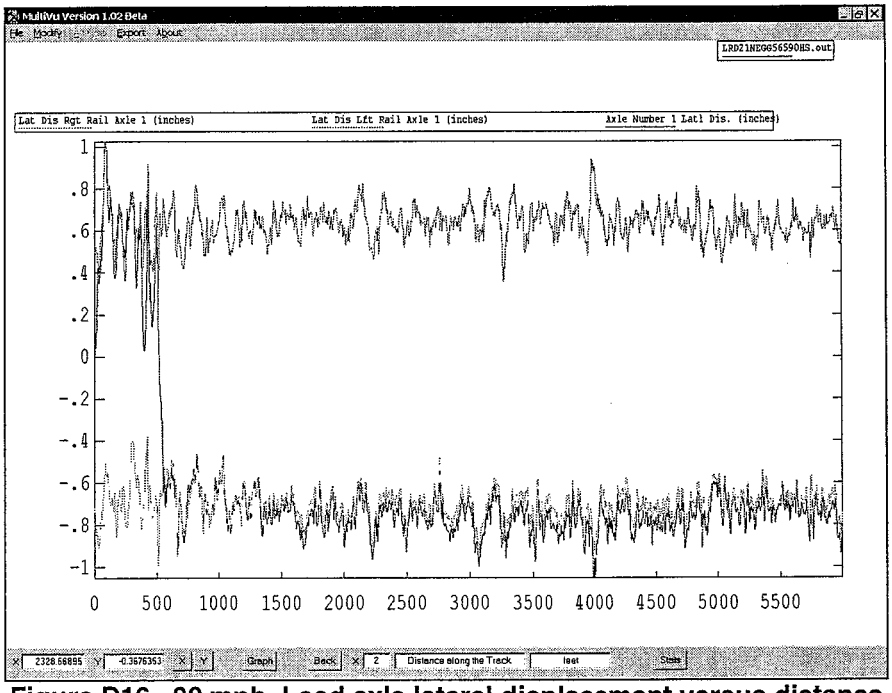

Figure D16. 90 mph, Lead axle lateral displacement versus distance (loaded RCV, hollow worn wheel on tangent worn track at 56.5-inch gage)

Hollow Worn Wheelset with Minimal Flange Wear

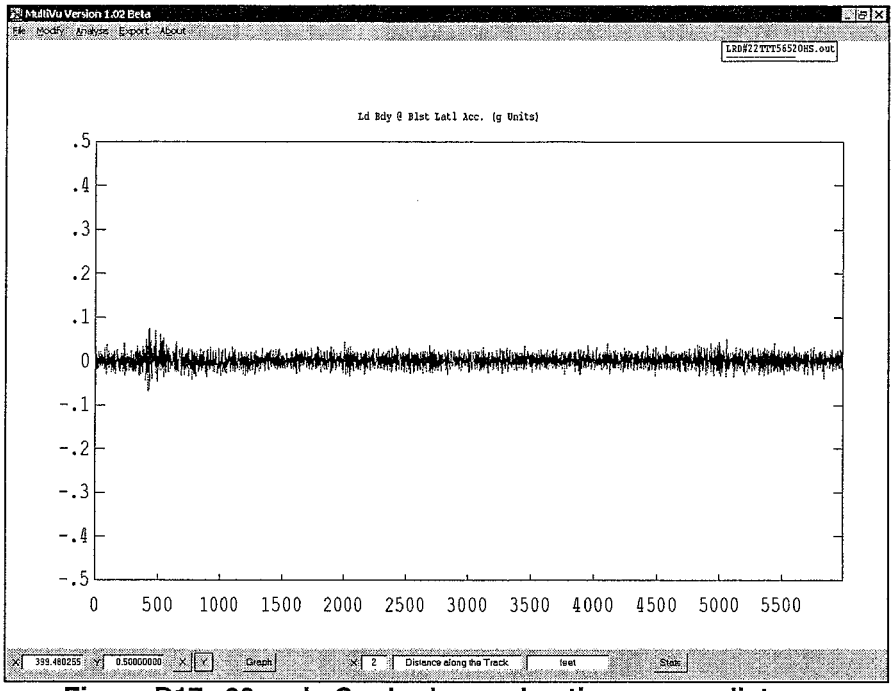

Figure D17. 20 mph, Car-body acceleration versus distance (loaded RCV, hollow worn wheel with minimal flange wear on TTC's TTT at 56.5-inch gage)

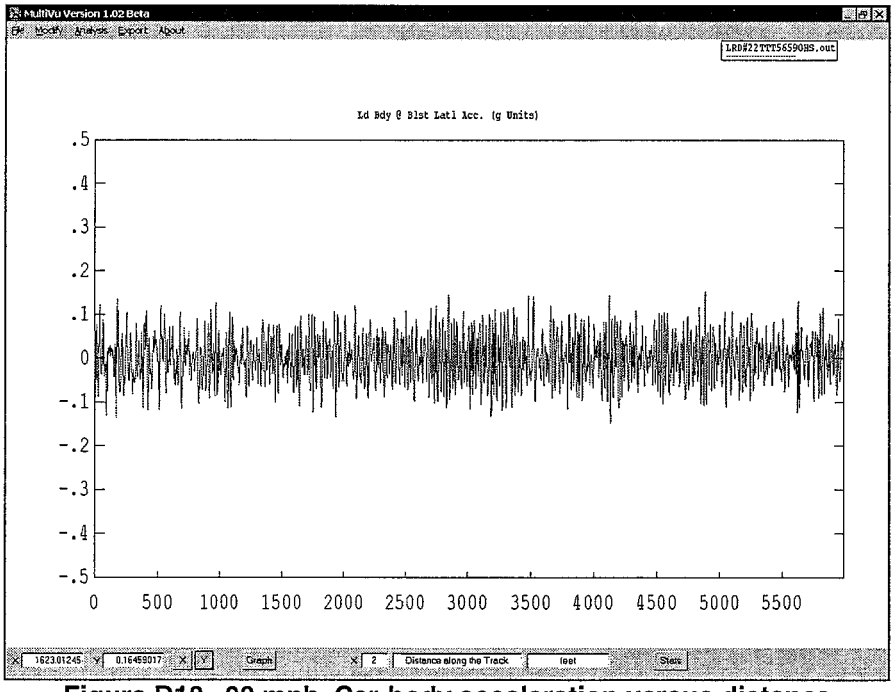

Figure D18. 90 mph, Car-body acceleration versus distance (loaded RCV, hollow worn wheel with minimal flange wear on TTC's TTT Track at 56.5-inch gage)

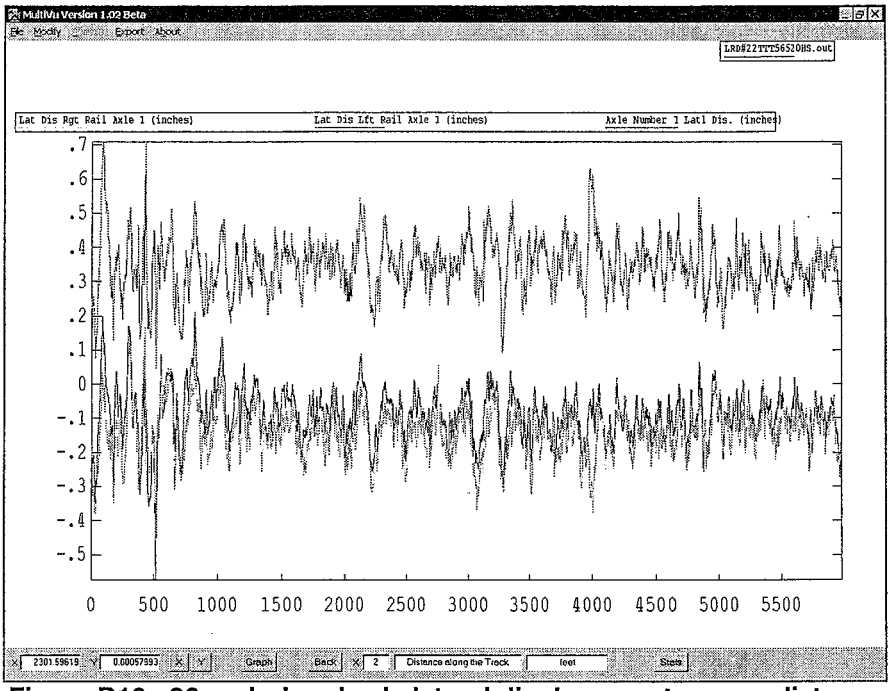

Figure D19. 20 mph, Lead axle lateral displacement versus distance (loaded RCV, hollow worn wheel with minimal flange wear on TTC's TTT at 56.5-inch gage)

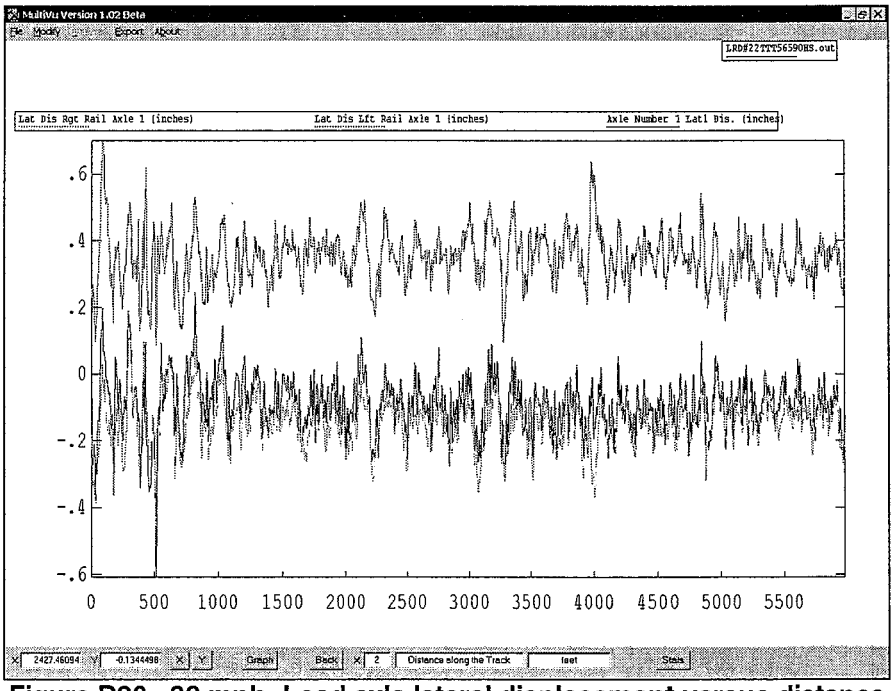

Figure D20. 90 mph, Lead axle lateral displacement versus distance (loaded RCV, hollow worn wheel with minimal flange wear on TTC's TTT at 56.5-inch gage)